Communications Research Centre

GALLIUM ARSENIDE MATERIALS AND DEVICES AND THE GUNN EFFECT

by

W.D. EDWARDS, W.A. HARTMAN, A.B. TORRENS AND D.L. BUTLER

CRC REPORT NO. 1303

Department of Communications
Ministère des Communications

OTTAWA, DECEMBER 1976

IC
.5
e
3

COMMUNICATIONS RESEARCH CENTRE

DEPARTMENT OF COMMUNICATIONS
CANADA

GALLIUM ARSENIDE MATERIALS AND DEVICES AND THE GUNN EFFECT

by

W.D. Edwards, W.A. Hartman, A.B. Torrens and D.L. Butler

(Space Technology Branch)

CRC REPORT NO. 1303

December 1976
OTTAWA

CAUTION
This information is furnished with the express understanding that:
Proprietary and patent rights will be protected.

TABLE OF CONTENTS

PREFACE vii

SYMBOLS AND ABBREVIATIONS USED viii

PART 1 - GALLIUM ARSENIDE GUNN EFFECT DEVICES 1

References to Part 1 3

PART 2 - MATERIAL PROCESSING 5

1. Alignment and Cut-off 6

2. Lapping 6

3. Polishing 6

4. Scribing 7

5. Etching 7

5.1 Thinning and Polishing 7

5.2 Selective Etching 9

6. Sample Washing and Storage 10

7. References 10

PART 3 - GALLIUM ARSENIDE VAPOUR EPITAXIAL GROWTH 21

1. General Description 22

2. Apparatus and Materials 23

3. Substrate Preparation 23

4. Growth Procedure 23

5. Quality of the Layers Grown 25

6. Conclusions 25

7. References 26

TK 5102.5 C673e #1303 c.b

DD 5320734
DL 5320786

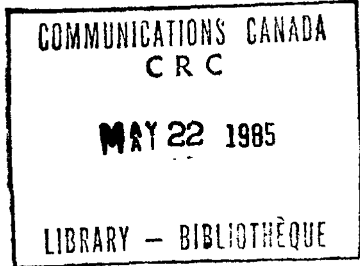
COMMUNICATIONS CANADA
CRC
MAY 22 1985
LIBRARY – BIBLIOTHÈQUE

PART 4 - MATERIAL ASSESSMENT 35

1. Epitaxial-Layer Thickness Measurement 36

2. Resistivity and Doping Measurements 37

3. Conclusions and Summary 39

4. References 39

PART 5 - CONTACTS TO GALLIUM ARSENIDE 45

1. Introduction 46

2. Contact Evaluation 46

3. Experimental 47

3.1 Au:Ge:Ni Contacts 47
3.1.1 Substrate Preparation 47
3.1.2 Equipment and Material 47
3.1.3 Contact Application 48
3.1.4 Measurements 49
3.1.5 Analysis and Results 49

3.2 Tin Dot Contacts 49

4. Discussion 51

5. References 52

Reprint from: Solid-State Electronics, 1972 59

PART 6 - DIODE FABRICATION AND TESTING 67

1. Diode Fabrication 68

2. Testers for Unencapsulated Diodes 68

3. Plot of the I vs. V Characteristic 69

3.1 DC Measurements 69

3.2 Pulse Measurements 69
3.2.1 High-Voltage Pulse Generator 69
3.2.2 High-Current Pulse Generator 70
3.2.3 Graphical Display of the I vs. V Characteristics . 71

4. Microwave Performance 72

5. Conclusion and Summary 72

PART 7 - THEORY OF STEADY HIGH-FIELD DOMAINS 81

1. Introduction 82

2. Study of Small Steady HFD's 82

3. Computations 83

4. Discussion 84

5. Conclusion 86

6. References 86

PART 8 - COMPUTER-SIMULATIONS OF NDC DIODES 97

1. Computer Programs 98

1.1 Relation Between the Field E and the Voltage U 99

2. Parastability 99

2.1 General 99

2.2 Outside Field E_U 100

2.3 Anode Field 100

2.4 Subthreshold Parastability 101

3. Dependence of Parastability on Doping Profile and Voltage . . . 101

3.1 Effect of Doping Inhomogeneities in the Bulk 102

3.2 Effect of an Anode Doping-Inhomogeneity 102

4. Response of a Parastable Diode to Voltage Modulation 103

4.1 Voltage Variations 103

4.2 Sinusoidal Modulation 103

5. Conclusion and Summary 104

6. References 105

PART 9 - THE GUNN EFFECT: FUTURE APPLICATIONS 119
1. Introduction 120
2. References 121

PREFACE

GALLIUM ARSENIDE MATERIALS AND DEVICES AND THE GUNN EFFECT

W.D. Edwards, W.A. Hartman, A.B. Torrens and D.L. Butler

ABSTRACT

A program of experimental and theoretical studies on Gallium Arsenide material and devices was undertaken at the Communications Research Centre (CRC) in 1968 for the following purposes:

- to develop a facility for growing epitaxial material suitable for the fabrication of negative-differential-conductivity (NDC) (e.g. Gunn) devices.
- to develop techniques for fabricating NDC devices for microwave applications
- to explore the theoretical aspects of NDC devices.

This report on the work carried out at CRC is made up of nine parts, each of which is, subtitled, and provided with an abstract. The report may thus be read as follows:

73-552-1 – Gallium Arsenide Gunn Effect Devices

73-552-2 – Material Processing

73-552-3 – Gallium Arsenide Vapour Epitaxial Growth

73-552-4 – Material Assessment

73-552-5 – Contacts to Gallium Arsenide

73-552-6 – Diode Fabrication and Testing

73-552-7 – Theory of Steady High Field Domains

73-552-8 – Computer Simulations of NDC Diodes

73-552-9 – The Gunn Effects – Future Applications

Although the program was officially terminated in 1970 some of the results presented in this report were obtained in the following three years. The pressure of other work delayed the issue of this report. Its appearance now is timely in view of the renewed interest in gallium arsenide material & devices.

SYMBOLS AND ABBREVIATIONS USED

A	cross-section area of an NDC diode, area of a Schottky barrier
c	domain velocity
C	domain characteristic (pt. 7, Figure 2)
D	device line (pt. 7, Figure 2)
D	electron diffusivity
e	elementary charge (electron charge = -e)
E	electric field
E_D	maximum domain field (pt. 7, Figure 1)
E_p	peak electric field (pt. 7, Figure 1)
E_{par}	low field outside a parastable layer (pt. 8, sec. 2.2)
E_U	field outside a high-field domain (pt. 7, Figure 1)
f	frequency
f_p	pulse repetition frequency
HFD	high-field domain (pt. 7)
J	current density
L	diode length, sample thickness
n	electron concentration
N	doping concentration, net ion concentration
N_p	value of N above which parastability occurs (pt. 8, sec. 2)
N_r	reference, or nominal, value of N in a nonuniformly-doped diode
P	peak point of the v vs. E characteristic (pt. 7, Figure 3)

t time

t_p pulse duration

T absolute temperature

U diode voltage

U_0 average value of U (pt. 8, sec. 4.2)

$\hat{U}_1$ amplitude of the modulation U_1 of U (pt. 8, sec. 4.2)

U_d domain excess voltage (pt. 7, sec. 1)

v electron drift velocity (pt. 7, Figure 3)

v_p peak electron drift velocity (pt. 7, Figure 3)

z position in a diode (pt. 7, eq. 4)

z_L position of a charge layer in a diode

μ electron mobility

μ_e equilibrium electron mobility

σ electrical conductivity ($\sigma \stackrel{d}{=} Ne\mu$)

σ_r reference electrical conductivity ($\sigma_r \stackrel{d}{=} N_r e \mu_e$)

ρ electrical resistivity ($\rho \stackrel{d}{=} 1/\sigma$)

GALLIUM ARSENIDE MATERIALS AND DEVICES AND THE GUNN EFFECT

by

W.D. Edwards, W.A. Hartman, A.B. Torrens and D.L. Butler

PART 1

GALLIUM ARSENIDE GUNN EFFECT DEVICES

by

W.D. Edwards, W.A. Hartman, A.B. Torrens and D.L. Butler

ABSTRACT

Gallium arsenide, NDC effects, and their applications to microwave devices are briefly reviewed. The subject matter of the remaining eight parts of the report is introduced.

PART 1

GALLIUM ARSENIDE GUNN EFFECT DEVICES

Gallium arsenide was selected as the material with the most potential for microwave and optical communications devices such as sources, modulators, detectors, and amplifiers. Microwave power (at 10 GHz, for example) may be produced from a tiny chip of GaAs subjected to a low voltage (e.g., 10 V). This is extremely important for military and civil communications applications, e.g. in satellites, where microwave systems are needed without the weight and high voltages of conventional microwave sources such as klystrons, and with the reliability and long life of solid-state devices. Oscillators and amplifiers have been made with noise figures approaching those of klystrons[1-3]. In 1952 GaAs was shown to be a semiconductor[4]. Gallium arsenide proved difficult to process, and transistor action was not demonstrated until[5] 1958. In the early 60's, the GaAs laser and the Gunn effect[6] in GaAs firmly established the importance of the material. It is a III-V compound with an intrinsic band gap of 1.4 eV and thus is a potential material for the fabrication of devices capable of operation up to 300°C.

The Gunn effect, discovered[6] in 1963, is one manifestation of the transferred-electron phenomenon. When an electric field is applied to gallium arsenide the electrons gain energy from the field. At high fields, they (or, more precisely, the points representing their states in the k-space) "transfer" from low-energy, high-mobility states to high-energy, low-mobility states[7]. As a result, the current density vs. field relationship for the material exhibits negative differential conductivity (NDC) for fields beyond a peak field E_p which is about 0.32 MV/m for n-type GaAs (Figure 3 of pt. 7). This NDC underlies all so-called "Gunn", "LSA", "bulk", and "transferred-electron" effects and devices.

When the material is biased in the NDC range, it is unstable. A small fluctuation grows into a large but finite electrical inhomogeneity, usually a high-field domain (HFD) (Figure 1 of pt. 7). Such a domain propagates at a velocity of about 100 km/s.

The most common NDC device is a diode, consisting usually of two parallel ohmic contacts applied to the two faces of a GaAs slice. If the product of the doping density N and the length (distance between contacts) L of the diode is larger[7,8] than $10^{16} m^{-2}$, the diode oscillates spontaneously when the voltage U between the contacts exceeds the value $L.E_p$. The oscillation frequency is the reciprocal of the HFD transit-time: $f = c/L$.

The transferred-electron effect is a true bulk effect as distinct from interface effects, e.g., those associated with a p n junction. Under certain operating conditions, such as the LSA (limited space-charge accumulation) mode, the device is not transit-time limited. This independence from transit time opens the way to production of high power at high frequencies. Pulsed oscillations of 6 kW at 1.75 GHz have been obtained with 14.6% efficiency[9]*. Pulses of 100 kW at 10 GHz with efficiencies of up to 20% are predicted[7,12].

---

* *Note added in 1975*

L.S.A. devices are still essentially laboratory devices and the quoted power figure is still the highest published [10]. Pulsed Gunn oscillators have provided 70W at X band [1].

The motion of the Gunn domain at approximately 100 km/s can be used as a basis for sophisticated high-speed scan and function generators[13], optical modulators[14], phase shifters[15], and logic applications[16].

The performance of these devices in terms of noise, reliability, efficiency, and power is critically dependent upon the production of uniform material and low-resistance ohmic contacts. The initial intent of the project was therefore the production of material and contacts suitable for the fabrication of Gunn diodes.

Material processing, epitaxial material growth, and assessment methods are described in pts. 2, 3 and 4 respectively. The emphasis on materials was subsequently redirected to devices and later to the necessary ohmic contacts to the devices (pts. 5 and 6). Attainment of the techniques necessary to process the somewhat intractable gallium arsenide has therefore occupied a major fraction of the effort and time allocated to the project. Pt. 7 sheds some new light on the behaviour of Gunn diodes near threshold bias. Concurrently, a computer-simulation program of NDC devices was undertaken to explore further the necessary material properties for efficient microwave oscillators and amplifiers (Pt. 8).

REFERENCES TO PART 1

1. *Gunn-Effect Oscillators Aim at Klystron Markets*, Electronics 41, No. 13, 157 (24 June, 1968).

2. Fitzsimmons, G.W., *Microwave Generation with Avalanche Diodes and Two Valley Gunn and LSA Mode Devices*, Microwave J. 11, 45 (1968).

3. Ohtomo, M., *Experimental Evaluation of Noise Parameters in Gunn and Avalanche Oscillators*, IEEE Trans. MTT 20, 425 (1972).

4. Welker, H., *Discussion on New Semiconductor Compounds*, Naturforsch 7a, 744 (1952).

5. Jenny, D.A., *The Status of Transistor Research in Compound Semiconductors*, Proc. I.R.E. 46, 959 (1958).

6. Gunn, J.B., *Microwave Oscillators of Current in III-V Semiconductors*, Solid State Commun. 1, 88 (1963).

7. Butcher, P.N., *The Gunn Effect*, Rep. Prog. Phys. 30, 97 (1967).

8. McCumber, D.E., and A.G. Chynoweth, *Theory of Negative Conductance Amplification and Gunn Instabilities in Two Valley Semiconductors*, IEEE Trans, ED13, 4 (1966).

9. Jeppsson, B., P. Jeppesen and Cayuga Associates, *A High Powered LSA Relaxation Oscillator*, Proc. IEEE 57, 1218 (1969).

10. Hobson, G.S., *Recent Developments in Transferred Electron Devices*, J. Phys. E: Sci- Inst. Vol 6, 1973.

11. Stevens, R., D. Tarrant + F.A. Myers, *Pulsed Gunn-diode Oscillator 40W at 16 GHz*, Electron Lett. Vol 10, December 1974.

12. Eastman, L.F., *The Capabilities and State-of-the-art of Gunn and LSA Devices*, XVI General Assembly URSI, Ottawa (1969); Proc.: Prog. Radio Sci. 1966-1969: 3.405 (1971).

13. Sandbank, C.P., *Synthesis of Complex Electronic Junctions by Solid State Bulk Effects*, Solid State Electron. 10, 369 (1967).

14. Cohen, M.G., S. Knight and J.P. Elward, *Optical Modulation in Bulk GaAs Using the Gunn Effect*, Appl. Phys. Lett. 8, 269 (1966).

15. Dean, R.H., A.B. Dreeben, J.F. Kaminski and A. Triano, *Travelling-Wave Amplifier Using Thin Epitaxial GaAs Layer*, Electronic Lett. 6 975-6 (1970).

16. Hartnagel, H.L., *Theory of Gunn Effect Logic*, Solid State Electron. 12, 19 (1969).

GALLIUM ARSENIDE MATERIALS AND DEVICES AND THE GUNN EFFECT

by

W.D. Edwards, W.A. Hartman, A.B. Torrens and D.L. Butler

PART 2

MATERIAL PROCESSING

by

W.D. Edwards and D.L. Butler

ABSTRACT

The basis material processes are described. Purchased GaAs ingots are X-ray oriented, sawed and lapped. The slices are first polished with grit or, more successfully, with a 5% NaOC1 solution. The slices are then scribed and cleaned.

Of the etches used to thin and polish samples, $CH_2OH:Br$ *and* $H_2SO_4:H_2O_2:H_2O$ *mixtures gives the best results. The best selective etch is an* $AgNO_3:CrO_3:HF:H_2O$ *mixture. No etch reliably delineates an* n^+n *interface.*

PART 2

MATERIAL PROCESSING

GaAs single crystals containing a variety of dopants at various concentrations were obtained commercially. On receipt, a number of the samples were checked for resistivity and uniformity. The processing steps which were developed are described below.

1. ALIGNMENT AND CUT-OFF

Bulk material was received in ingot form and sliced off into suitable wafers, using the diamond saw shown in Figure 1. Device processing was carried out in relationship to specific crystal planes, e.g. 111 or 100, and therefore the crystal was oriented with respect to the cutting blade (Figure 2). The crystal was mounted on a specially designed jig (Figure 3), which incorporated a Jarrel-Ashe goniometer, to allow orientation determination by the X-ray (Laue) method and then transfer of the jig to the cut-off machine. Crystal alignment, transfer and cut-off to within 0.5° was possible. A typical Laue pattern is shown in Figure 4. The smallest thicknesses successfully obtained were 0.1 mm.

2. LAPPING

The cut-off machine introduces surface uneveness and damage. Slices of approximately equal thicknesses are needed for the polishing operation. The slices were therefore ground down to the desired thickness on a rotary lapping machine. Typically, three slices were cemented to a lapping block with a low melting-temperature wax - glycol phthalate, which melts at 150°C. The block was placed on the machine and the slices were successively ground with grinding powders of sizes down to 1 micron. A typical surface finish is shown in Figure 5. The thickness of the slice was measured with a specially designed dial gauge (Figure 6).

3. POLISHING

A continuation of the lapping operation, or use of a polishing wheel, with grit sizes to 0.1μ or with other polishing materials such as rouge, gives a mechanical polish.

A number of such approaches were tried but the most successful was a mechanical-chemical method. This approach has been shown by X-ray topography to produce damage-free wafers[1].

Before commencing, it was necessary to rid the sample surfaces of all grinding power to avoid scratching the polished surface. A scanning electron microscope (SEM) was used to determine the minimum time necessary to rid the surface of grinding particles in an ultrasonic cleaning bath. Typical SEM

photographs are shown in Figure 7. It was necessary to ultrasonically clean a lapped surface for 90 seconds in water and for 90 seconds in freon to clean away all the nine-micron lapping grit.

Three slices were then mounted on a polishing block with the aid of a wax, which is both thermo-setting and soluble in trichloroethylene. The block was then placed upon a pellon pad soaked in 5% sodium hypochlorite[2]. The solution was replenished using a pipette at 1 ml per minute during the polishing operation. The pellon pad was rotated at about 60 rpm and, as a result of the special support arm, the polishing block also rotated with respect to the pad (Figure 8). The polish-etch rate, as determined with the dial gauge shown in Figure 6, was about 8 microns/min. The chemical polishing action was terminated by flooding the pad with distilled water. Very highly polished surfaces were obtained with most of the curvature at the sample edges; typically, 50 interference lines were observed across a 1 cm slice.

A disadvantage of the method was that three slices had to be polished at once and they therefore had to be prelapped to approximately equal thicknesses. A single slice on a different type of polishing mount (Figure 9) was equally smooth but had more curvature.

4. SCRIBING

Gallium arsenide has a preferred cleavage plane - the 110. A slice usually had some part of its perimeter broken off along a cleavage plan and this edge was used to visually align the slice on an automatic scribing machine*. It was necessary to attach the small wafers to a glass slide to ensure adequate coverage of the vacuum chuck. The height, position and pressure of the 4-pt truncated diamond scribe tip was then adjusted. The chuck could be rotated by 90° or 120°depending on the crystal orientation to give the correct angle for further scribe lines. Then, the die dimensions were set and the automatic scribing was started.

The wafer was removed from the mounting plate and either rolled using a rubber roller on a semi-pliable base, or individually pressured, to cleave the wafer at the scribe lines. At least 85% of the slice was usable after this procedure.

5. ETCHING

Chemical etches were used for the following purposes: to thin down samples, to polish, to determine crystal orientation, and to reveal dislocations.

5.1 THINNING AND POLISHING

It was found to be preferable to use a polish etch to thin down samples. The etches used on the (100) face, together with the average etch rates observed, are shown in Table 1.

* *Tempress Industries, Inc., 980, University Ave., Los Gatos, Calif. 95030*

TABLE 1

			Etch rate in μm/min. at 25°C	at 55°C
$3H_2SO_4$:	$1H_2O_2$:	$2H_2O$	2.0	4.4
5% NaOCL :			1.5	1.8
1 Br :	50 methanol		4.1	2.3
1 Br :	100 methanol		2.1	1.0
1 Br :	200 methanol		0.9	0.3
1 Br :	50 Freon TF (Dupont)		1.1	0.92
1 Br :	100 Freon TF (Dupont)		.66	0.58
1 Br :	200 Freon TF (Dupont)		.46	0.55

The reagents used were 49% HF, 97% H_2SO_4, 70% HNO_3, and 30% H_2O_2

All samples were etched in a 25 ml Erlenmeyer flask set in a constant-temperature water bath. The flask was set at an angle and slowly rotated so as to give a tumbling action to the samples. Samples were etched for three different periods of several minutes duration. The etch rates were found to be constant during the etching process, for $(6mm)^2$ samples in 10 ml of fresh etch.

The first etch solution in Table 1 ($3H_2SO_4$:H_2O_2:$2H_2O$) may deteriorate rapidly and must be freshly prepared. Bromine-methanol etches were quenched in methanol at the end of the action to prevent staining. All of the etches gave good polish finishes with the bromine-methanol etches giving the best finish. The bromine-freon etches were tried as a means of eliminating water from the process, but the etch rates were small and erratic and the use of this etch was therefore discontinued. It should be noted that the bromine-methanol etch rate appears to decrease with increase in temperature. It is thought that this anomaly was due to the loss of bromine from the etch as the temperature rose.

Samples cut with (111) faces exposed may be polished with an etch consisting of 1 HF : 3 HNO_3 : 2 H_2O.

Another very good etch, although it slightly differentiates the "A" and "B" faces, is the mixture 7 H_2SO_4:$1H_2O_2$:$1H_2O$ used at 80°C and quenched with H_2O. This etch also has the advantage that it does not deteriorate for several weeks if kept in the dark.

5.2 SELECTIVE ETCHING

Structure-sensitive etches were used to reveal dislocations, orientation and layer interfaces on pre-polished surfaces.

On the (100) faces, dislocations were revealed by applying, for two minutes, an etch consisting of 2 ml H_2O, 8 mg $AgNO_3$, 1 g CrO_3 and 1 ml HF. This was more satisfactory than using a mixture of HNO_3, HF and H_2O as a dislocation etch.

On the (111) faces, the etch 1 H_2SO_4: 1 H_2O_2 : 1 H_2O revealed dislocations. The following etches gave a more pronounced etch pit array on the "A" face than on the "B" face and hence may be used to determine face polarity, when necessary:

(a) Five minutes in 1 HNO_3: 3 H_2O;

(b) Five minutes in 1 HF : 1.5 H_2O_2 : 5 H_2O;

(c) One minute in 1 HNO_3: 3 H_2O: 1% of $AgNO_3$;

(d) One minute in 1 HF: 6 HNO_3: 10 H_2O;

(e) Approximately three minutes in 1 H_2SO_4: 1 H_2O_2: 1 H_2O;

(f) Approximately three minutes in 2 $HC\ell$: 1 HNO_3: 2 H_2O.

Etches a, b and c gave the best results. A typical result is shown in Figure 10.

For the delineation of the junction between an epitaxial layer and the substrate, it was necessary to find an etch sensitive to the small difference in chemical potential existing between the layers. The etch may be applied to a cleaved surface or, for greater accuracy, to a surface angle-lapped at approximately 5° to the plane of the junction (Figure 11). The sample was mounted, either with "Elephant wax" or glycol phthalate, onto the piston of the special angle-lapping tool. After lapping with 0.3 micron powder, the surface was washed and then stained (etched) with one of the following solutions:

(i) 3 HNO_3: 1 HF : 4 H_2O, for 20 to 30 seconds.

(ii) 5 $HC\ell$: 3 HF: 5 H_2O_2: 30 H_2O, for 3 minutes.

(iii) 1 HNO_3: 10 H_2O, for 2 minutes.

(iv) 1 HF: 1 H_2O_2: 10 H_2O, for 20 seconds.

None of these etches was very successful. The interfaces between the epitaxial layers and the substrates were poorly defined. When demarcation lines were observed, the calculated epitaxial layer thickness did not agree with the measurements made by an infra-red technique (ch. 4) or with the manufacturer's specifications. The etch technique was therefore not used to define epitaxial layers.

6. SAMPLE WASHING AND STORAGE

After etching, the sample must be carefully washed free of acids and metal ions. Approximately ten rinses in deionized water, followed by a rinse in a 5% KCN solution in water was sufficient to remove surface copper ions. This was followed by a further twenty rinses in 15 MΩ/cm water. The samples were stored submerged in alcohol for the short period preceding their use. In aqueous solution, alcohols have a reducing effect and hence minimize surface oxidation of samples stored in such a solution.

7. REFERENCES

1. Meiran, E.S., *Evaluation of Bulk and Epitaxial GaAs by Means of X-Ray Topography*, Trans. AIME 242, 413 (1968).

2. Reisman and Rohr, *Room Temperature Chemical Polishing of Ge and GaAs*, J. Electrochem. Soc., 1425 (1964).

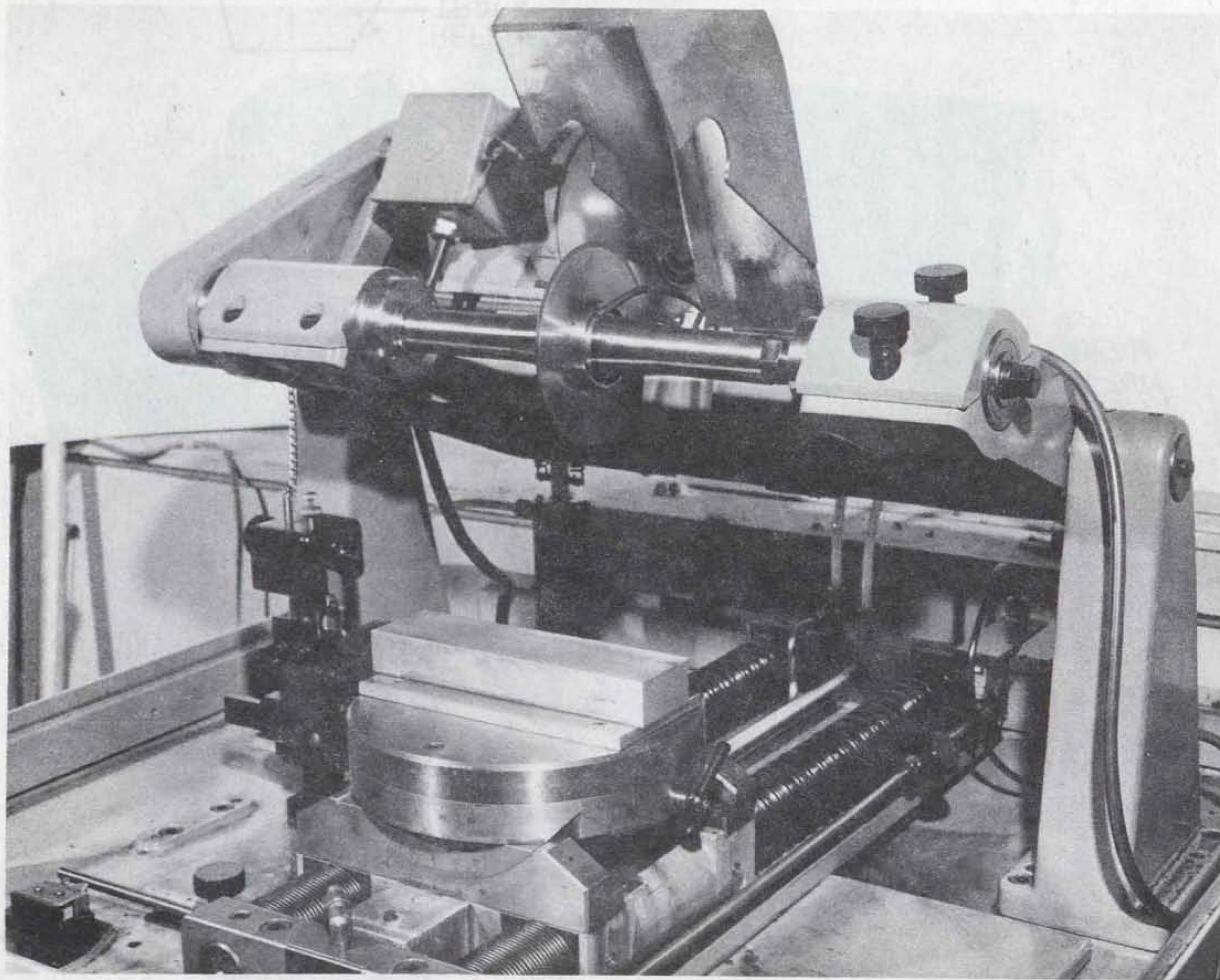

Figure 1. Diamond cut-off saw

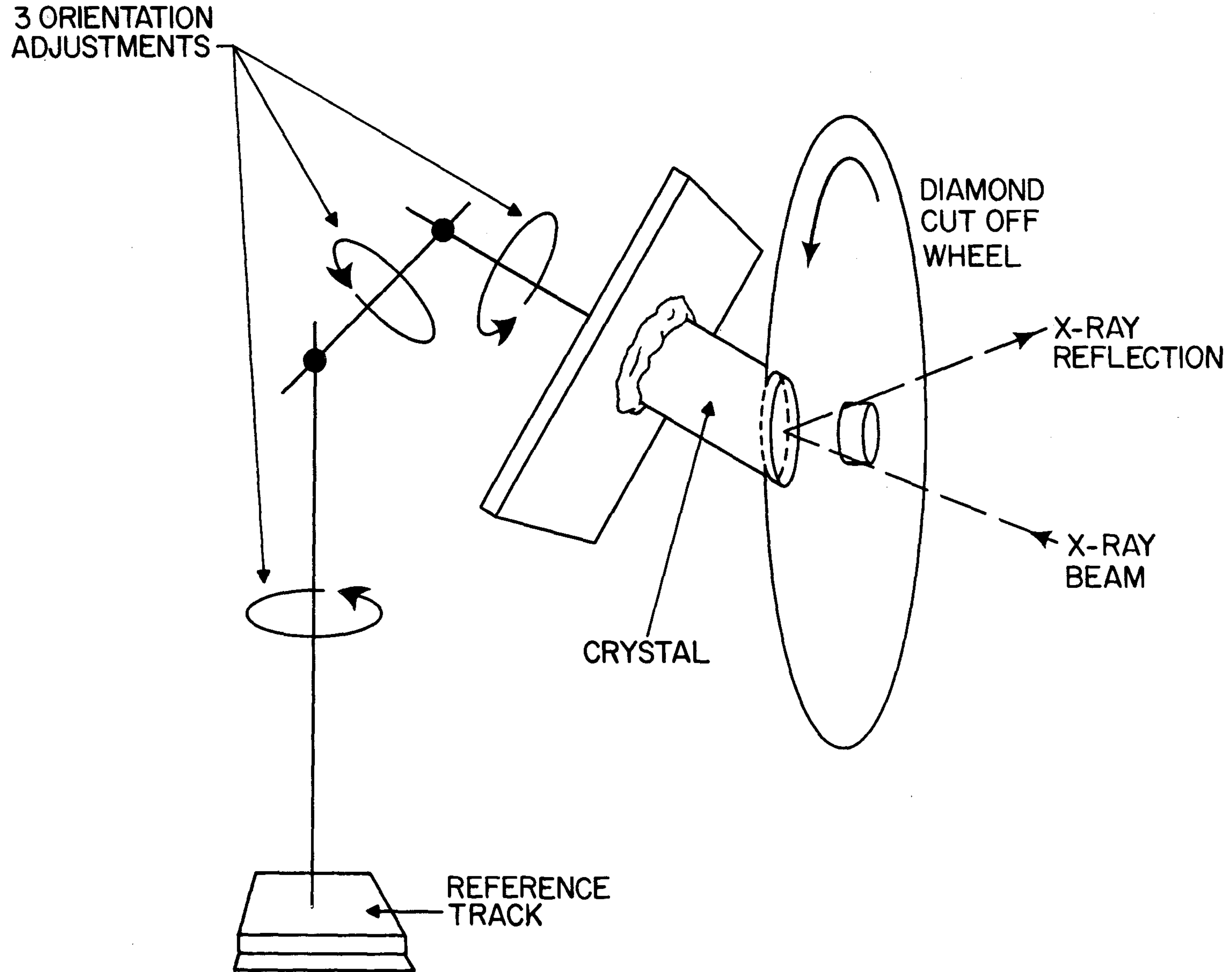

Figure 2. GaAs ingot mounted for wafer slicing, after X-ray orientation.

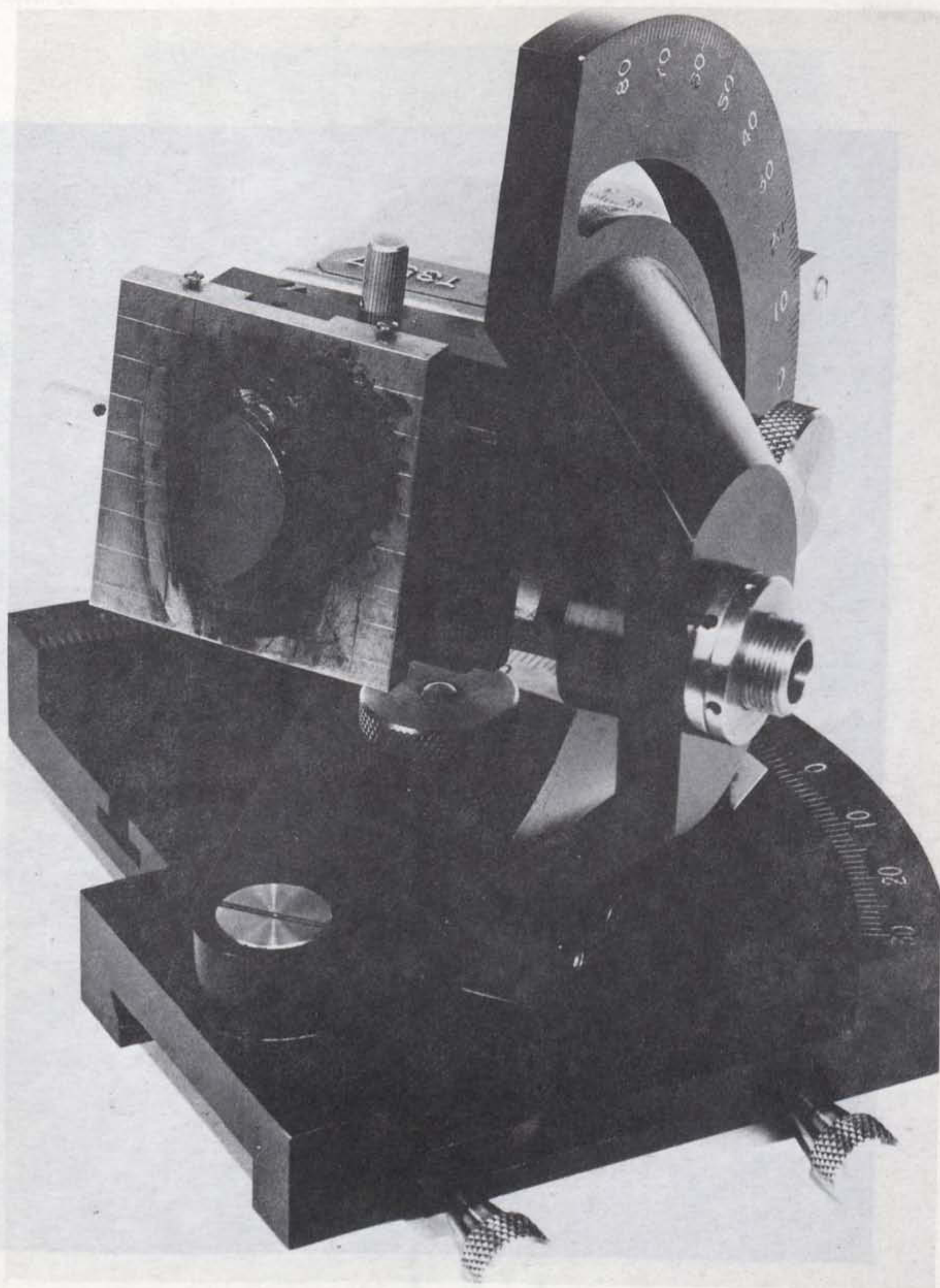

Figure 3. Jarrel-Ashe goniometer and jig for transfer of aligned crystal to the cut-off machine

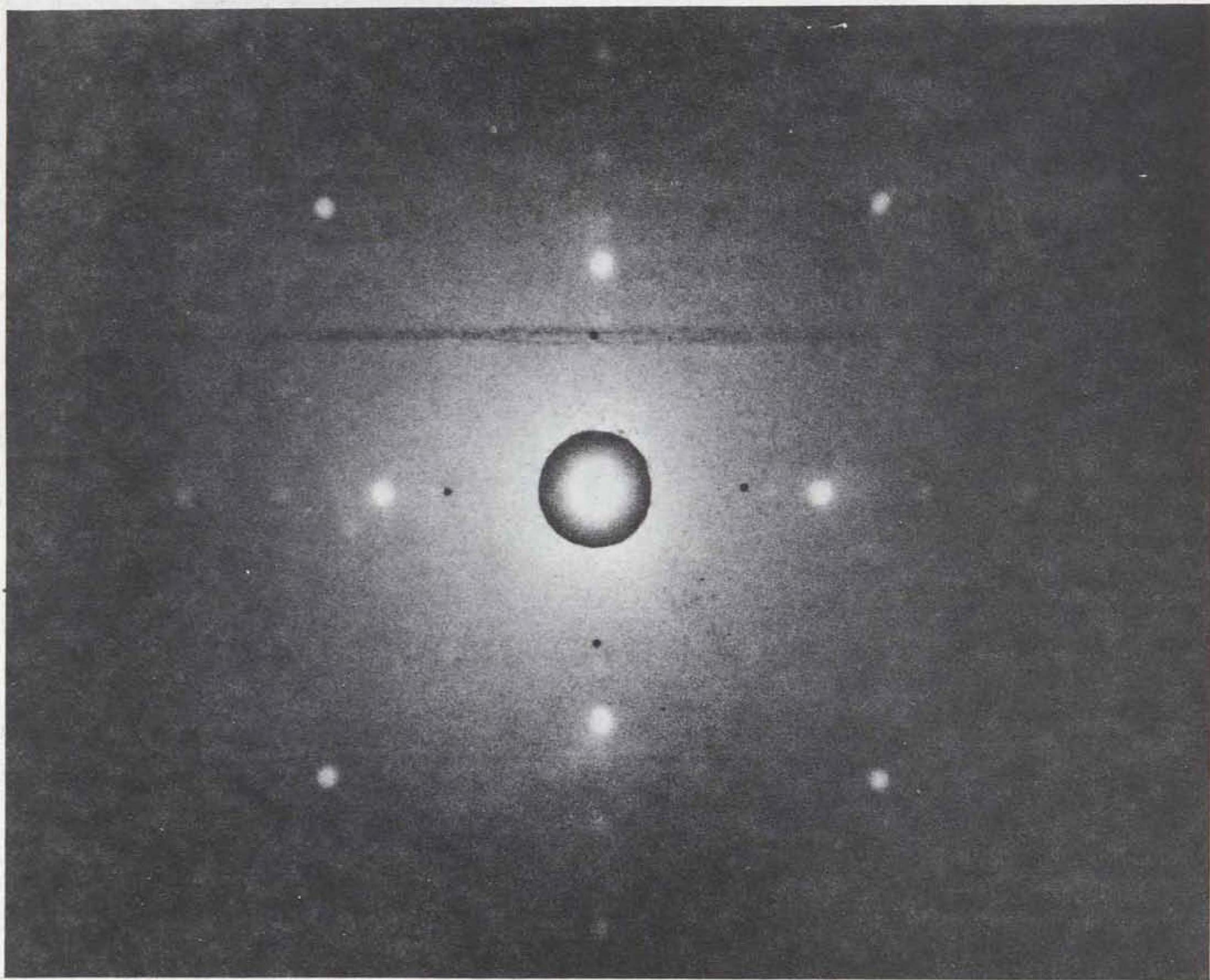

Figure 4. Laue pattern from the (100) plane of a GaAs crystal

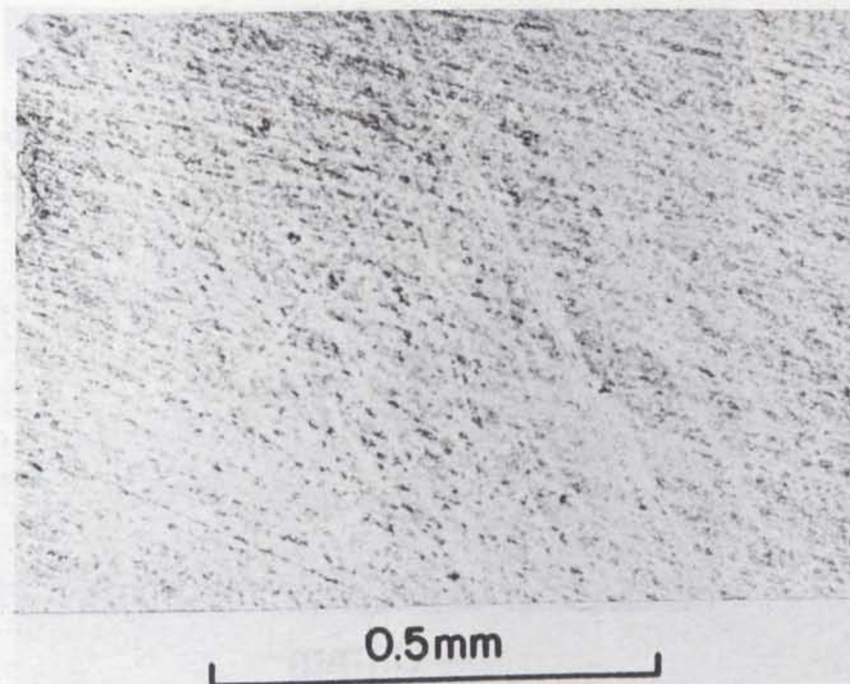

Figure 5. Surface finish of a GaAs wafer after lapping with 1 μm size grit

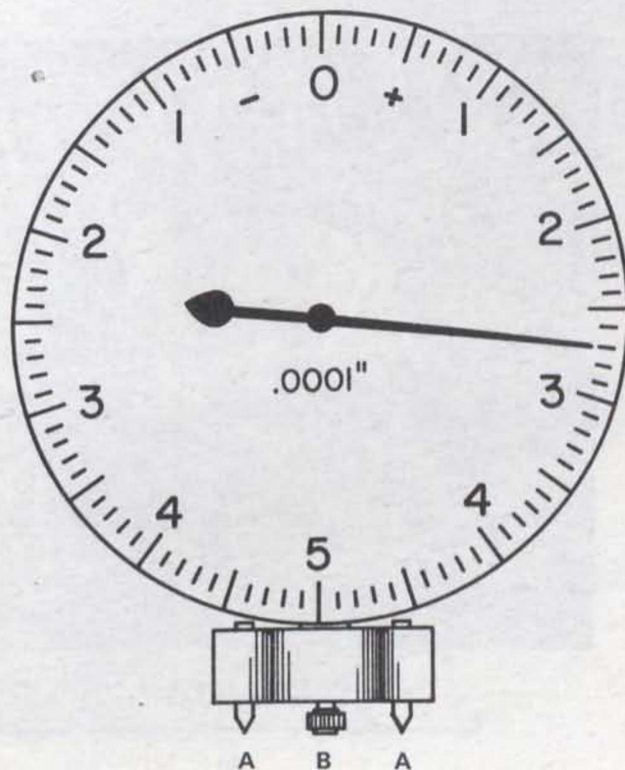

Figure 6. Dial gauge for wafer thickness measurement. The two feet labelled "A", straddle the sample which is placed on a flat surface and presses against piston "B".

(a)

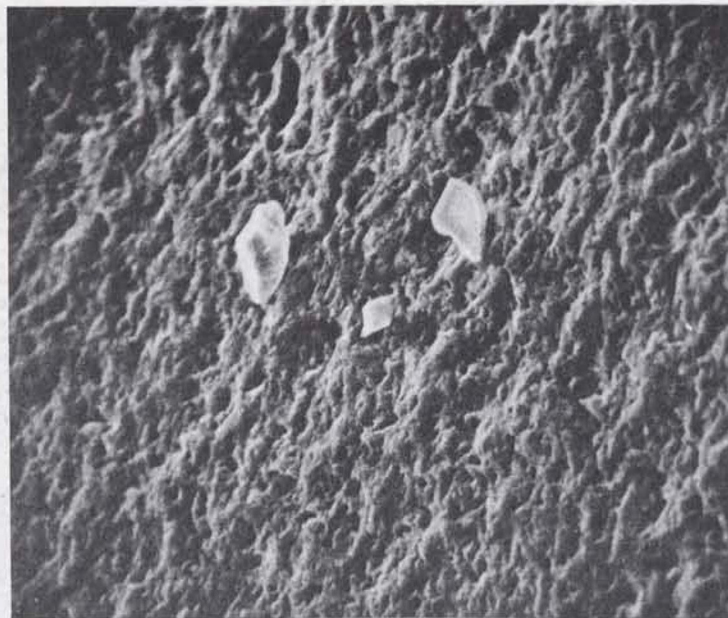

(b)

Figure 7. Scanning electron microscope micrographs of the surface of a GaAs wafer, showing particles left after lapping with 9 μm grit

Figure 8. Polishing machine

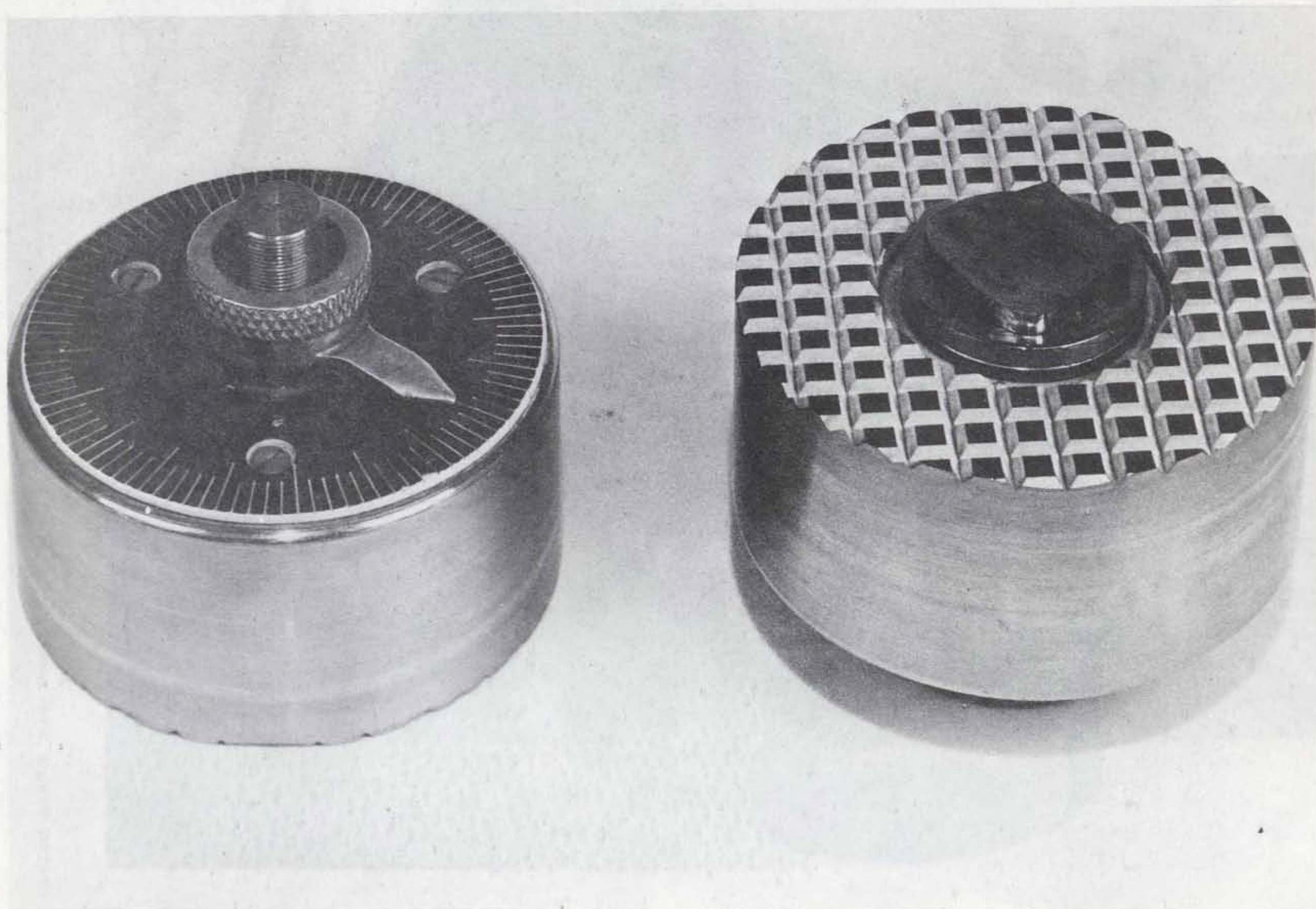

Figure 9. On the right-hand side is shown a single slice mounted on the piston of the lapping tool. At the left, a top view shows the calibrated piston.

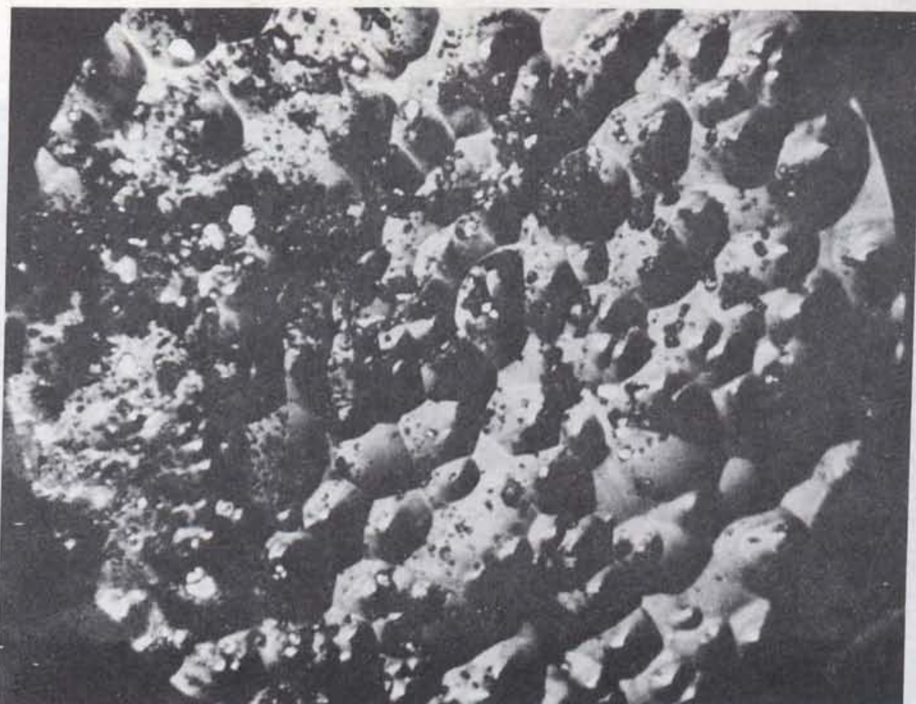

The "A" Face

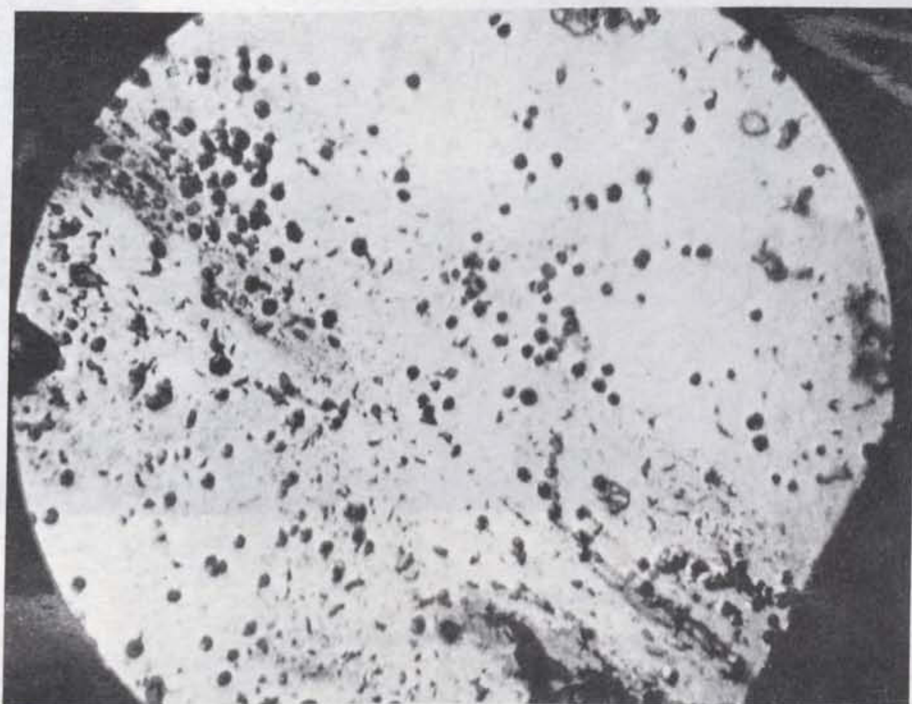

The "B" Face

Figure 10. Differentiation of the "A" and "B" (111) faces by etching

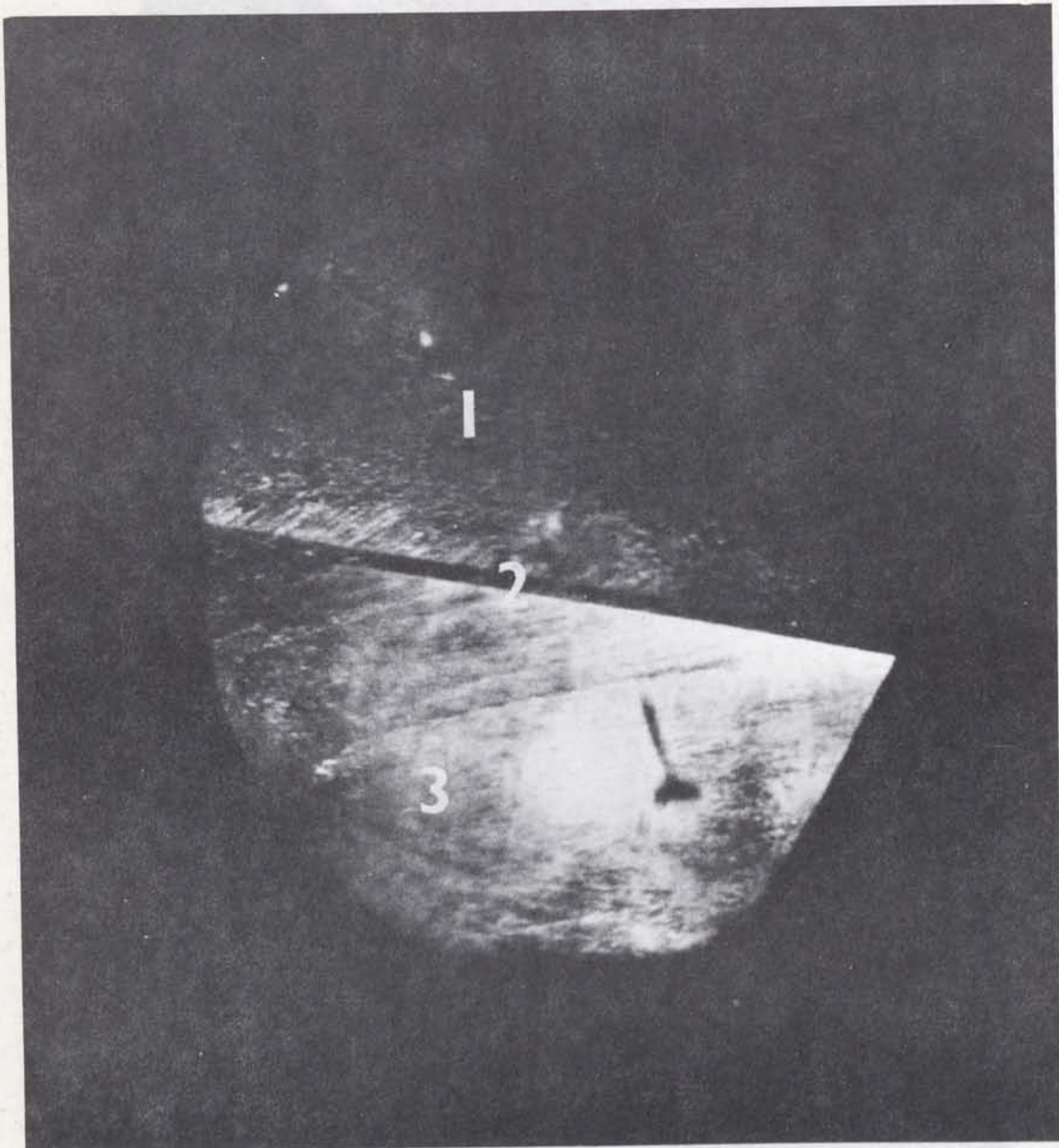

1. The ground substrate.
2. The ground and stained epitaxial layer.
3. The epitaxial layer.

Figure 11. Epitaxial layer of GaAs angle-lapped at 5° and then stained.

GALLIUM ARSENIDE MATERIALS AND DEVICES AND THE GUNN EFFECT

by

W.D. Edwards, W.A. Hartman, A.B. Torrens and D.L. Butler

PART 3

GALLIUM ARSENIDE VAPOUR EPITAXIAL GROWTH

by

W.A. Hartman

ABSTRACT

Epitaxial GaAs is grown on a n^+ substrate by the H_2-$AsCl_3$ method in a three-zone furnace, part of a system assembled at CRC. Etch-back is sometimes performed in the furnace to remove superficial damage. The microscopic or SEM examination of the layer obtained reveals defects such as pyramid growth. The lowest defect density obtained is $10(cm)^{-2}$. The doping values typically obtained are of the order of $10^{17}(cm)^{-3}$.

PART 3

GALLIUM ARSENIDE VAPOUR EPITAXIAL GROWTH

Bulk material of the required doping (of the order of 10^{15} $(cm)^{-3}$), mobility, and homogeneity, is especially difficult to produce. Also bulk gallium arsenide often contains deep traps which lead to a negative temperature coefficient of resistivity. Epitaxial material can be prepared with the more desirable positive temperature coefficient, better mobility and homogeneity[1]. It may also be laid down upon semi-insulating substrates and hence is ideal for integrated circuit applications[2]. The effort was therefore directed to the production of epitaxial material upon bulk material obtained commercially. The system which gave the earliest success was a vapour epitaxial method[3]. This is described here.

1. GENERAL DESCRIPTION

Vapour epitaxy is the chemical deposition, from the vapour phase onto a crystalline surface, of material whose lattice structure and orientation are essentially continuations of those of the substrate. In the case of gallium arsenide, one particular technique[4] has been most successful in producing high-purity epitaxial layers with high-mobility carriers.

A schematic diagram of the reactor used in this process is shown in Figure 1. Hydrogen, purified by palladium diffusion, is bubbled through arsenic trichloride, and then diluted with a hydrogen carrier stream. The mixture is next passed over pure gallium metal contained in a boat located in a three-zone furnace. In the first zone, arsenic forms by the reduction of the arsenic trichloride vapour by hydrogen, according to the equation:

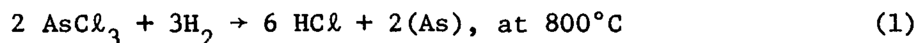

$$2\ AsC\ell_3 + 3H_2 \rightarrow 6\ HC\ell + 2(As),\ \text{at } 800°C \qquad (1)$$

The arsenic then combines with gallium to form GaAs. When the melt is completely saturated at the chosen temperature, a crust of gallium arsenide forms over the surface. The arsenic now flows downstream to condense on cooler parts of the system.

When this crust appears, the system is ready for epitaxial growth, which occurs in the second zone of the furnace. The arsenic trichloride flow is stopped, the prepared substrate material inserted into the furnace, and the arsenic trichloride re-started when the substrate is up to temperature. The gallium arsenide crust reacts with the arsenic trichloride according to the following equations:

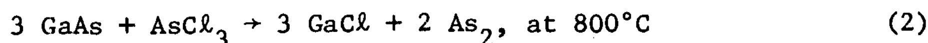

$$3\ GaAs + AsC\ell_3 \rightarrow 3\ GaC\ell + 2\ As_2,\ \text{at } 800°C \qquad (2)$$

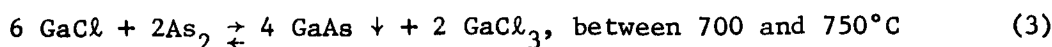

$$6\ GaC\ell + 2As_2 \rightleftarrows 4\ GaAs \downarrow + 2\ GaC\ell_3,\ \text{between 700 and } 750°C \qquad (3)$$

If the correct temperature distribution has been established, this leads to gallium-arsenide deposition on the prepared substrate.

2. APPARATUS AND MATERIALS

The open-tube flow system as shown in Figure 1 was chosen for this work. A three-zone diffusion furnace, with a 50 mm i.d. quartz reactor tube, was used; Figure 2 shows the furnace system in more detail.

A gas distribution system was assembled. It incorporated flowmeters to measure the main hydrogen flow, the $AsC\ell_3$: H_2 flow, and the flow in two other lines to be used for the doping of the grown layers. The growth system could be purged with ultra-high purity nitrogen or argon, or evacuated through a "molecular-sieve" filter. A palladium-diffusion hydrogen purification unit was installed in the hydrogen inlet line to the system.

The system was constructed with stainless-steel tubing and Swagelok* compression fittings of the same material up to the flowmeters. The valves were also of stainless steel and contained Viton A seals. The rest of the system, from the flowmeters to the reactor tube, was constructed of Pyrex glass with a limited number of shrinkable PTFE connectors and PTFE compression fittings for joints which required occasional dismantling. The entire system was made leak-proof with the aid of a helium leak-tester.

The reagents chosen were gallium (Eagle-Picher Industries, 99.99999% purity), arsenic trichloride (Asarco Intermetallics, 99.999% purity), and hydrogen (Matheson, ultra-high purity grade).

3. SUBSTRATE PREPARATION

Most of the growth attempts were made on semi-insulating (oxygen-doped) slices of (100) orientation obtained from Monsanto. Attempts number 8 and 9 were made with slices from a silicon-doped, n^+ ingot from Mining and Chemical Products, Ltd. The ingot was X-ray oriented and the slices cut 2° off the (100) orientation as explained in pt. 2. The lapping and polishing operations are also described in pt. 2. The substrates used for the first four attempts were polished sequentially with 1 and 0.3 micron powders. The rest were done chemo-mechanically, using sodium hypochlorite solution, which provided a better surface finish.

Immediately before growth, each substrate was lightly etched for about one minute in a hot (50°C) mixture of 3 H_2SO_4 : 1 H_2O: 1 H_2O_2, followed by at least 10 rinses with deionized water. To complex absorbed copper ions, the substrate was then soaked in 10% KCN solution for 5 minutes; this step was followed by further rinses in deionized water. The final step was a 30-minute wash in a Soxhlet apparatus using electronic-grade isopropanol[5].

4. GROWTH PROCEDURE

The gallium source (25 grams) was placed in a quartz "bucket" fixed to the end of a length of quartz tubing so that a thermocouple could be used to

* *Crawford Fittings Ltd., Niagara Falls, Ontario.*

monitor the source temperature. The quartz tube passed through an air-tight sliding seal to the outside of the furnace. Fresh gallium sources were initially saturated with gallium arsenide at 800°C. With a hydrogen flow of 100 ml/min through the $AsCl_3$, the saturation required about 50 minutes. Once saturated, a source was used for two or three growth attempts. Over the course of the experiments, three different gallium melts were used.

The substrates were either placed on a flat silica plate or held approximately vertical in slots in the plate, which was attached to a long quartz tube bearing a thermocouple. This tube was passed to the outside of the furnace in the same fashion as the tube on the gallium source; thus the position of the substrates could be changed during growth.

Before a growth or gallium source saturation, the system was flushed thoroughly with nitrogen, then purged with hydrogen for approximately an hour. The $AsCl_3$ bubbler was also flushed with hydrogen for several minutes.

The actual epitaxial growths, once a gallium source had been saturated, were carried out as outlined previously. To remove superficial damage a vapour etch, above 800°C, of the substrate was carried out in some instances (eq. 2). The etching was allowed to proceed for about 10 minutes with the normal flow of $AsCl_3 : H_2$, after which the substrate temperature was reduced to the growth temperature of about 750°C. The hydrogen flow rates used ranged (at n.t.p.) from 125 to 420 cm^3/min, of which about 100 cm^3/min flowed through the $AsCl_3$ bubbler. A summary of the growth attempts is given in Table 1. In attempts 1 to 5 the substrates were placed flat on the substrate holder; for the other growths, they were approximately vertical, with the growth surface perpendicular to the gas flow.

TABLE 1

Summary of GaAs Vapour Epitaxial Growth Attempts

Attempt Number	Substrate Number	$AsCl_3/H_2$ Flow (cm^3/min)	Total H_2 Flow (cm^3/min)	Vapour-etched Prior to Growth (min)	Growth time (min)
1	69/4/12	100	420	4	75
2	69/4/11	110	280	10	60
3	69/4/9/1	50	125	10	60
4	69/4/9/2	110	280	10	60
5	69/6/1	110	280	0	60
6	69/6/2/1	50	190	0	75
7	69/6/3/2	50	210	0	60
8	69/7/2/1	50	210	0	30
9	69/7/1/7	60	130	0	60

Gallium source temperature for all attempts: 800°C.
Substrate temperatures for growth: ~750°C.
Volumes measured at n.t.p., i.e. at 20°C and 1 atmosphere.

5. QUALITY OF THE LAYERS GROWN

At this stage in the project, methods of assessing the properties of the layers were limited. Because of the difficulty in obtaining consistent ohmic contacts and satisfactory Schottky barriers, only a few CV measurements to determine layer doping levels were made. Also, the standard method[6] of cleavage and chemical etching to delineate the junction between the substrate and an epitaxial layer could not be made to work consistently (sec. 5.2 of pt. 2). Thus, in most cases, the thickness of any layer grown could not be accurately determined.

Microscopic examination of the surfaces of all the growth attempts was made with both an optical microscope and a scanning electron microscope. A photographic record of the surface features, such as growth pyramids, was made for each substrate.

Growth attempts 2, 3, and 4 were the most successful. The layers were uniform with a bright, reflective surface. The surfaces had an overall gently hilly finish with some growth pyramids and other defects (Figure 3). Substrate 69/4/9/1 had very many of these defects, while 69/4/9/2, which was the best of all the layers, had fewer than ten per cm^2 (Figure 4). The doping levels of 69/4/11 and 69/4/9/2 were found by CV techniques to be $(1.0 \pm 0.5) \times 10^{17}$ and $(3.3 \pm 0.5) \times 10^{17}$ cm^{-3} respectively.

The layer on 69/6/1 had a dull finish, and the surface was covered with very fine, almost geometrically-regular projections or pits. Some large defects were present, with what appear to be particles of foreign matter at their centres (Figure 5).

A uniform layer, similar to that of 69/4/11, was obtained on substrate 69/6/3/2.

Growth attempts 6 and 8 resulted in patchy layers. The very rough growth on 69/6/2/1 is shown in Figure 6. A SEM photograph of sample 69/7/2/1 examined in the cathodoluminescent mode shows white areas where the luminescent n^+ substrate was not covered by the layer (Figure 7).

There did not appear to be any growth on substrates 69/4/12 and 69/7/1/7.

6. CONCLUSIONS

A facility for the vapour epitaxial growth of GaAs has been built and used successfully to grow layers with physical features similar to those reported by others[4,7]. Preliminary measurements put the doping levels of these layers at approximately $10^{17}cm^{-3}$. This is higher than the 10^{14} to $10^{15}cm^{-3}$ levels which are required for the production of Gunn-effect devices.

Further work is required to determine the correct conditions (gas flow rates, $AsC\ell_3$ partial pressure, substrate temperature, etc.) for growth of high-quality layers. This would also require that proper methods for evaluating the layers be developed.

Some improvements to the reactor system were suggested by the preliminary results. These were an improved $AsCl_3$ bubbler design, and the use of a large-bore (35 mm) stopcock to separate the growth portion of the furnace tube from a forechamber as described by Tietjen and Amick[8]. This chamber could then be purged separately with hydrogen before insertion of the substrates into the furnace. Contamination of the growth region during insertion and withdrawal would then be minimized, and the furnace tube could be kept always isolated from the atmosphere. However, the project was terminated before these improvements could be incorporated.

7. REFERENCES

1. Berson, B.E., and S.Y. Narayan, *L Band Epitaxial Gunn Oscillators*, Proc. IEEE, 55, 1078 (1967).

2. Mause, K., *Simple Integrated Circuit with Gunn Devices*, Electron. Lett. 8, 62 (1972).

3. Knight, J.R., D. Effer and P.R. Evans, *The Preparation of High Purity Gallium Arsenide by Vapour-Phase Epitaxial Growth*, Solid State Electron. 8, 178 (1965).

4. Effer, D., *Epitaxial Growth of Doped and Pure GaAs in an Open Flow System*, J. Electrochem. Soc. 112, 1020 (1965).

5. Steward, C.E.E., *Preparation of GaAs Surfaces for Epitaxial Deposition*, Solid-State Electron. 10, 1199 (1967).

6. Herzog, A.H., *Measuring Epitaxial Layer Thickness of Gallium Arsenide Wafers by Cross Section Staining Destructive*, Semicond. Products, 5, 25 (December 1962).

7. *Proceedings of the International Symposium on GaAs*, The Institute of Physics and the Physical Society, London, 1967:

   a. Eddols, D.V., J.R. Knight, and B.L.H. Wilson, *The Preparation and Properties of Epitaxial Gallium Arsenide*, 3

   b. Shaw, D.W., R.W. Conrad, E.W. Mehal and O.W. Wilson, *Gallium Arsenide Epitaxial Technology*, 10

   c. Bolger, D.E., J. Franks, J. Gordon, and J. Whitaker, *Preparation and Characteristics of Gallium Arsenide*, 16.

8. Tietjen, J.J., and J.A. Amick, *The Preparation and Properties of Vapour: Deposited Epitaxial $GaAs_{1-x}P_x$ Using Arsine and Phosphine*, J. Electrochem. Soc. 113, 724 (1966).

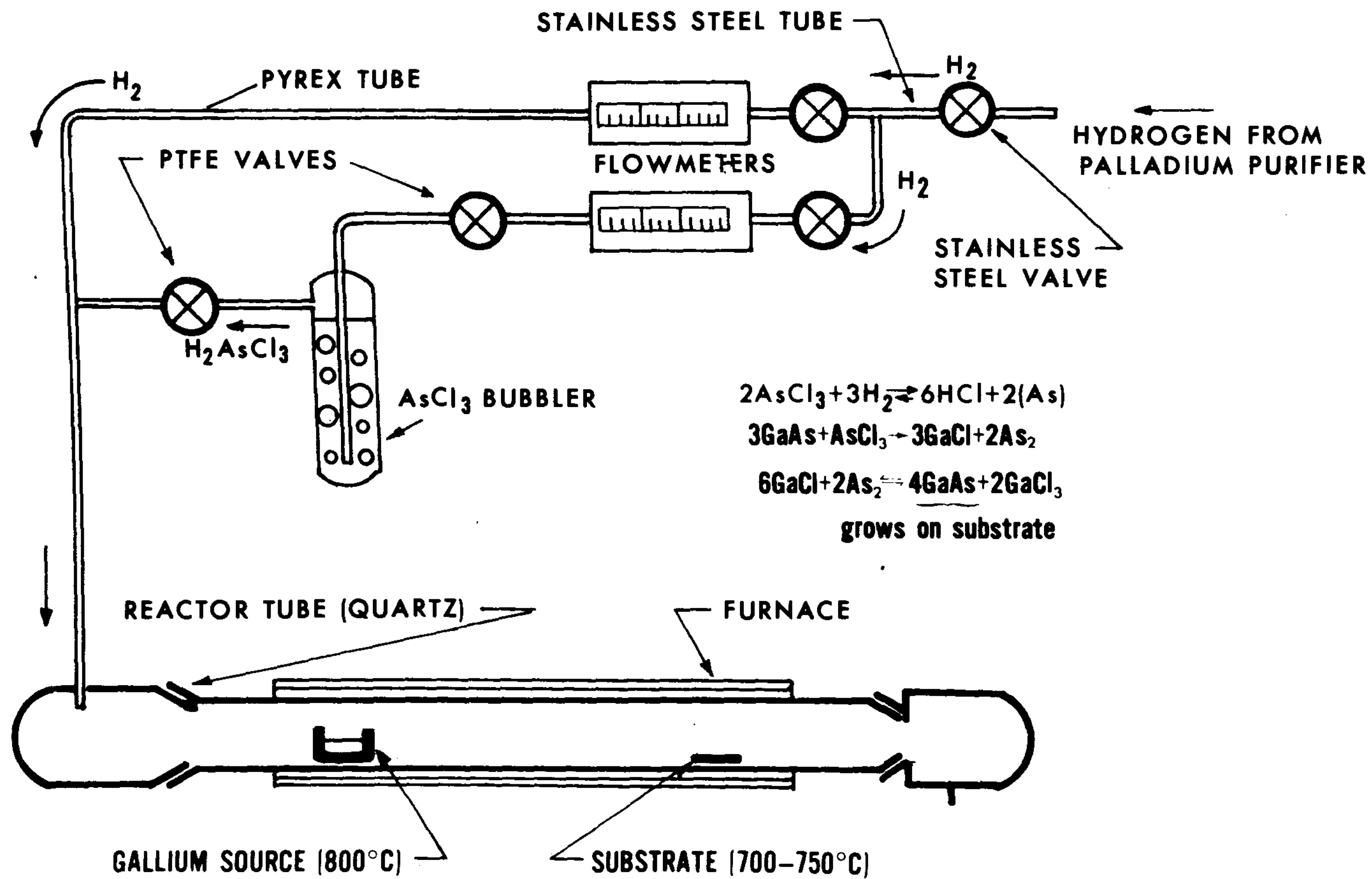

Figure 1. Gallium-arsenide vapour-phase epitaxial reactor

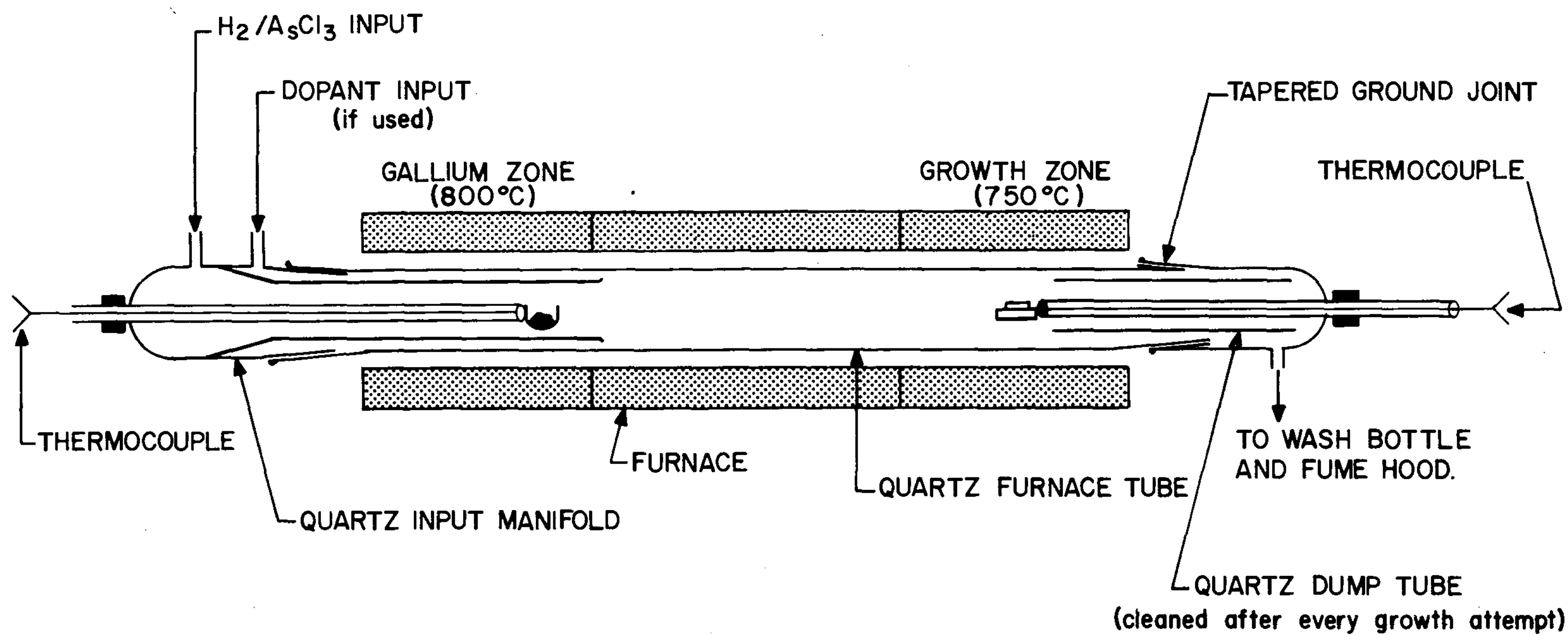

Figure 2. Detail of the epitaxial reactor

(a) SEM micrograph (emissive mode) of growth pyramid

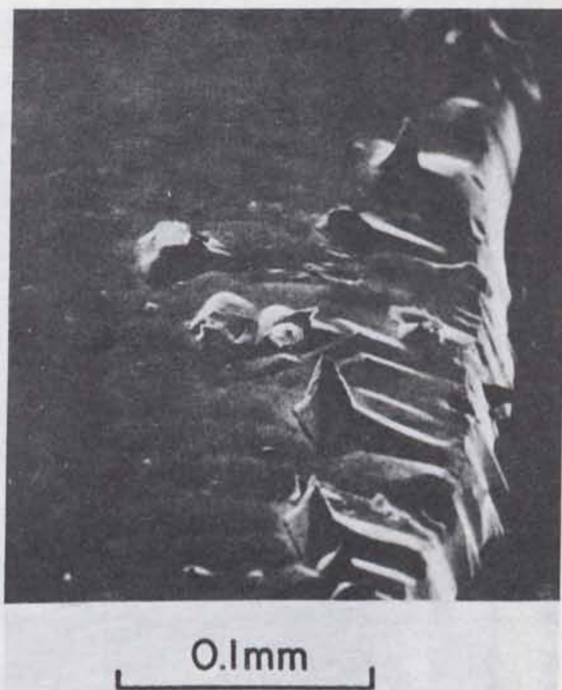

(b) SEM micrograph of edge of substrate

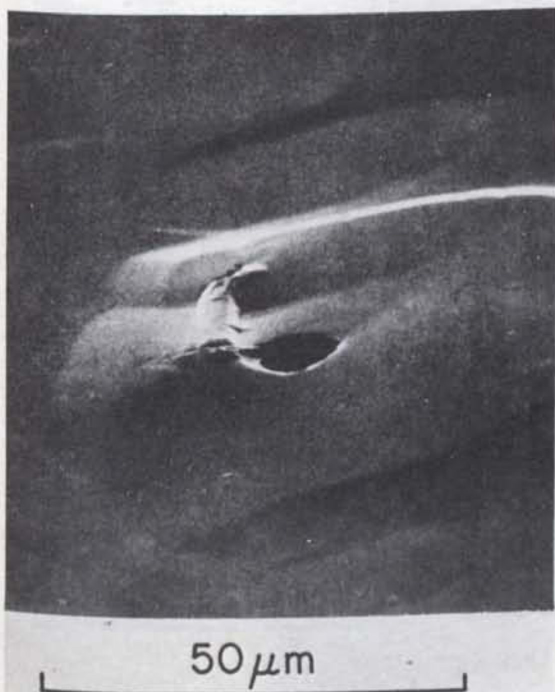

(c) Surface feature

(d) Optical photomicrograph showing surface finish

Figure 3. Surface detail of epitaxial growth on substrate 69/4/11

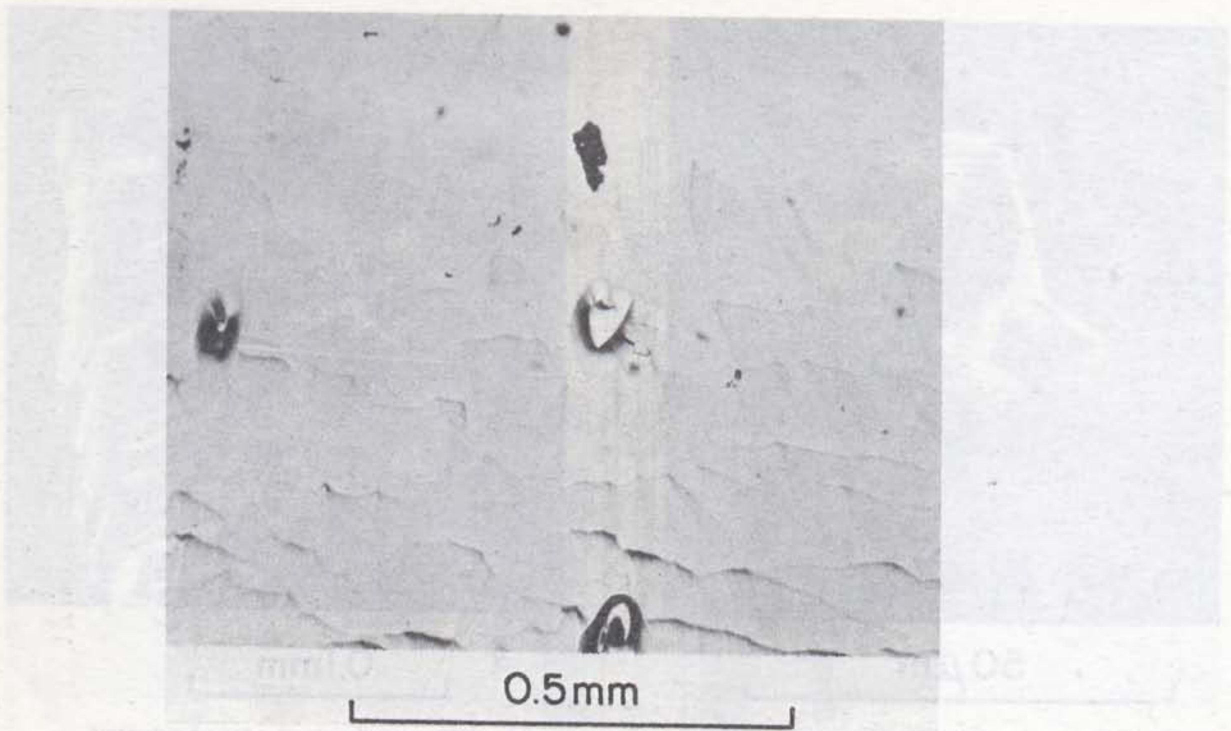

(a)

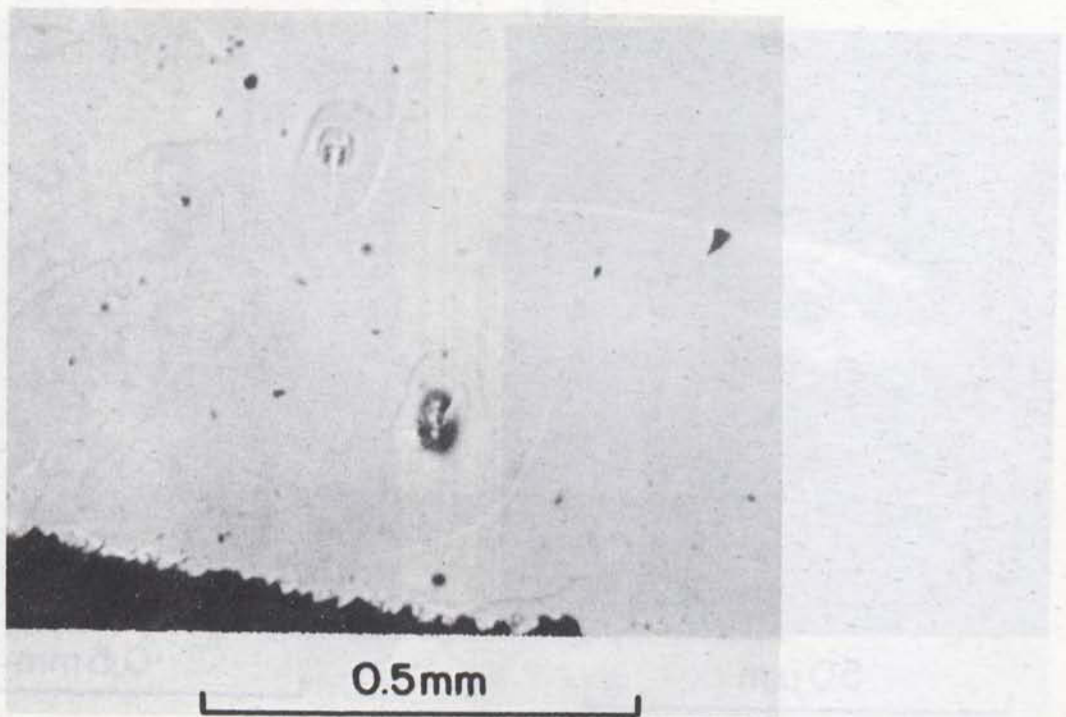

(b)

Figure 4. Growth pyramids and surface detail of 69/4/9/2

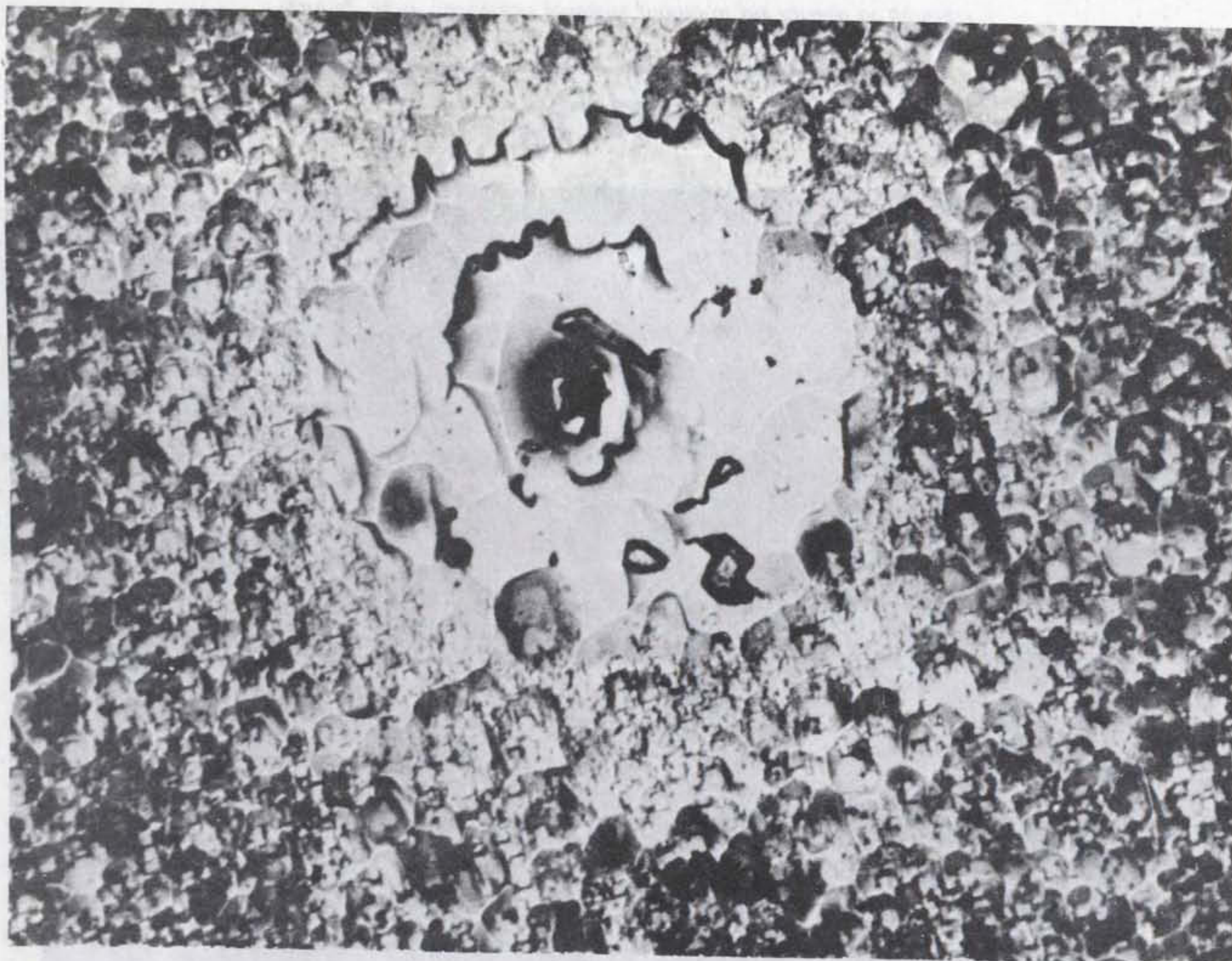

0.5mm

Figure 5. Typical surface feature of 69/6/1

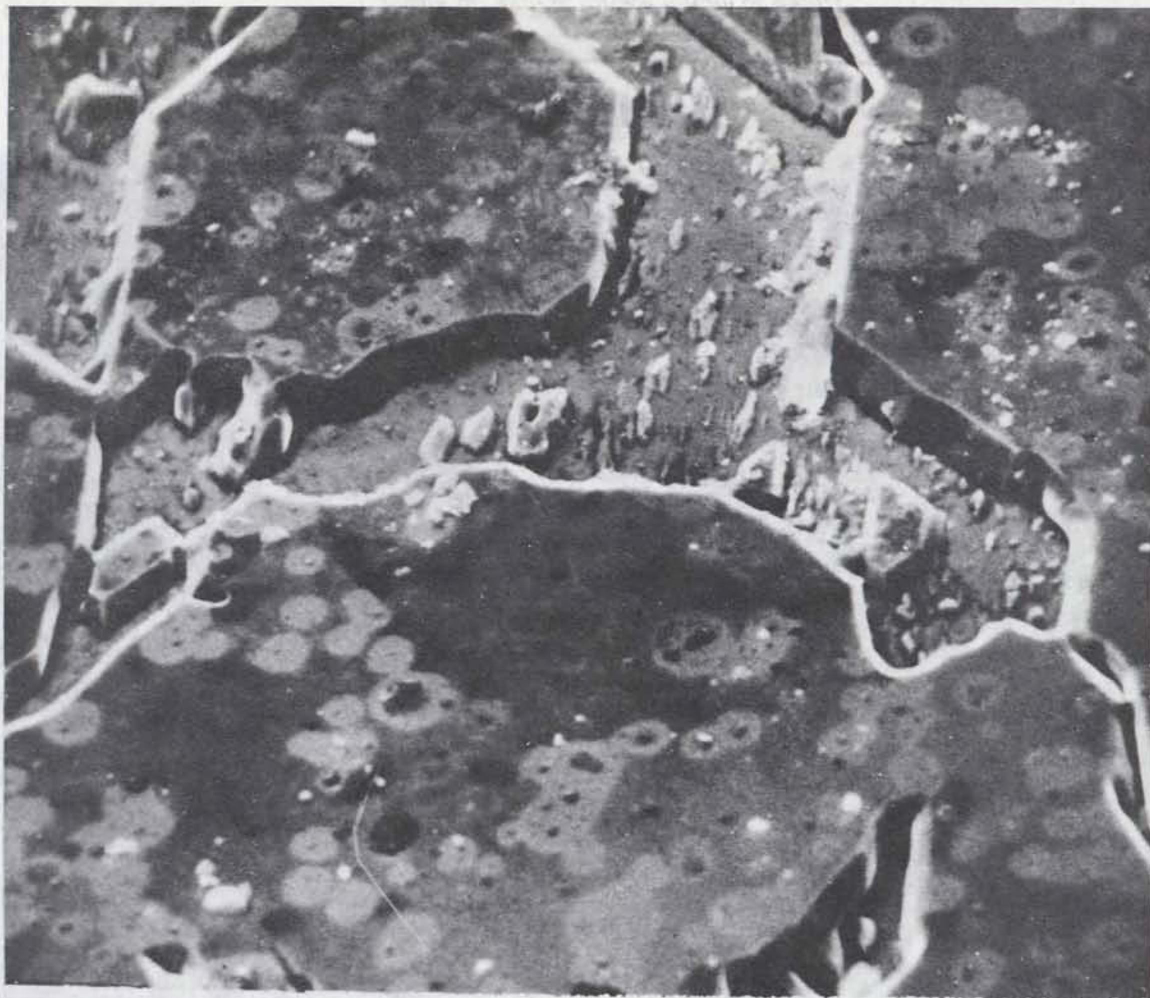

Figure 6. SEM micrograph (emissive mode) of the surface of 69/6/2/1

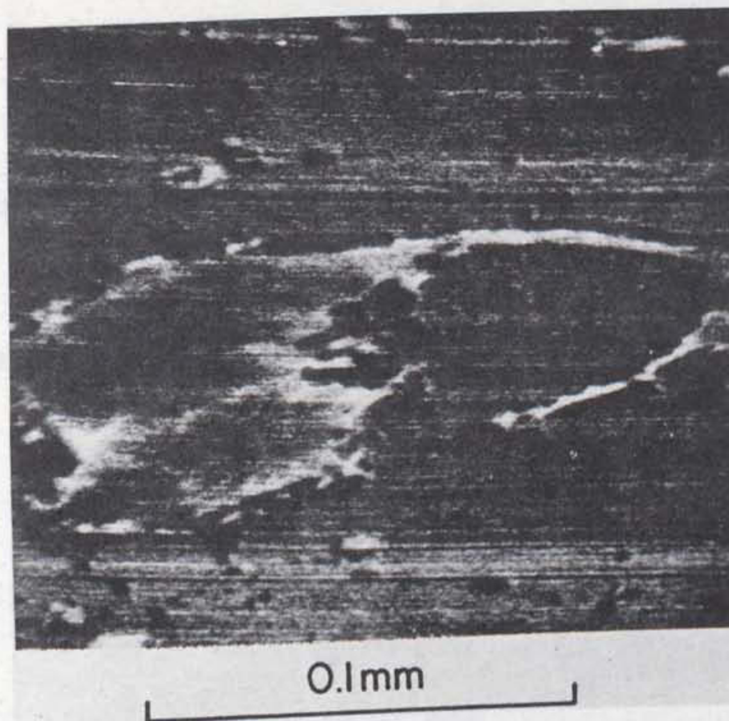

(a) cathodoluminescent mode

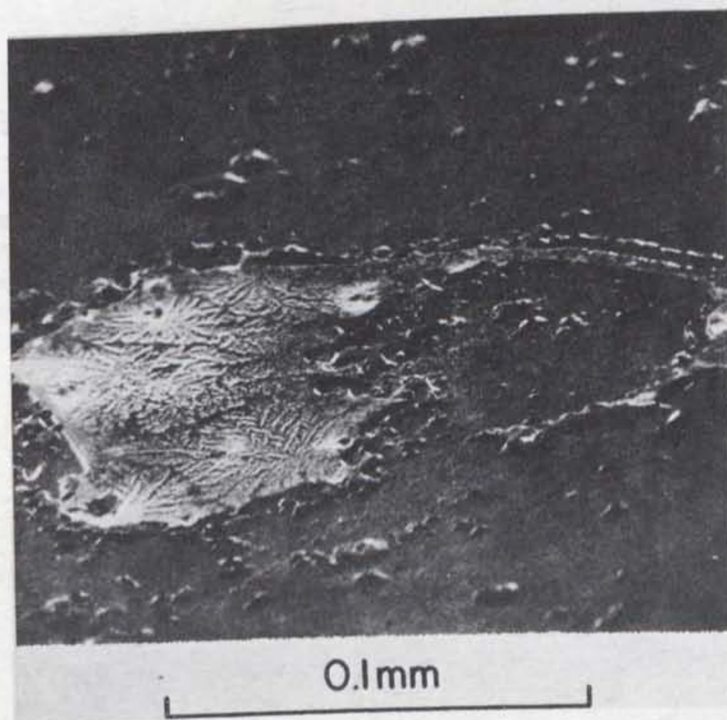

(b) emissive mode

Figure 7. SEM micrographs of surface of 69/7/2/1, showing incomplete coverage of substrate

THIS PAGE INTENTIONALLY LEFT BLANK

GALLIUM ARSENIDE MATERIALS AND DEVICES AND THE GUNN EFFECT

by

W.D. Edwards, W.A. Hartman, A.B. Torrens and D.L. Butler

PART 4

MATERIAL ASSESSMENT

by

W.D. Edwards and D.L. Butler

ABSTRACT

The thickness of epitaxial layers is measured by an infra-red interferometric method with a grating spectrophotometer. The resistivities and carrier mobilities of materials are measured by the Hall method, from -190°C to +100°C on automatic equipment. A Schottky-barrier capacitance measurement technique is used to obtain the doping profiles of samples, and reveals the existence of a lower-conductivity layer at the nn^+ interface.

PART 4

MATERIAL ASSESSMENT

The sample preparation processes were assessed optically and with a scanning electron microscope. It was assumed that the most desirable surface was a highly polished, optical flat with no visible blemishes under a magnification of 100. A typical surface finish after mechanical polishing is shown in Figure 1. After chemical-mechanical polishing, approximately 300 structural blemishes/cm^2 could be seen when viewed under a magnification of 100. Epitaxial materials obtained from outside sources were examined to establish a set of judgement criteria. A wide latitude in surface finish on epitaxial samples supplied was found as shown in Figure 2. These are to be compared with a CRC epitaxial finish shown in Figures 3 and 4 of ch. 3.

1. EPITAXIAL-LAYER THICKNESS MEASUREMENT

The thickness of an epitaxial layer may be measured by angle lapping and chemical delineation (staining). This is a destructive method and the technique was described in sec. 5.2 of pt. 2.

The infra-red interference method as described by Groves[1] was adapted to the non-destructive thickness-measurement of epitaxial gallium arsenide layers. In this work, the technique was applied to lightly-doped n-type layers on highly-doped n^+ substrates. A Perkin-Elmer 337 grating infra-red spectrophotometer and a Beckman microreflectance attachment were used for these measurements. Spectral scans from 8.0 to 25.0 microns wavelength were made of the radiation reflected by the epitaxial layer of a sample in the microreflectance attachment. From the interference pattern of intensity maxima and minima, the thickness of the layer can be calculated.

A detailed outline of the theory involved is given by Groves[1]. For the case of an undoped or lightly doped (about 10^{17} carriers per cm^3) epitaxial layer on a heavily-doped n-type substrate, the thickness L is given by:

$$L = 0.153\ m/\gamma_m \qquad (1)$$

where m is the order of the maximum or minimum wavenumber γ_m. The quantity m/γ_m is essentially constant in the range 2µm to 16µm.

A sample fringe spectrum and calculations are shown in Figure 3. The following procedure is used for calculating the thickness:

(i) Values of γ_m, the wavenumbers at which maxima and minima occur in the spectrum, are estimated.

(ii) To index the maxima and minima:

(a) Select a low-order (low-frequency) maximum, γ_m, and a high-order maximum, γ_{m+x}. The number of cycles between γ_{m+x} and

γ_m is x. In Figure 3,

$$\gamma_m = 575 \text{ cm}^{-1},$$

$$\gamma_{m+x} = 790 \text{ cm}^{-1},$$

$$x = 1.$$

(b) $m \approx \dfrac{x \cdot \gamma_m}{\gamma_{m+x} - \gamma_m}$

m = order of peak at γ_m, usually a half odd integer, (i.e., 1/2, 3/2,....,etc.)

In Figure 4, x = 1, and m = 790 - 575 ≈ 2.5

(iii) Index the other maxima and minima in order, with an interval of 1/2, the higher orders corresponding to higher frequencies (see second row of numbers in Figure 3, labelled m).

(iv) Tabulate the quotients m/γ_m. These should be nearly constant. The m/γ_m values in Figure 3 have been converted to microns.

(v) Average the values of m/γ_m to obtain $\overline{m/\gamma_m}$, which is in eq. 1 to give the thickness. For the example of Figure 3,

$$L = 0.153 \times 43.6 \ \mu m = 6.7 \ \mu m$$

The manufacturer's value of thickness for the layer on this wafer (CRC 5) is 7.1 μ.

From the measurements that have been made, this method appears capable of resolving thickness differences of approximately 0.5 μm.

2. RESISTIVITY AND DOPING MEASUREMENTS

A single-probe method of resistivity measurement[2] was tried. At the doping levels of interest here, less than $10^{16}/cm^3$, the method was of little use as the scatter in the resistivity values was excessive.

The four-probe method of resistivity measurement[3] was also found to be unsuitable for the gallium arsenide of interest. The two alternate methods used were destructive, considerably more time-consuming, and involved several process steps.

Simple in principle, but time-consuming, is the preparation from the material of interest, of either a parallelepiped-shaped sample or a Van der Pauw sample[4], (Figure 4a,b) of known dimensions. The sample is prepared as

described earlier in pt. 2. Contacts are either evaporated or alloyed directly onto the samples. After alloying the contacts with one of the developed processes (pt. 5), the sample is measured geometrically and electrically. In the case of the parallelepiped-shaped sample, a simple calculation gives the resistivity from $\rho = RA/L$. The arbitrary shape of the Van der Pauw sample requires a more sophisticated formula:

$$\rho = \frac{\pi\ Lf}{2\ \ln 2}\left(R_{AB.CD} + R_{BC.DA}\right) \quad ,$$

where L is the sample thickness, $R_{AB.CD}$ a resistance given by the potential difference between contacts C and D when a current flows through contacts A and B, and f is a function which depends on the ratio $R_{AB.CD}/R_{BC.DA}$.

A measurement of resistivity alone gives the product of n, the carrier density, and μ, the carrier mobility. The methods just described give resistivity values. The sample shapes shown in Figure 4 may be used to measure the Hall coefficient, $R_H = \alpha/nq$ where α is a factor near unity and q the electron charge. The measurements are made in a magnetic field over a wide range of temperature, e.g., -190°C to +100°C.

An automatic measurement system was constructed. Essentially the instrument is an auto-ranging voltmeter (Vidar). Voltages proportional to sample currents, the temperature, magnetic field, etc., are selected every few seconds by an input scanner. The digital voltmeter measures the signals and the output is taken through a coupling unit to a paper-tape punch. The sample is cooled to liquid nitrogen temperature and allowed to warm up. A specially-built controller selects the other sample operating conditions: current, current direction, magnetic field magnitude and direction. Computer programs were written so that the paper-tape information could be presented in tabular and graphical form.

An alternative method of measuring the resistivity depends upon the fabrication of a Schottky barrier upon a piece of material adjacent to that of interest. The capacitance of such a barrier is related to the majority-carrier distribution by[5]:

$$n = \frac{-C^3}{\varepsilon e A^2}\left(\frac{dC}{dV}\right)^{-1}$$

where n(x) is the carrier concentration at the distance x from the surface, C the differential capacitance, ε the semiconductor permittivity, V the voltage applied to the barrier, and A the contact area.

A thin molybdenum mask was made such that small (0.25 in diameter) dots of gold could be deposited upon the gallium arsenide to form Schottky barriers. An ohmic contact, formed by one of the methods described in pt. 5, had to be applied to the sample prior to the evaporation of the Schottky barrier. A small tin dot was used on the end of the measuring probe to avoid damage to the fragile Schottky-barrier contact.

Capacity vs. applied voltage values were obtained with a Boonton 71 A-F capacity meter. Initially, the results were taken manually and, later, pro-

vision was made to sweep the voltage and to record the capacity on an xy recorder. A computer program was written to calculate dC/dV values from the sequential experimental values and finally the corresponding values of n vs. depth.

A representative computer plot is shown in Figure 5 for a vapour-grown epitaxial layer. Over a depth range of about 50 nm, the doping is less than $10^{17}(cm)^{-3}$. This type of lower-conductivity layer occurs fairly often in GaAs epitaxy[6,7].

3. CONCLUSIONS AND SUMMARY

Facilities, including an automatic Hall system, were established and techniques mastered for the measurement of bulk and epitaxial material properties. Surface finish, epitaxial-layer thickness, impurity concentration and Hall coefficient were measured.

4. REFERENCES

1. Groves, W.O., *Measurement of Thickness of Gallium Arsenide Epitaxial Films by the Infrared Interference Method (Non-Destructive)*, Semicond. Products 5, 25 (December 1962).

2. Frank, H., and S.A. Axim, *Measurement of Diffusion Profile on Zu in n-type GaAs by a Spreading Resistance Technique*, Solid-State Electron. 10, 727 (1967).

3. Edwards, W.D., and A.L. Barry, *Circuit to Facilitate the Measurement by Four-Probe Method of the Resistivity*, J. Sci. Inst. 39, 119 (1962).

4. Van der Pauw, L.J., *A Method of Measuring Specific Resistivity and Hall Effect of Disc of Arbitrary Shapes*, Philips Res. Rep. 13, 1 (1958).

5. Schottky, W., *Simplified and Expanded Theory of New Semiconductor Components*, Z. Phys. 118, 539 (1942).

6. Harris, J.S., Y. Nannichi and G.L. Pearson, *Ohmic Contacts to Solution Grown Gallium Arsenide*, J. Appl. Phys. 40, 4575 (1969).

7. Saito, T., and F. Hasegawa, *Cause of the High Resistance Region at Vapour Epitaxial GaAs Layer Substrate Interface*, J. Appl. Phys. 10, 197 (1971).

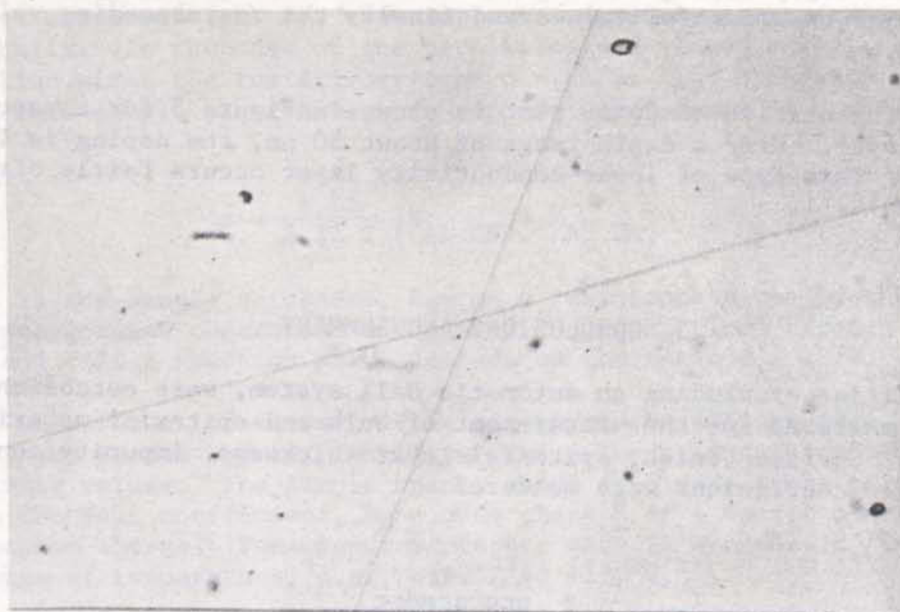

0.5 mm

(a) Normal illumination

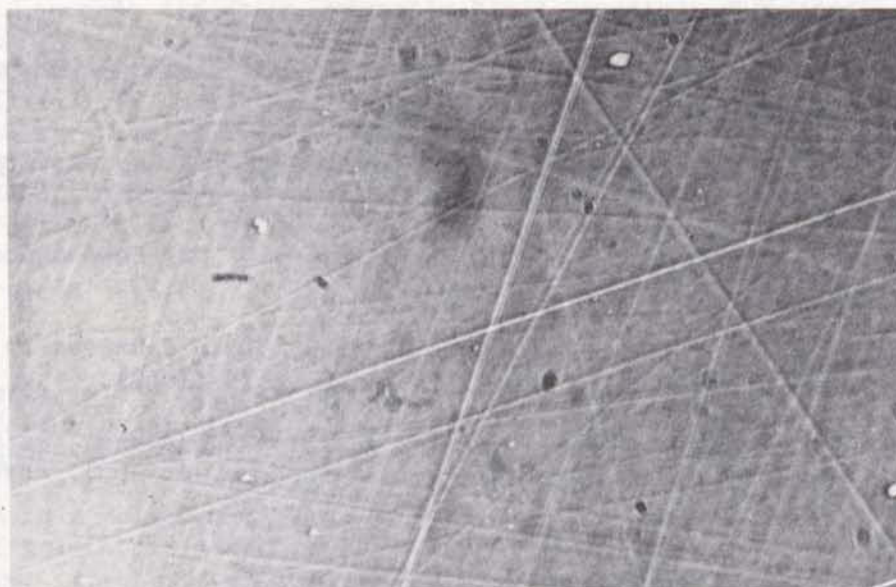

0.5 mm

(b) Phase contrast

Figure 1. Typical surface finish obtained on GaAs with a 1 μm aluminum–oxide grinding powder

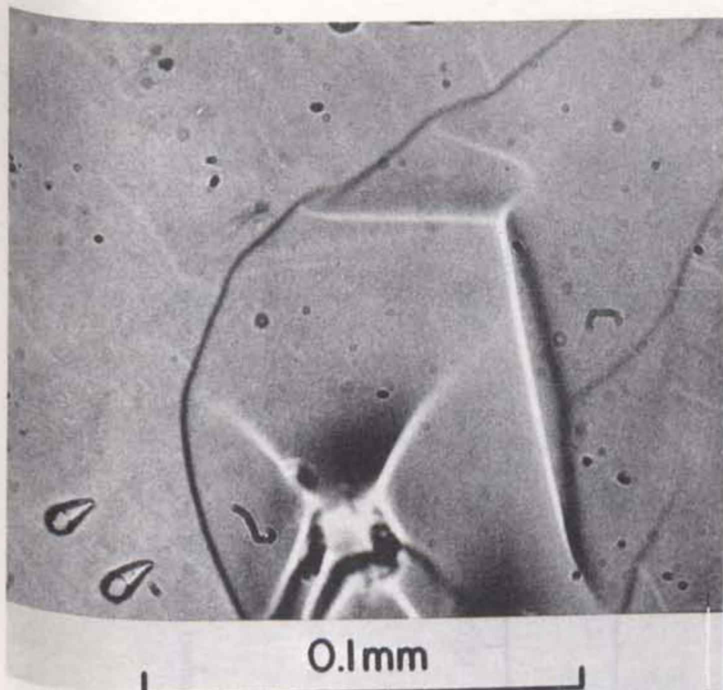

(a) Mullard Research Co. epitaxial ($n - n^+$) layer

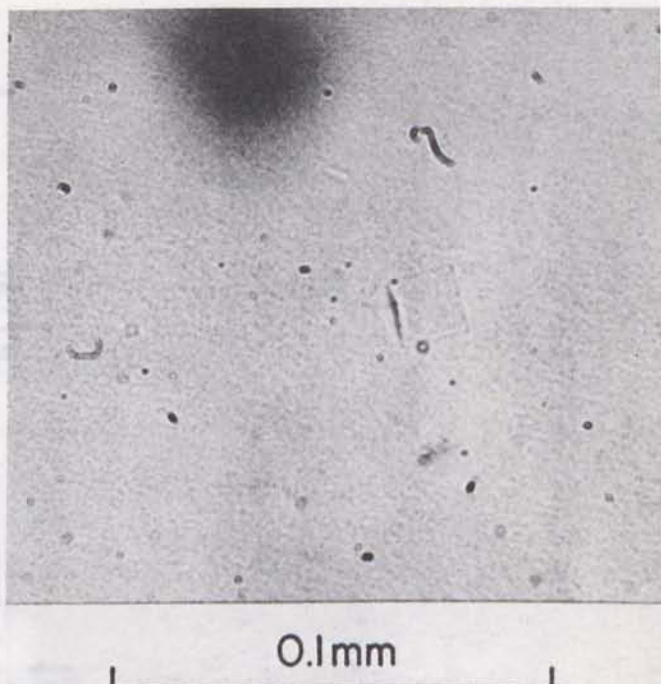

(b) Monsanto epitaxial layer

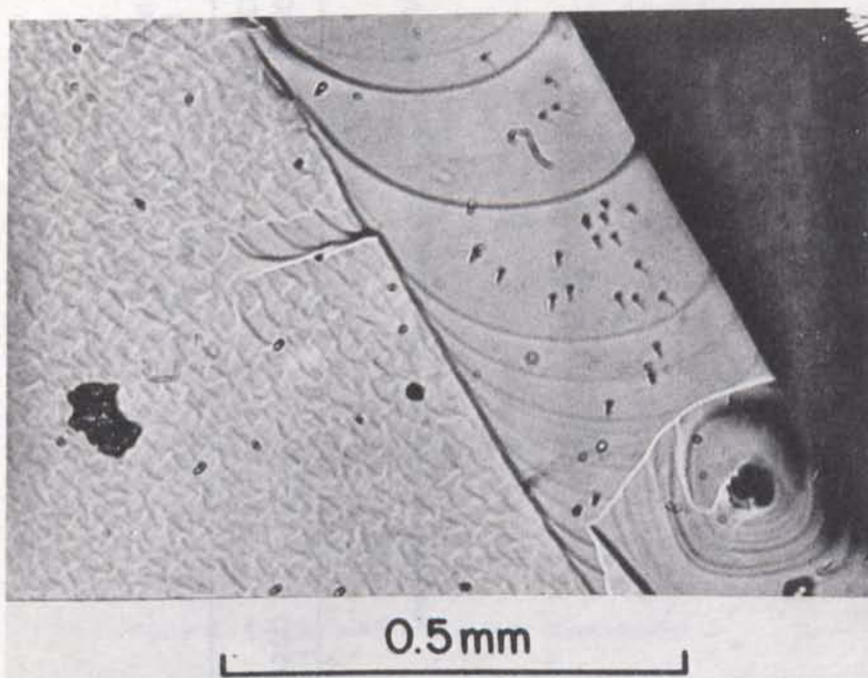

(c) Transverse Gunn diode constructed by RRE.
The photograph shows the surface roughness of the epitaxial layer used.

Figure 2. Surface finishes observed on non-CRC epitaxial layer samples

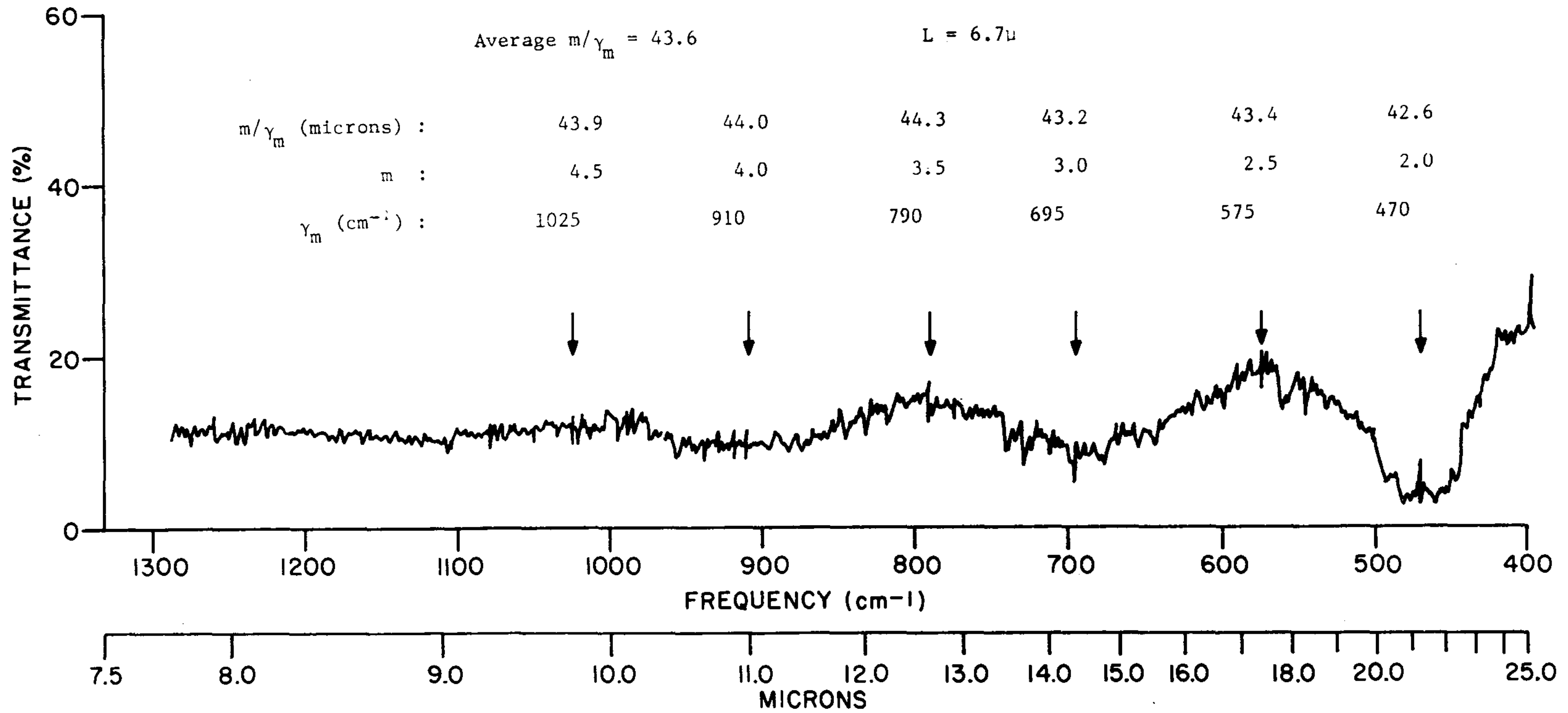

Figure 3. Sample fringe spectrum illustrating the infra-red interference method of measuring the epitaxial-layer thickness

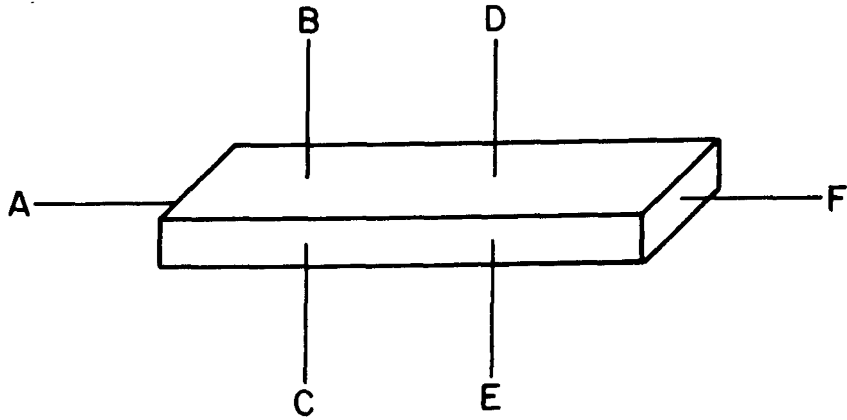

(a) Parallelepiped-shaped

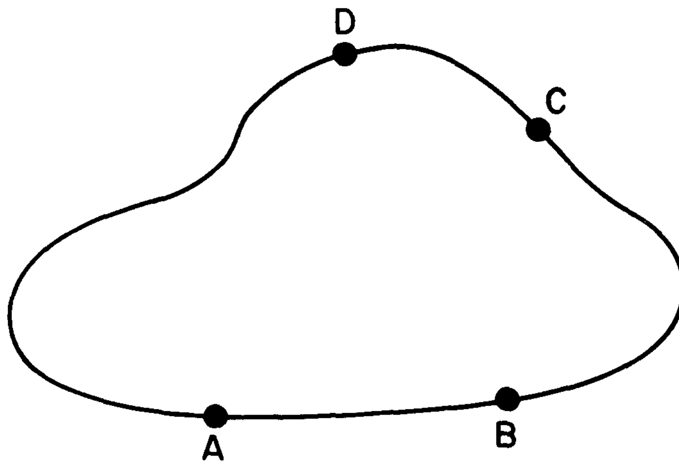

(b) Van der Pauw

Figure 4. Samples used for resistivity measurements

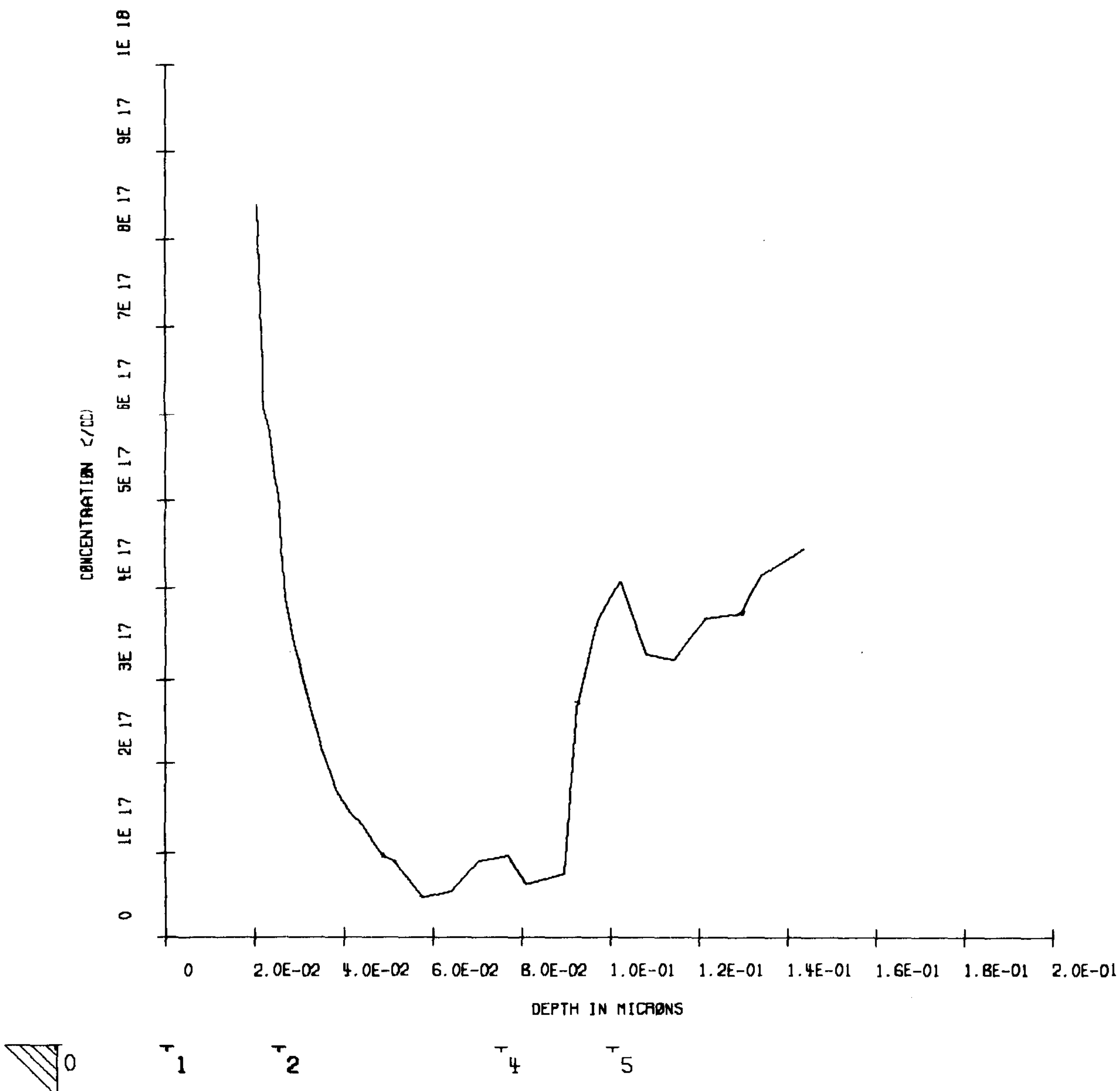

Figure 5. Computer-produced impurity concentration profile for a vapour-grown epitaxial layer of GaAs

GALLIUM ARSENIDE MATERIALS AND DEVICES AND THE GUNN EFFECT

by

W.D. Edwards, W.A. Hartman, A.B. Torrens, and D.L. Butler

PART 5

CONTACTS TO GALLIUM ARSENIDE

by

W.D. Edwards, W.A. Hartman, A.B. Torrens, and D.L. Butler

ABSTRACT

Au:Ge:Ni contacts are applied by evaporation from a W boat under vacuum. Alloying is done in an H_2 flow at a temperature which exceeds 400°C for about 10 min. The specific contact resistance, measured on dot contacts, is found to vary inversely proportionally to the doping.

Sn-dot contacts are also applied on GaAs. The addition of HCℓ to the ambient H_2 atmosphere critically determines the electrical and mechanical qualities of the contact obtained.

PART 5

CONTACTS TO GALLIUM ARSENIDE

1. INTRODUCTION

This work was carried out as part of a program to develop techniques for making uniform, reproducible, low-resistance ohmic contacts to lightly-doped n-type gallium arsenide. Different contacting metals and metal alloys were investigated in the program, as well as the variation of contact quality with surface preparation and material resistivity.

2. CONTACT EVALUATION

To evaluate ohmic contacts, the total current resistance must be separated into spreading, contact, and residual resistances. This can be accomplished by using a method discussed by Cox and Strack[1]. The total resistance can be written as:

$$R_T = \frac{\rho}{d\pi} \text{ Arc tan } \left(\frac{4L}{d}\right) + \frac{4R_c}{\pi d^2} + R_o, \tag{1}$$

where ρ is the resistivity of the material, d is the contact diameter, L is the thickness of the material, and R_c is the specific contact resistance. Residual resistances, such as the contact resistance of the back contact, are denoted by R_o. In this work, tests have shown R_o to be of the order of 0.5 ohms or less, and thus it is neglected in the analysis. Eq. 1 assumes that the spreading resistance of a circular disc contact can be written as

$$R_s = \frac{\rho B}{2d} \quad , \tag{2}$$

where B is a correction factor for the finite thickness of the material. This factor is approximated by:

$$B \simeq \frac{2}{\pi} \text{ Arc tan } \frac{4L}{d} \quad . \tag{3}$$

If the total resistance of contacts of different diameters is measured, curve-fitting methods can be used with eq. 1 to obtain the specific contact resistance and the material resistivity, if the sample thickness is known.

Wafers with two planar parallel contacts were more suited to specific contact resistance measurement. The resistance R_T of these samples is related to R_c by:

$$R_T A = \rho L + 2R_c \quad ,$$

where L is the sample length and A its area. Samples of various lengths were used and a plot of R_TA vs. L gives a figure for R_c and a value for the resistivity. Resistivity values were checked by alloying dots to parallelepiped shaped samples.

3. EXPERIMENTAL

The gallium arsenide slices and epitaxial wafers prepared as previously described were scribed into pieces approximately 2.5 mm square. Ohmic contacts were alloyed to these samples by a number of methods, some of which are now described.

3.1 Au:Ge:Ni CONTACTS

3.1.1 Substrate Preparation

The substrates were polished chemo-mechanically with sodium hypochlorite and, after being removed from the polishing fixture, given a preliminary degreasing in electronic-grade acetone, followed by a rinse in isopropanol. Each substrate was then etched in a hot (50°C) mixture of 3 parts H_2SO_4, 1 part H_2O, and 1 part H_2O_2, for 30 seconds. The wafer was then rinsed on a glass frit with hot (just below boiling) distilled water. This was followed by a 5-minute soak in 10% potassium cyanide solution, to rid the surface of copper, followed by several rinses with deionized water.

For sample 5/13, however, an attempt was made to avoid possible contamination from the glass beakers in which the rinse water was heated. Samples 5/13 and 5/14 were processed simultaneously, the differences being that 5/13 was rinsed with cold deionized water directly from the source, and 5/14 was processed as outlined above. The specific contact resistance found for 5/13 was not significantly different from that for 5/14 or for other samples.

For the first few samples processed (up to and including 4/3), the final step was brief degreasing in hot isopropanol vapour. For sample 4/4 and all following ones, the final step was a thirty-minute rinse in electronic-grade isopropanol in a Soxhlet. The substrate was then placed onto the mask in the vacuum deposition chamber.

3.1.2 Equipment and Material

The contact material was obtained commercially in the form of small ingots, weighing approximately 100 mg. each, of an Au:Ge eutectic alloy (88% Au, 12% Ge by mass). Each evaporation charge consisted of two of these ingots with about 11 mg of pure Ni wire. Several evaporation charges were prepared at one time, and degreased and stored in small wire-mesh baskets in a vapour degreaser containing electronic-grade isopropanol.

The evaporation mask was constructed by drilling a pattern of holes in 50 μm molybdenum sheet. The basic pattern consisted of five holes of different diameters: 0.05, 0.1, 0.2, 0.25, and 0.5 mm; this pattern (Figure 1) was repeated on 2 mm centres to form a 3 x 3 array. Mechanical fabrication of the mask was used as photoetching methods did not give the definition

required through a 50 μm thick mask. The mechanical approach was also more simple.

To check the hole diameters, gold was evaporated through the mask onto a piece of a microscope slide under the same conditions as for contact evaporation. Photomicrographs of the evaporated dots were made and the diameters measured. Because of a tendency of the gold to flake off the slide, not all the dots could be measured; however, a satisfactory average value was obtained for each of the different diameters. These averages were in most cases well within a 10% deviation from the nominal values for the hole diameters and were used in all calculations involving contact diameters. The contact diameters, as evaporated, are

Nominal Diameter (μm)	Actual Diameter (μm)
50	56 ± 5
100	112 ± 3
200	201 ± 3
250	267 ± 10
500	518 ± 5

The contact evaporation system was a modified Edwards 12-inch vacuum coater unit, model 12EA/484. The original oil diffusion pump was replaced with an Edwards F403 four-inch pump, fitted with a liquid-nitrogen cold trap which permitted lower ultimate pressures (about 8×10^{-7} torr) to be obtained. Evaporations were performed at pressures of 1×10^{-6} to 2×10^{-6} torr and these were reached within one to two hours of starting evacuation.

An assembly was built onto the baseplate of the system to support the evaporation mask so that the substrate was approximately three inches above the tungsten source boat. A manually-operated shutter was installed so that the substrate surface could be protected from any impurities driven from the source in the initial stages of evaporation.

3.1.3 Contact Application

The contact evaporation required two operations: evaporating a dot pattern onto one surface of a GaAs substrate, followed by the evaporation of a large-area contact (covering as much of the surface as possible) onto the other surface. A tungsten boat was used to evaporate the contact material. A boat usually survived several evaporations. When it became necessary to install a new boat, it was first vapour-degreased and mounted in the vacuum system, which was then pumped down to about 10^{-6} torr. The boat was cleaned by heating at white heat for five minutes.

The procedure for each evaporation was as follows: first, the charge of about 200 mg of Au:Ge eutectic and 11 mg of Ni was placed in the boat, and the appropriate mask was installed in the holder. Then the GaAs specimen, prepared as described previously, was placed on the mask. The sample was transferred under isopropanol and the vacuum system immediately evacuated. The shutter was in place between the specimen substrate and the tungsten boat. After the vacuum system was pumped to about 1×10^{-6} torr,

the source boat was heated until the contents just melted together. Then the temperature of the boat was raised to white heat, the shutter withdrawn, and the material evaporated completely. The nickel evaporated last and covered the Au:Ge deposit.

Alloying of the contacts was carried out in a continuous-flow, pure-hydrogen atmosphere, using the alloying curve of Figure 2. The nickel surface coat prevented balling of the Au:Ge alloy. The samples were bonded to modified TO-5 headers at the same time as the alloying took place. This was done by using Au:Ge eutectic alloy preforms (25 μm thick and 1.27 mm in diameter). Several of these were distributed about the header so that the whole back surface of sample could be contacted. The GaAs sample was then placed, with back contact down, on top of the preform so that when the whole assembly was heated, the back contact was bonded to the header (Figure 3).

3.1.4 Measurements

The contact arrays were applied to many samples of bulk GaAs of different thicknesses and resistivities. For each contact, a graph of the d.c. I vs. V characteristic, measured through the bulk GaAs to the header, was obtained for currents of several hundred milliamperes in both current directions.

The characteristics for most of the contacts appeared ohmic at the lower current densities, i.e., the curves were straight lines through the origin. However, at higher current levels, the characteristics became curved, indicating decreasing contact resistances. Later, when pulse methods were used to display the I vs. V characteristics of the same contacts, the characteristics were ohmic out to the Gunn threshold, indicating that the curvature of the d.c. plots was the result of local heating.

The total resistance of each contact was calculated from the slope of the I vs. V characteristic at the origin.

3.1.5 Analysis and Results

The values of contact resistance listed in Table 1 were found by least-squares curve fitting of eq. 1 to the measured value of the total resistance. For these calculations, the values of resistivity supplied by the manufacturer were assumed to be correct. Figure 4a shows typical results.

Then the data were analyzed by the same type of curve fitting to give values for both the resistivity and the specific contact resistance for each sample. Negative values for the contact resistance were sometimes obtained; these are discussed in Ref. 2 (appended). Plots are given of the fitted curves for the results that fit the model reasonably well (Figure 4b to f). A summary is given in Table 2.

3.2 TIN DOT CONTACTS

The procedure followed was essentially that described by Bott[3]. The gallium arsenide chips were degreased in acetone, etched for one minute in bromine methanol 1:200, rinsed in deionized water and finally placed in a

Soxhlet containing isopropanol before loading into the furnace shown in Figure 5a.

TABLE 1

Specific Contact Resistances, Calculated by using Manufacturers' Values for Sample Resistivity

Sample No.	Thickness (μm)	Resistivity (ohm·cm)	Specific Contact Resistance (10^{-3} ohm·cm^2)
3/1, 4/1, 4/3	345	0.47	2.1
4/5	169	0.47	0.69
4/6			0.18
5/3			1.9
5/9	106	0.47	0.13
5/13			0.16
5/14			0.44
5/5	8	1.4	4.0
5/7			5.5
5/8			2.4
6/2	100	1.85	1.8
6/3		1.85	1.3
6/4	193	10	2.6
6/5			

TABLE 2

Specific Contact Resistance and Bulk Resistivity Calculated from Total-resistance Data

Sample No.	Thickness (μm)	Resistivity (ohm·cm)	Specific Contact Resistance (10^{-3} ohm·cm^2)
3/1, 4/1, 4/3	345	0.63	1.5
4/6	169	0.54	0.04
5/3	169	0.60	0.75
5/9, 5/13, 5/14	106	0.45	0.35
6/2, 6/3	100	1.4	2.5

A platinum. spiral heater winding is surrounded by a silica hearth. Eight depressions are ground into the opposite side of the hearth into which fit the stubs of the Gunn-diode package. The control thermocouple fits into the centre of the hearth (Figure 5b). The optically-flat viewing window attached to a ground glass cone is removed for loading the gallium arsenide wafers, diode packages, etc. The choice of furnace atmosphere, hydrogen or

hydrogen plus hydrogen chloride, is selected by a two-way tap. The tap is motor-driven to facilitate timing of the gas addition. The thermocouple signal is fed to a strip-chart recorder with preselected profiles to provide feedback to the furnace heater power supply.

In this manner the furnace atmosphere and temperature can be changed according to a preselected program whilst the alloying process is observed through a microscope. The hydrogen chloride vapour addition was found to be the most critical step. The addition was limited to a few seconds at the peak of the temperature cycle as too early an addition of the hydrogen chloride gave erratic results in the form of poor and irregular mechanical bonds, Schottky barriers, etc.

Tin dots of diameter 0.1 mm to 0.5 mm were alloyed to epitaxial and bulk samples of several thicknesses. The back, or large-area, tin contact between the gallium arsenide and the gold-plated stub was preferably made at the same time as the tin dot contacts. With multiple loads in the furnace this was difficult to achieve and in these instances the stubs were tinned in a separate operation.

After alloying, the contact areas were measured optically. By sectioning completed devices or, more effectively, by rolling the dots off the wafers in the alloy furnace before cooling commenced, it was established that alloying occurred over the whole area. This last experiment showed that wetting occurred uniformly over the whole surface, and also gave a value for the dissolution depth.

Current vs. voltage measurements were made on the completed devices in the same manner as described for the Au:Ge:Ni contacts. The contact areas were measured with a microscope.

The specific contact resistances were calculated from eq. 1. The average values obtained, for a given material resistivity, are plotted in Figure 1 of Ref. 2 (appended), together with an indication of the spread in the values.

4. DISCUSSION

The ohmic contacts studied were linear and were quite symmetrical on current reversal. There was no evidence that the contact resistance was rectifying[4]. Such ohmic contacts can be characterized by their specific resistance as defined in Ref. 2 (appended). Specific contact resistance values for a range of sample resistivity and contacting methods are plotted in Figure 1 of Ref. 2 (appended). Also shown are results, found by other workers for more heavily-doped material. There does appear to be an approximately linear relationship between specific contact resistance and material resistivity, as pointed out by Goldberg and Tsarenko[5]. A similar relationship has been indicated for silicon[6].

Further discussion of the results obtained[2] will be found in Ref. 2 (appended).

5. REFERENCES

1. Cox, R.H., and H. Strack, *Ohmic Contacts for GaAs Devices*, Solid State Electron. 10, 1213 (1967).

2. Edwards, W.D., W.A. Hartman and A.B. Torrens, *Specific Contact Resistance of Ohmic Contacts to Gallium Arsenide*, Solid State Electron. 15, 387 (1972) (appended).

3. Bott, I.B., C. Hilsum and K.C.H. Smith, *Construction and Performance of Epitaxial Transferred Electron Oscillators*, Solid State Electron. 10, 137 (1967).

4. Hooper, R.C., J.A. Cunningham and J.C. Harper, *Electrical Contacts to Silicon*, Solid State Electron. 8, 831 (1965).

5. Goldberg, Yu.A., B.V. Tsarenko, *Dependance of the Resistance of Metal Gallium Arsenide - Ohmic Contacts on Carrier Density*, Soviet Phys. Semicond. 3, 1447 (1970).

6. Hoare, R., Northern Electric, unpublished manuscript (1970).

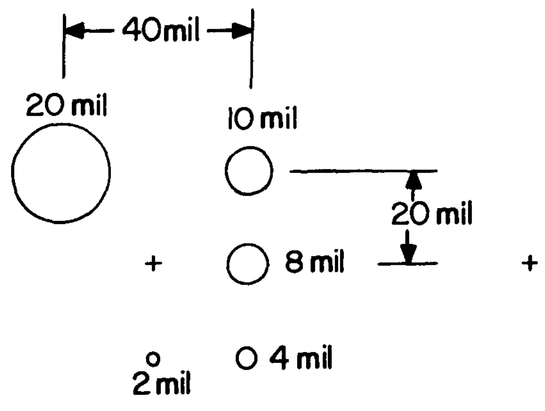

Figure 1. Basic pattern of holes in contact evaporation mask

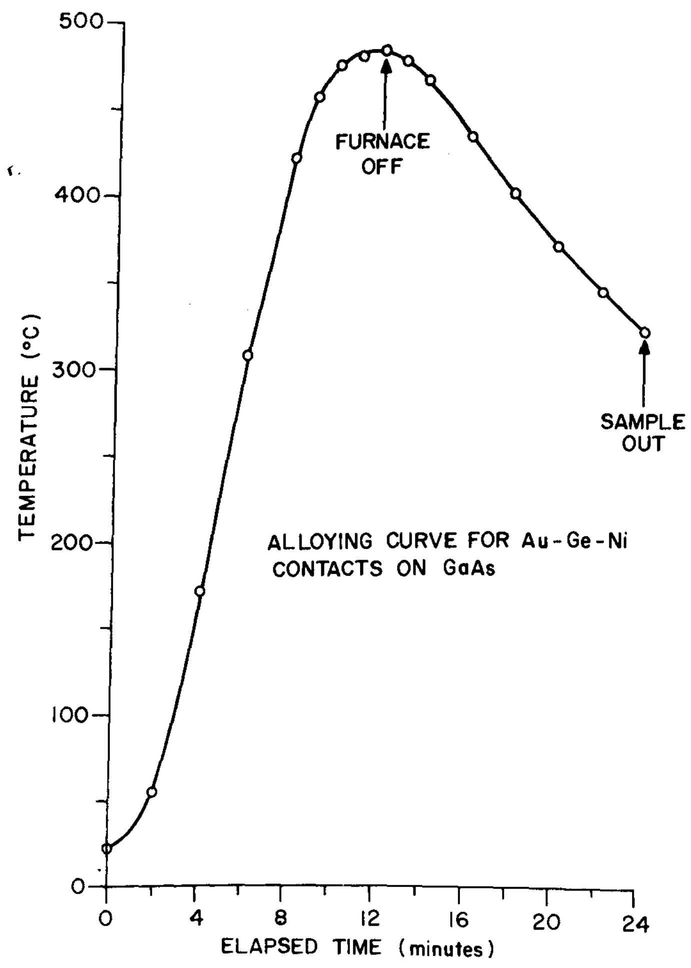

Figure 2. Temperature profile for alloying evaporated Au:Ge:Ni contacts

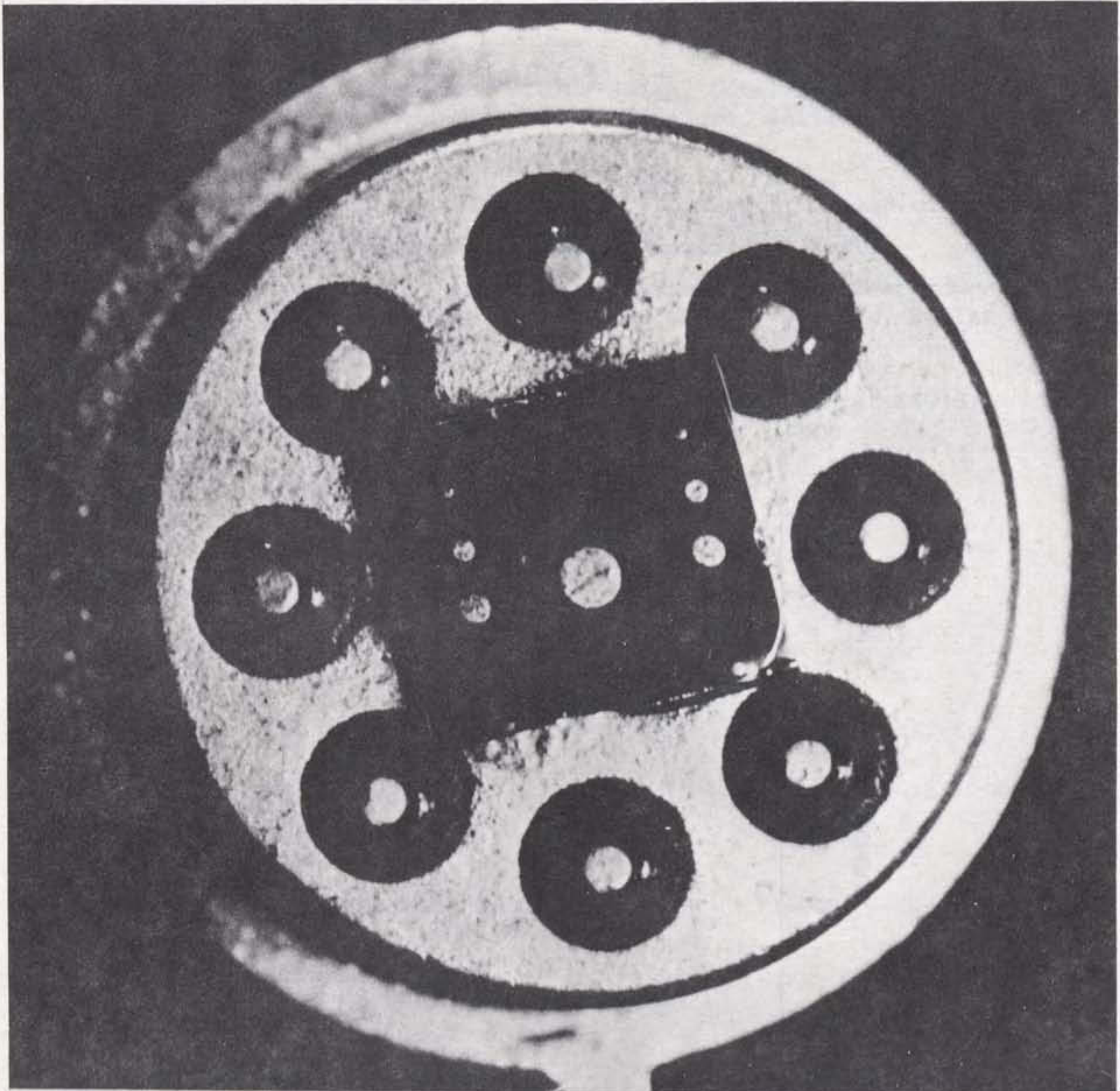

Figure 3. Evaporated contacts on GaAs chip, after alloying and bonding to header

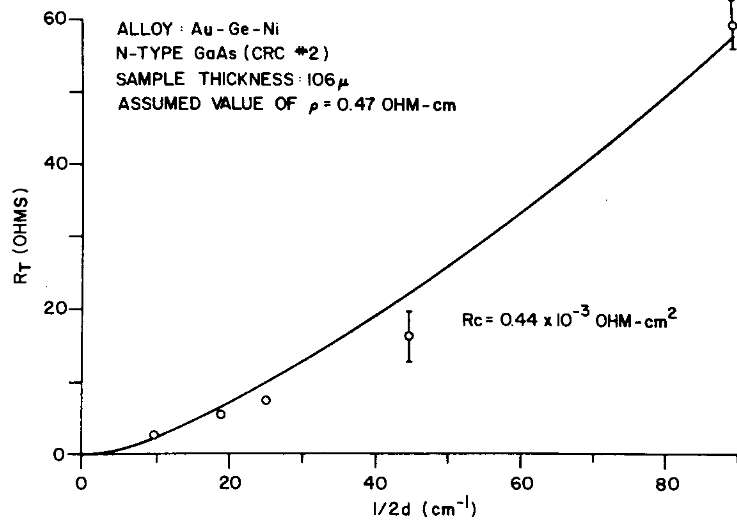

(a)

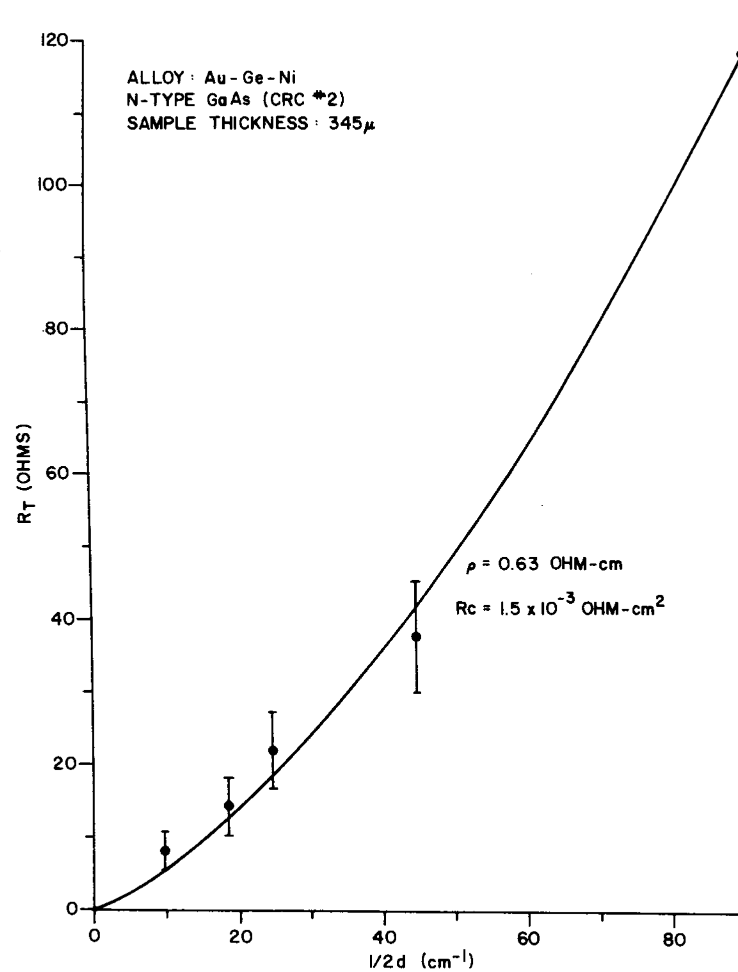

(b)

Figure 4. Contact resistance vs. reciprocal contact diameter for six samples (Sheet 1 of 3)

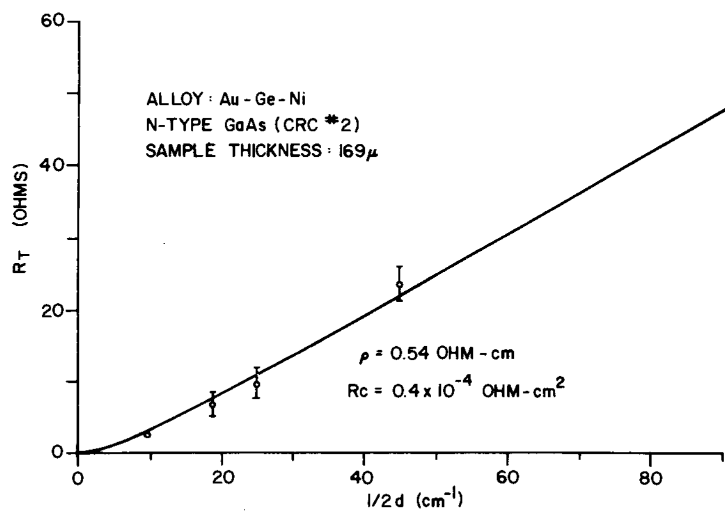

(c)

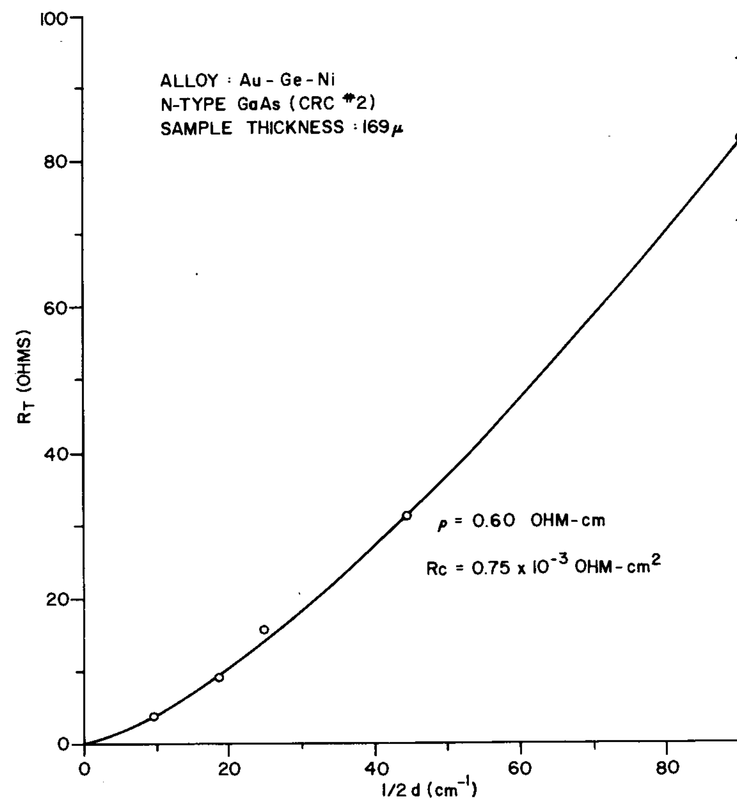

(d)

Figure 4. Contact resistance vs. reciprocal contact diameter for six samples. (Sheet 2 of 3)

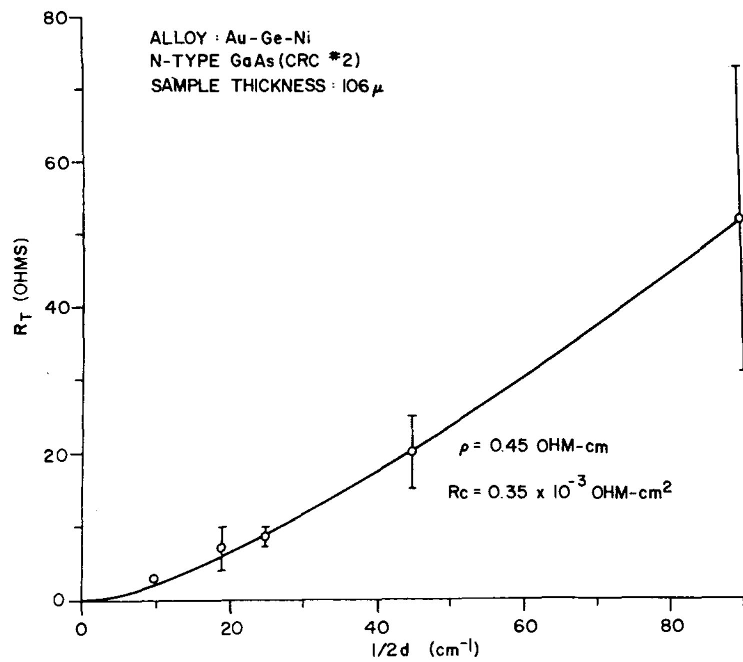

(e)

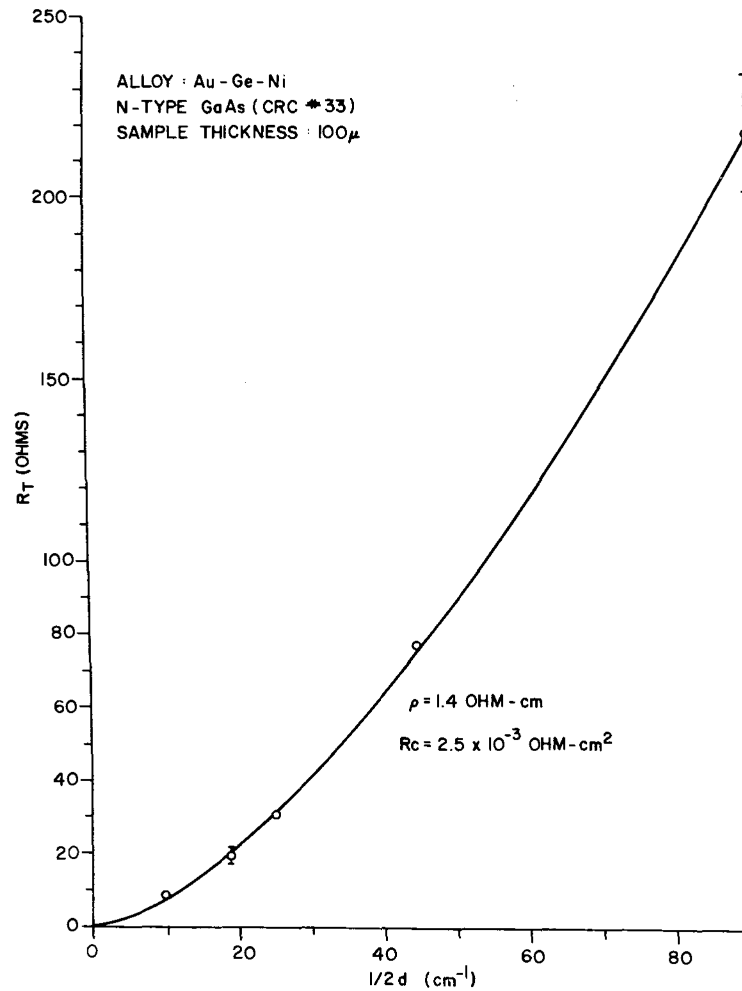

(f)

Figure 4. Contact resistance vs. reciprocal contact diameter for six samples. (Sheet 3 of 3)

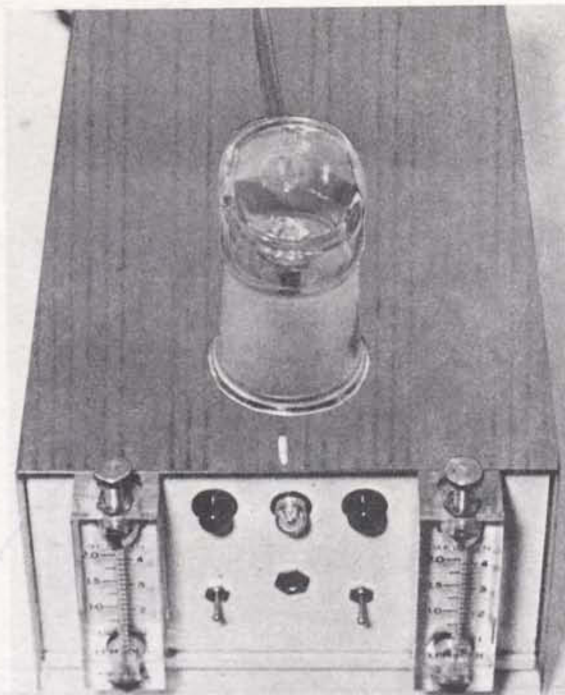

(a) General view showing controls

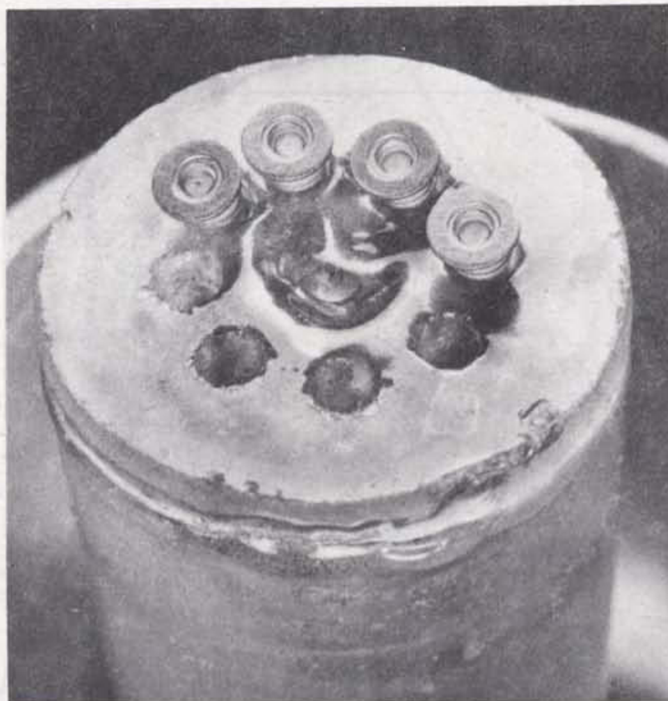

(b) Hearth load with Gunn diode headers (ground quartz cap removed)

Figure 5. Tin-dot contact alloying furnace

Reprint from: *Solid-State Electronics*, 1972, Vol. 15, pp. 387–392. Pergamon Press.

SPECIFIC CONTACT RESISTANCE OF OHMIC CONTACTS TO GALLIUM ARSENIDE

W.D. Edwards, W.A. Hartman and A.B. Torrens

Communications Research Centre, P.O. Box 490, Station "A", Ottawa, Canada

(Received 22 January 1971; in revised form 29 June 1971)

Abstract – Values of specific contact resistance R_c have been obtained for Sn, Sn:Ag, and Au:Ge:Ni contacts to N-type gallium arsenide of resistivity 0.4 to 30 Ω cm. An approximate relationship $R_e \propto 1/N$, where N is the bulk carrier concentration, was shown to apply. The relationship between the value of R_c and the contact structure is discussed. It is pointed out, in particular, that R_c may be negative when its usual, phenomenological definition is used.

Résumé – On obtient des valeurs expérimentales de résistance spécifique de contact R_c pour des électrodes de Sn, Sn:Ag et Au:Ge:Ni appliquées à de l'arséniure de gallium de type N et résistivité 4 à 300 mΩm. On trouve que R_c est, en général, inversement proportionnel à la concentration d'électrons. Dans une discussion de la relation entre R_c et la structure du contact, on fait remarquer, entre autres, que R_c peut être négatif, si on le définit de la façon phénoménologique habituelle.

1. INTRODUCTION

Gallium arsenide is of interest as the basic material for both light emitters and microwave devices. Ohmic contacts must be made to the material and, for microwave devices, the relatively low doping of the gallium arsenide gives rise to difficulties. Many papers have been published on methods of making ohmic contacts to gallium arsenide but specific contact resistance values were seldom provided[1–5], especially for lightly-doped material.

Values of specific contact resistance are reported here. It is shown that a simple relationship between specific contact resistance and bulk resistivity exists. The specific contact resistance may be positive or negative when defined as the difference between the total measured resistance and the calculated bulk resistance.

2. CONTACT PROCEDURES

The gallium arsenide used was obtained commercially in bulk, slices and epitaxial form with resistivities in the range 0.4 to 30 Ωcm. Slices were cut from the bulk parallel to the {111} and {100} planes with a diamond cut-off wheel. To reduce slice damage and the consequent introduction of dislocations to a minimum, no lapping was done. The slices were reduced to the desired thickness and polished by a chemical-mechanical method. The etch was a freshly prepared 5% NaOCl solution carried on a rotating Corfam pad.

The polished slices and epitaxial wafers were then scribed and divided into pieces approximately 2.5 mm square prior to final etching and cleaning. A number of alloys and processing variables were tried. The processes reported on below gave the lowest specific contact resistances.

2.1 Tin Dot Contacts

The procedure followed was essentially that described by Bott *et al.*[6]. The gallium arsenide chips were degreased, etched, carefully rinsed in water and finally cleaned in a soxhlet containing isopropanol before being loaded into the furnace. The furnace atmosphere and temperature were varied according to a prearranged programme, whilst the alloying process was observed through a microscope. The hydrogen chloride addition was the most critical step. The gas injection was limited to a few seconds at the peak of the temperature cycle. Earlier addition of the hydrogen chloride gave erratic results such as poor and irregular mechanical bonds or Schottky barriers.

Tin dots of diameter 0.1 to 0.5 mm were alloyed to epitaxial and bulk samples of several thicknesses. The back, or large area, tin contact between the gallium arsenide and a gold-plated stub was made at the same time as the tin dot contacts. After alloying, the areas of the contacts were measured optically. By sectioning completed devices or, more effectively, by rolling the dots off the wafers in the alloy furnace before solidification commenced, it was established that alloying occurred over the whole area. This last experiment showed that wetting occurred uniformly over the whole surface and also gave a value (~ 2 μm) for the dissolution depth.

2.2 Au:Ge:Ni Contacts

The techniques used to prepare these contacts were similar to those reported elsewhere [7,8]. Polished wafers of known thicknesses, about 6 mm square, were degreased and then etched for 30 sec in a hot (50°C) mixture of 3:1:1 parts by volume of H_2SO_4:30% H_2O_2:H_2O. After a rinse in distilled water, the wafers were given a 5-min soak in 10% KCN solution, followed by further rinses in water and isopropanol.

Another etch that gave comparable results was a mixture of 7:1:1 parts by volume of H_2SO_4:30% H_2O_2:H_2O used at 80°C. The samples were washed in water and acetone before etching. The etch was quenched with distilled water, and the samples were dried on filter paper prior to storage in isopropanol.

The contact material was an eutectic alloy of 88% Au and 12% Ge (mass proportions), with about 5% Ni added. The contacts were applied by vacuum evaporation on to each side of the wafer of about 0.15 g of the alloy from a tungsten boat placed about 0.1 m below the substrate. When desired, one uniform deposition was replaced by the deposition of an array of circular dots through a 50 μm-thick molybdenum mask. The basic mask pattern consisted of five drilled holes of 50, 100, 200, 250 and 500 μm diameters; this pattern was repeated on 2 mm centres to form a 3 X 3 array.

When evaporation took place the nickel evaporated last, forming a layer over the Au:Ge deposit. This nickel coat inhibited balling of the Au:Ge during the alloying step, and gave more uniform contacts. However, it was more difficult to maintain the complete coverage after alloying on the 30 Ωcm material. On {111} samples, fragmentation of the contact was more severe on the 'A' face, the more poorly polished side.

A pre-evaporation sputter-clean of the gallium arsenide wafers did not affect the contact resistance and was therefore not included in the normal process. The contacts were alloyed at 480 ±5°C for about 3 min, in a continuous flow of pure hydrogen. At the same time the back contact of the wafer was bonded to a TO-5 header by means of several Au:Ge eutectic alloy preforms.

In another procedure, the sample was not mounted on a header. It was alloyed in a heated graphite dish, in a chamber which was first evacuated, then filled with hydrogen up to atmospheric pressure.

2.3 Other Contacts

Vacuum-deposited tin does not usually give satisfactory contacts on GaAs because the tin balls on melting in the alloying process. To prevent balling, one can deposit a very thin film of silver before the tin[9,10], or add silver to the tin deposition[8,11,12]. After simultaneous evaporation of about 170 mg of tin and 85 mg of silver and alloying in hydrogen, excellent wetting was obtained with formation of a crystalline layer. The diodes obtained were ohmic.

Electrodes obtained by evaporating 11 mg of aluminum and 290 mg of gold (eutectic proportions) and alloying exhibited good mechanical adherence but the contacts were not ohmic.

3. MEASUREMENTS

The VI characteristics of contacts made by all methods were measured up to, and beyond, the Gunn threshold. At low levels where the heat dissipation was insignificant d.c. currents were used to obtain the VI plots on an XY recorder. At higher power levels, short voltage pulses were used to examine the device characteristics in the non-linear region. Simple integrating circuits allowed the characteristics measured with pulses to be plotted on a standard XY recorder (see Appendix). Below the threshold region the plots showed that the current was a linear function of the voltage and no evidence of rectification[13] was seen. The resistance of the samples was obtained from the slope of the VI plots.

Devices of the dot and planar back-contact type were analyzed by the method described by Cox and Strack[3]. The measured device resistance R for such a structure is given by:

$$R = \frac{\rho}{\pi d} \text{Arc tan} \frac{4L}{d} + \frac{4R_c}{\pi d^2} + R_r, \tag{1}$$

where ρ is the resistivity, d the contact diameter, L the wafer thickness, R_c the specific contact resistance and R_r the residual resistance due to the back contact. As tests had shown R_r to be of the order of 0.5 Ω or less, it was neglected in the analysis.

Curve-fitting methods were used to analyze the resistance data in terms of the contact diameter and the wafer thickness to give values for both R_c and ρ.

Wafers with two planar-parallel contacts were also used to obtain specific contact resistance values according to the relation

$$R = \frac{\rho L}{A} + 2\frac{R_c}{A} \tag{2}$$

where A is the sample area. For samples of various thicknesses, a plot of RA vs. L gives values for R_c and ρ. Resistivity values were checked by alloying contact dots along the sides of bar-shaped samples.

The operation of a number of samples at microwave frequencies was observed by mounting the wafers under a pressure contact on a piece of 50 Ω microstrip. The samples were driven by 0.25 μsec pulses at 1000 Hz. The microstrip was coupled to a triple stub tuner by a 200 pF capacitor. The tuner was followed by a power meter, sampling scope or spectrum analyzer, as appropriate. The particular sample described in Fig. 3 had a specific contact resistance of $6.56 \times 10^{-3}\,\Omega(\mathrm{cm})^2$, bulk resistivity of 1.85 Ωcm and operated in the circuit described at 1.08 GHz with an efficiency of 2.5 per cent. It was observed that samples made from bulk material with two planar contacts parallel to the $\{111\}$ planes could be reversed in the pressure holder with very little effect on the efficiency of operation. Negative differential resistance was observed in the 0.47 Ωcm samples over the whole range of specific contact resistance.

4. DISCUSSION

If a current of density J flows through an ohmic contact from a metal to a semiconductor, the voltage drop induced by the current between a point P in the metal and a point Q in the semiconductor can be written:

$$\tilde{V}_{PQ} \overset{d}{=} \tilde{V}_Q - \tilde{V}_P = R_{PQ}J \tag{3}$$

where $\tilde{V}$ is the deviation of the potential V from its equilibrium value and R_{PQ} is, by definition, the specific resistance between points P and Q. If P and Q are taken very close to the junction, R_{PQ} is the specific contact resistance. This definition is, however, not precise without a detailed physical model which allows one to determine where the points P and Q should be taken[14].

In this paper, we consider points A and B in the bulk of the materials, outside of their contact layers. A contact layer is defined as the volume over which the material is locally modified by the contact, for such reasons as surface damage, regrowth, and diffusion from the surface. It also includes any resistive layer (e.g., oxide layer [13,14]) which may exist between the metal and the semiconductor. The specific contact resistance is defined as the difference between the actual resistance R_{AB} and the resistance expected from the bulk material resistivities and the dimensions involved:

$$R_c \overset{d}{=} R_{AB} - (\rho_m a_m + \rho a)$$

where a_m and a are the distances from the junction to the points A and B, respectively. Usually, the contribution $\rho_m a_m$ of the metal may be neglected:

$$R_c = R_{AB} - \rho a. \tag{4}$$

It is this definition of R_c which is implied in relations (1) and (2), and, essentially, in the methods used by other workers[1–4, 15, 16, 21].

An important property of R_c as defined by relation (4) is that it may be positive or negative, depending on the structure of the contact layer. It is to be noted that negative values of R_c arise only as a result of the definition used. With a more 'physical' — as opposed to phenomenological — definition, such as relation (3), the contact resistance R_{PQ} could never be negative. If, after the contact has been applied, surface defects or local diffusion of impurities have decreased the carrier mobility or concentration near the contact, or if there is a thin resistive layer between the metal and the semiconductor[13, 17, 22, 23, 24], R_c will be positive. But the opposite ($R_c < 0$) can also be expected if, for example, diffusion from the contacting metal increases the doping near the contact. Such overdoping will occur at contacts where regrowth of an N^+ layer takes place. A

fairly long doping 'tail' extending from Au:Ge:Ni contacts on GaAs was observed by Harris *et al.* [18]. Thus, negative experimental values of R_c based on relation (4) may be meaningful and have indeed been obtained[5, 16]. In the present work, all six contacts on one particular dice had negative specific resistance with average value about $-3 \times 10^{-4} \Omega(cm)^2$.

In some cases, overdoping of the semiconductor could be combined with a thin resistive layer at the junction. In other cases, a short overdoped region near the contact could occur with a long, slightly compensated region extending farther into the bulk, due to a fast-diffusing impurity such as copper[15]. Then R_c could be nearly zero.

The above considerations indicate that R_c alone does not adequately characterize an ohmic contact. Ideally, a good contact should affect the semiconductor over only a very short distance from the junction, and its specific contact resistance would be nearly zero, possibly slightly negative. But such a value of R_c does not guarantee the contact to be good. Furthermore, if a contact 'a' has a short overdoped region and if another one 'b' has a long overdoped region, contact 'a' would likely be preferable despite the fact that R_c is larger for 'a' than for 'b'.

R_c could be expected to depend on the crystal orientation as do etching, surface regrowth and wetting (Section 2.2), although Dale[19] found no evidence of this. R_c will also depend on the materials and process used to make the contact. On the other hand, R_c should be independent of any geometric dimension. However, when two contacts are made and the sample is so thin that the two contact layers overlap, definition (4) cannot be used because the semiconductor bulk is not defined any more. Then, one can use relation (1) or (2) to define R_c; however, (i) ρ must be chosen somewhat arbitrarily (for example, the resistivity of the material before contact application) and (ii) R_c depends on L and no longer is characteristic of the contact alone. Therefore, care should be exercised in interpreting measurements on very thin samples such as those used by Colliver *et al.* [5] and in comparing such measurements with those obtained on thick samples.

Specific contact resistance values for a range of sample resistivity and contacting methods are plotted in Fig. 1. Results published by other authors, mainly for the more heavily-doped material, are also shown. The specific contact resistance appears to be approximately proportional to the reciprocal of the carrier concentration, as pointed out by Goldberg and Tsarenkov[4]. A similar relationship has been observed for silicon and germanium[20].

Since the measurements of the diode lengths and resistances were relatively accurate, the scatter in the values of R_c can be ascribed to the following causes:

(1) The tendency of the metallic electrodes to fragment on alloying, which raises an uncertainty in the determination of the effective area. Such fragmentation was sometimes visible with a microscope when high-resistivity material was used. Its occurrence poses the question of what proportion of the metallic layer is making electrical contact.

(2) In the usual case where $|R_c| \ll \rho a$, even a small relative uncertainty in ρ results in a large relative uncertainty in R_c. Three reasons for uncertainty in the value of ρ are (a) The crystal is not homogeneous[20]. (b) The quantity ρ in relations (1), (2) and (4) is the material resistivity *after* the diode has been fabricated. It may be significantly different from the resistivity of the material before the fabrication process, especially for lightly-doped material and for contact-alloying temperatures of the order of 500°C. Even if the resistivity measurements and diode fabrication are performed upon adjacent pieces of material, the bulk resistivity of the completed diode may be different from that of the measured piece because of the higher temperature of the contact fabrication process. (c) The resistivity change during diode fabrication may be poorly reproducible. A random error is then introduced in the value of ρ used in relations (1), (2) or (4); this could account for the large scatter in values of R_c at high ρ (Fig. 1).

The sources of error (b) and, to some extent, (c) should be less important when ρ is obtained at the same time as R_c from measurements on a number of diodes made simultaneously. Such methods include that using relation (1) and curve fitting methods and that using relation (2) and samples of various lengths.

(3) The physical structure, i.e., band structure, impurity profile, etc., of the obtained contact depends on the materials and processes used and, for a given material, on uncontrollable variations of the process. In particular, there is, *a priori,* no reason why two different alloys should give, on the same material, contacts with equal specific resistances.

The fact that a common law – $R_c \propto N^{-1}$ – holds approximately for a number of results pertinent to different materials and methods indicates that a particular band structure that is fairly independent of the materials and processes used often occurs at the contact. Other structures, or combinations of structures, could account for the existence of results which do not follow the above law.

Acknowledgement – The authors wish to thank D. Butler, J. Bingham, and G. Pinkney for help with the experiments. The receipt of a preprint from B.R. Gossick is gratefully acknowledged.

REFERENCES

1. K.L. Klohn and L. Wandinger, *J. electrochem. Soc.* **116**, 507 (1969).

2. B. Schwartz and J.C. Sarace, *Solid-St. Electron.* **9**, 859 (1966).

3. R.H. Cox and H. Strack, *Solid-St. Electron.* **10**, 1213 (1967).

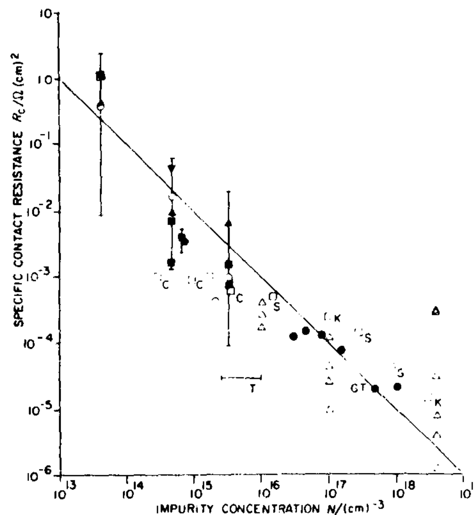

Fig. 1. Specific contact resistance R_c vs. impurity (bulk carrier) concentration:

(a) Results published by:
□ K, Klohn and Wandinger;
□ S, Schwartz and Sarace;
□ C, Cox and Strack; T, Colliver, Gibbs and Taylor;
● GT, (points and line) Goldberg and Tsarenkov;
Δ Matino and Tokunaga.
(b) Results obtained in the present work (only averages and uncertainties are shown):
■ Au:Ge:Ni contacts obtained by the first process.
▲ Au:Ge:Ni contacts obtained by the second process described in Section 2.
○ Sn dot contacts.
▼ Sn: Ag contacts.

4. Yu. Goldberg and B.V. Tsarenkov, *Soviet phys. Semicond.* 3, 1447 (1970).

5. D.J. Colliver, S.E. Gibbs and B.C. Taylor, *Electron. Letters* 6, 353 (1970).

6. I.B. Bott, C. Hilsum and K.C.H. Smith, *Solid-St. Electron.* **10**, 137 (1967).

7. N. Braslau, J.B. Gunn and J.L. Staples, *Solid-St. Electron.* **10**, 381 (1967).

8. M. Cathelin and B. Jarrousse, *Onde Electrique* **50**, 179 (1970).

9. T.B. Ramachandran and R.P. Santosuosso, *Solid-St. Electron.* 9, 733 (1966).

10. A.B. Torrens, PhD Thesis, University of British Columbia (1969).

11. C.R. Paola and S. Knight, *Proc. 134th. National Meeting of the Electrochemical Society,* p. 456 (1968).

12. A.L. Edridge, F.A. Myers, B.J. Davidson and J.C. Bass, *Electron. Letters* 5, 103 (1969).

13. R.C. Hooper, J.A. Cunningham and J.G. Harper, *Solid-St. Electron.* 8, 831 (1965).

14. B.R. Gossick, *Surface Sci.* 21, 123 (1970).

15. R.M.G. Bolton and B.F. Jones, *Electron. Letters* 5, 662 (1969).

16. R.D. Larrabee, W.A. Hicinbothem Jr. and M.C. Steele, *IEEE Trans. Electron Devices* ED17, 271 (1970).

17. G.A. Armantrout and J.C. Looney, *Solid-St. Technol.* **11**, 29 (1968).

18. J.S. Harris, Y. Nannichi, G.L. Pearson and G.F. Day, *J. appl. Phys.* **40**, 4575 (1969).

19. J.R. Dale and R.G. Turner, *Solid-St. Electron.* 6, 388 (1963).

20. F. Nibler, *J. appl. Phys.* 34, 1572 (1963).

21. H. Matino and M. Tokunaga, *J. electrochem. Soc.* **116**, 709 (1969).

22. T. Saito and F. Hasegawa, *Jap. J. appl. Phys.* **10**, 197 (1971).

23. R.H. Cox and T.E. Hasty, *Proc. 134th. National Meeting of the Electrochemical Society* p. 454 (1968).

24. B. Schwartz, *J. electrochem. Soc.* **118**, 657 (1971).

APPENDIX

DC plotting of IV characteristics measured with pulses

The circuit used to plot the IV characteristic of Gunn diodes is shown in Fig. 2. If the voltage u is constant or slowly varying, the (R_x, C_x) and (R_y, C_y) low-pass filters may be omitted, and one obtains the IV plot in the usual manner. The conditions for accuracy are:

$$|i_Y| \ll |i| \quad \text{and} \quad R \ll u/i \qquad \text{(A1)}$$

If the voltage u is pulsed periodically, i.e., has a value u_p for a time t and is zero for the rest of the period T, the (R, C) circuits shown in Fig. 2 are used. Typically, $R_xC_x = R_yC_y = 0.1$ sec. If the condition RC $\gg$ T is satisfied for both circuits, the voltages applied to the XY display device (typically, an electro-mechanical recorder) are continuous:

$$u_X = \bar{u} = u_p t/T,$$

$$u_Y = R\bar{i} = Ri_p t/T.$$

The final plot actually represents $\bar{i}$ vs. $\bar{u}$, which is, for a non-oscillating diode, i_p vs. u_p with the scale factor t/T. When $|u_p|$ is larger than the threshold voltage and the diode oscillates during the pulse, the current read from the scaled plot is the average current of the oscillating diode, because the oscillation period is much shorter than the pulse duration. Thus, the current plotted beyond threshold is close to, but larger than, the minimal instantaneous (so-called 'valley') current in the oscillating diode. Fig. 3 shows one of the plots obtained.

When $R|i_p|t/T$ becomes too small to drive the recorder and to be conveniently amplified, a synchronous (lock-in) a.c. amplifier may be used to amplify the fundamental of the pulsed voltage Ri. The amplitude of this fundamental is, for $t \ll T$, equal to $2R|i_p|t/T$, and is typically well above the sensitivity limit of commercial synchronous amplifiers.

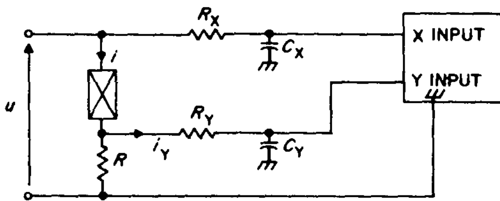

Fig. 2. Circuit for plotting the i vs. u characteristic of a diode with the voltage u pulsed. The XY display device is d.c.-driven.

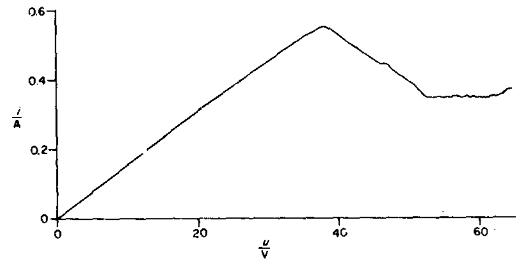

Fig. 3. IV characterisitc of one of the fabricated Gunn diodes, drawn on an XY recorder with the circuit shown in Fig. 2.

GALLIUM ARSENIDE MATERIALS AND DEVICES AND THE GUNN EFFECT

by

W.D. Edwards, W.A. Hartman, A.B. Torrens, and D.L. Butler

PART 6

DIODE FABRICATION AND TESTING

by

W.D.Edwards
With Acknowledgements
to J.A. Bingham

ABSTRACT

The chips, as obtained after dicing of a slice with contacts, are tested on needle or strip-type stations supplied with electrical pulses. Two pulse generators with 50V, 7A and 400V, 1A capabilities, are described. A special circuit is used to plot directly in DC current-voltage characteristics measured with pulses. In rudimentary microwave tests, diodes yield typical powers of 0.65W at 1.08 GHz with an efficiency of 2.9% in pulse operation.

PART 6

DIODE FABRICATION AND TESTING

1. DIODE FABRICATION

The dicing of a GaAs with its alloyed electrodes yields diodes which are essentially ready for testing. However, to facilitate handling of these devices as well as their insertion into practical microwave circuits, they should be mounted in some standard diode package. Such a package is illustrated in Figure 1. (Metronics Inc.)

Diodes made with tin dots were the only ones to be completely assembled. The gallium arsenide die was alloyed to the gold-plated stub as described in pt. 5. The ground section of a typical device (embedded in wax for grinding) is shown in Figure 2. A gold wire or ribbon was welded between the top tin contact and the flange of the package as shown in Figure 1b. The lid to the package was then welded into position with the aid of specially-shaped probe tips on the welding machine*. The completed package was then ready for testing.

However, most diodes were tested, unmounted, in special probing devices, because:

(1) The mechanical protection afforded by the package is not necessary for laboratory tests.

(2) No reliable encapsulation method was developed before the decision was taken to abandon the Gunn effect program. As a result, an attempt to mount a diode involved the risk of damaging an otherwise good device. Thus, the failure of an encapsulated device could not be associated with certainty to the device preparation or to the packaging step.

(3) Even at the stage where all devices can be encapsulated they should first be pre-tested.

2. TESTERS FOR UNENCAPSULATED DIODES

Three testing stations were used. In two of these the chip to be tested is laid on a metallic surface (usually gold-plated), grounded through a low-resistance sampling resistor. The other electrode is either a needle probe mounted on a micromanipulator (Figure 3a), or a gold-plated blade of beryllium-copper which can be lowered onto the chip with the help of a PTFE-tipped pressure screw (Figure 3b). The gold-plated blade forms with the base plate a strip-line of about 50Ω characteristic impedance. The blade is insulated with PTFE and connected to a BNC input connector. The current-

* *Model 1015, Weldomatic. Division of the Unitec Corporation Pasedena, California.*

sampling resistor is a low-reactance planar disc-resistor. Thus, this mount is expected to allow meaningful testing at microwave frequencies as well as at low frequencies.

The high-current pulser (sec. 3.2.2) uses neither of the above stations since it has its own needle probe (Figure 4).

3. PLOT OF THE I VS. V CHARACTERISTIC

Plotting was done with an xy recorder or, occasionally, an oscilloscope.

3.1 DC MEASUREMENTS

A reversible-polarity voltage-ramp was applied to the diode. The voltage and current signals were amplified by Keithley electrometers, the outputs of which were fed to an xy recorder. The voltage ramp was relatively slow and typically lasted a few seconds.

3.2 PULSE MEASUREMENTS

3.2.1 High-Voltage Pulse Generator

A high-voltage pulse generator was constructed (Figure 5). It comprises a pentode (6LQ6; peak cathode current: 1.2A) as a switch driven by a modified monostable which is triggered externally through a small coupling capacitor. Normally, the output pulse has the same duration as the input pulse. Using a monostable instead of a bistable insures that the tube be cut off if an insufficient triggering pulse is applied at the input, or when the unit is turned on. Furthermore, the capacitor C prevents the tube from staying "on" more than some 50 μs, should very long input pulses be accidentally applied.

The tube is turned off by a strong negative grid-cathode voltage, -130 V. Although, for most applications, a voltage of some -60 V would be sufficient, the tube would still conduct slightly, and this would affect the measurements described in section 3.2.3.

The characteristics of the pulser are:

- pulse voltage (negative): 0 to 500 V. (This depends on the tube supply voltage. 1 KV should be obtainable with the tube used).

- Pulse current: 0 to 1 A.

- Pulse duration: 0 to 50 μs, as determined by the drive. The maximum duration may be increased by increasing C (Figure 5). Pulses of more than 0.3 A should not last more than a few μs.

- Rise and fall times: about 25 ns on a 180-Ω load. Diodes can be tested with this pulser only up to the current I_M.

Therefore, at threshold:

$$ANev_p \leq I_M,$$

or

$$AN _ \frac{I_M}{ev_p} \approx 3 \cdot 10^{13} m^{-1} \quad .$$

(N is the doping and v_p the peak electron velocity, see Figure 3 of pt. 7.) Since it is, in practice, difficult to make the diode cross-section area A smaller than some $(0.2mm)^2$, only diodes made from material with a doping $N < 10^{21} m^{-3}$ could be conveniently tested. This condition was satisfied for the material mostly used, which has a doping of $4.6 \cdot 10^{20} m^{-3}$. However, the most conductive material used ($N = 4.1 \cdot 10^{21} m^{-3}$) did not satisfy this condition, so that only a few small diodes made of this material could be tested beyond the Gunn threshold with this tube pulser.

3.2.2 High-Current Pulse Generator - (Contributed by J.A. Bingham)

The pulse-prober head is mounted on a Kulicke and Soffa xyz positioner and the probe needle is viewed through a binocular microscope (Figure 6). A voltage pulse of short duration (30 to 50 ns) is produced within the probe head and applied to the device under test via the probe needle (Figure 4). A current transformer in series with the probe needle produces an output voltage proportional to the instantaneous current. As the voltage and current sense-lines are both terminated in 50-Ω loads, wide bandwidth operation is possible with a sampling oscilloscope. The bandwidth of the complete prober is limited by the current transformer and is 300 MHz with the Hewlett-Packard 1411A-1425A oscilloscope. The overall testing facility is shown in Figure 7.

The circuit diagram of the probe head is shown in Figure 8. A negative pulse from a pulse generator is brought into the probe head through the pulse input jack. Since the voltage amplifier stage is in an emitter-follower configuration, the pulse amplitude at the probe needle will be essentially equal to that of the input voltage pulse. The maximum pulse input to the probe head should never exceed the DC supply voltage and the latter is limited to 50V.

The emitter of Q1 is connected to the probe-needle support at which point the voltage waveform is sampled. This waveform has its output at the terminal labelled "V out" and is terminated at the oscilloscope in a 50-Ω load. The probe-needle support is a short hollow tube which passes through the centre of a current transformer which produces a voltage proportional to the current in the probe-needle support. The output of the current transformer is terminated at the oscilloscope in a 50-Ω load. The current transformer has a transformation ratio of 5 mV/mA. Small phase shifts may be corrected by lengthening or shortening the voltage pulse line from the probe head to the oscilloscope input.

A typical application of the probe is shown in Figure 4. Here the probe is being used to measure the V I characteristics of a tin-dot contact to a Gunn-effect diode mounted in a small microwave device package.

In conclusion, a simple prober has been described which will display the I vs. V characteristics of unpackaged components in the range 0 to -50V and to a maximum current of 8 A. Although the prober was developed for characterizing Gunn-effect diodes, it may also be used for displaying the characteristics of junctions in microcircuits or any resistive element which can be measured with reference to ground.

3.2.3 Graphical Display of the I vs. V Characteristics

Let U_p be the amplitude of the voltage pulse applied to the diode and I_p the amplitude of the resulting current pulse. In order to plot I_p vs. U_p with an electromechanical recorder, it is necessary to convert the pulses into DC signals proportional to their amplitudes. One can filter the pulses and apply their average values to the xy recorder. The circuit used is shown in Figure 2 on Page 66 of this Report.

Let t_p and f_p be the duration and the frequency of the pulses. If $R_xC_x >> f_p^{-1}$ and $R_yC_y >> f_p^{-1}$, the voltages applied to the xy unit are

$$U_x = \overline{U} = f_p t_p U_p$$

and

$$U_y = R\,\overline{I} = f_p t_p R_s I_p \quad .$$

Therefore, the quantities plotted are the pulse heights U_p and I_p except for known scale factors. As $|U_p|$ is increased slowly from zero, one obtains directly the current vs. voltage characteristic of the diode, if $R << U_p/I_p$, $I_y/I<<1$, and $\left|\frac{\tau dU}{U dt}\right| << 1$. Here, τ is the largest time constant associated with the system: it is equal to R_xC_x, R_yC_y, or is determined by the xy recorder itself.

As long as the current pulse remains rectangular, it is possible to plot the characteristic beyond the oscillation threshold of a diode. The current intensity plotted is then the average oscillation current because the pulse duration is much larger than the oscillation period.

The method is very convenient and allows the plotting of a curve in a few seconds. One of the plots obtained is shown in Figure 3 on Page 66 of this Report.

In practice, difficulties arise with thin, highly-doped diodes because both R and f_pt_p must be made small (to preserve accuracy and reduce heating), so that U_y becomes so small (less than 5 mV) that it is difficult to obtain a plot free of drift and noise. Then, instead of plotting the average values of U and R I, one can use a synchronous amplifier to amplify and convert one of their harmonics--usually, the fundamental--into a DC signal suitable to drive the xy recorder. This method is effective, although slightly more complex than the previous one.

In the average-value method (Page 66 of this Report), the residual voltage U_r between pulses must be zero. More precisely, if a relative error α is admissible, U_r must satisfy the condition:

$$|U_r/\overline{U}| < \alpha,$$

i.e.,
$$|U_r/U_p| < \alpha f_p t_p \quad .$$

If the duty factor $f_p t_p$ is 10^{-3} and if α is 10^{-2}, U_r/U_p must be less than 10^{-5} in magnitude. This condition is more stringent than the following, which is used when the only requirement is that the dissipation due to U_r be small:

$$(U_r/U_p)^2 << f_p t_p, \text{ e.g., } |U_r/U_p| < \sqrt{0.1 f_p t_p} = 10^{-2}.$$

4. MICROWAVE PERFORMANCE

Several devices were tested for microwave performance. DC tests on encapsulated diodes failed because the devices were destroyed before any oscillation could be observed.

Unencapsulated bulk diodes, typically 0.1 mm long, were mounted in a microstrip pressure-contact connected to a tunable triple-stub coaxial line. Bias voltage pulses of 0.25 μs duration were applied at a frequency of 1 kHz (sec. 3.2.1). Since the diodes were not designed for optimum microwave generation, the output power and efficiency were usually modest, e.g., 0.65 W max. and 2.9% max., both at 1.08 GHz. The bias polarity could be inverted with little change in performance, which indicates that the devices fabricated were symmetrical.

5. CONCLUSION AND SUMMARY

Adequate facilities were developed both for DC and pulse tests of unencapsulated diodes. The microwave testing of such diodes was also performed satisfactorily but was not refined sufficiently to yield efficiencies greater than a few percent.

More experimentation is needed to determine the best method of bonding and to achieve encapsulation of the diodes.

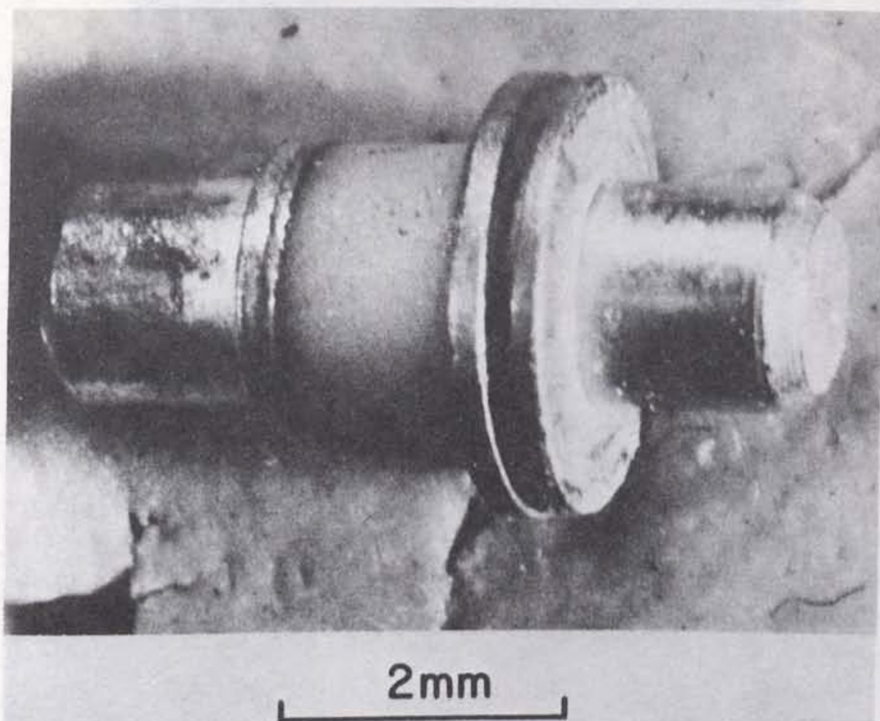

(a) External view

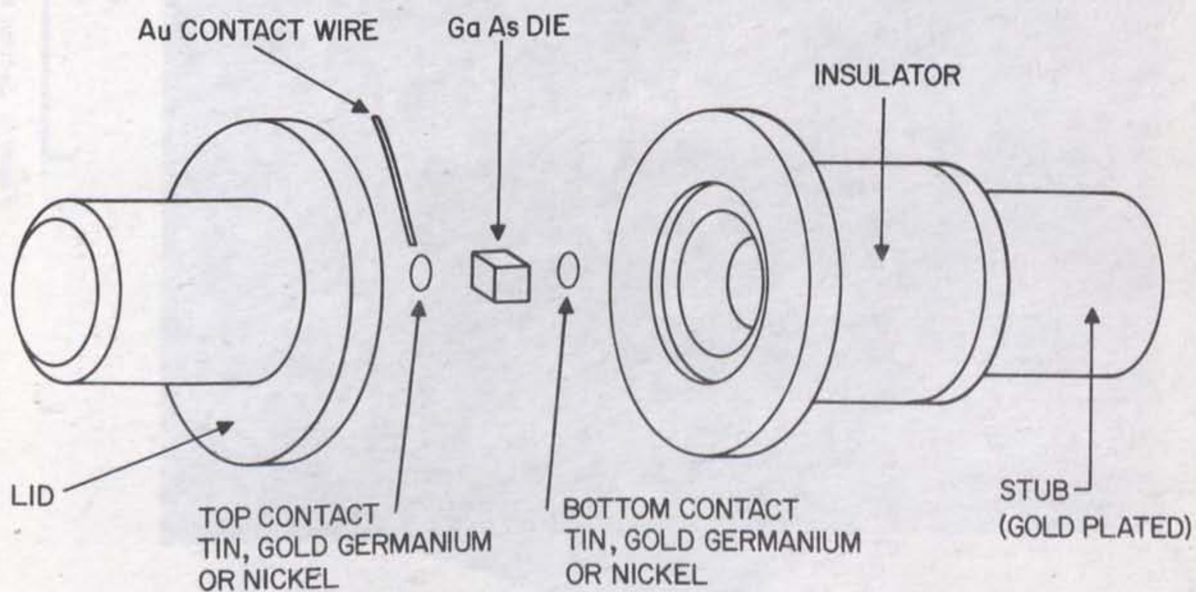

(b) Internal view

Figure 1. Encapsulation of a GaAs chip

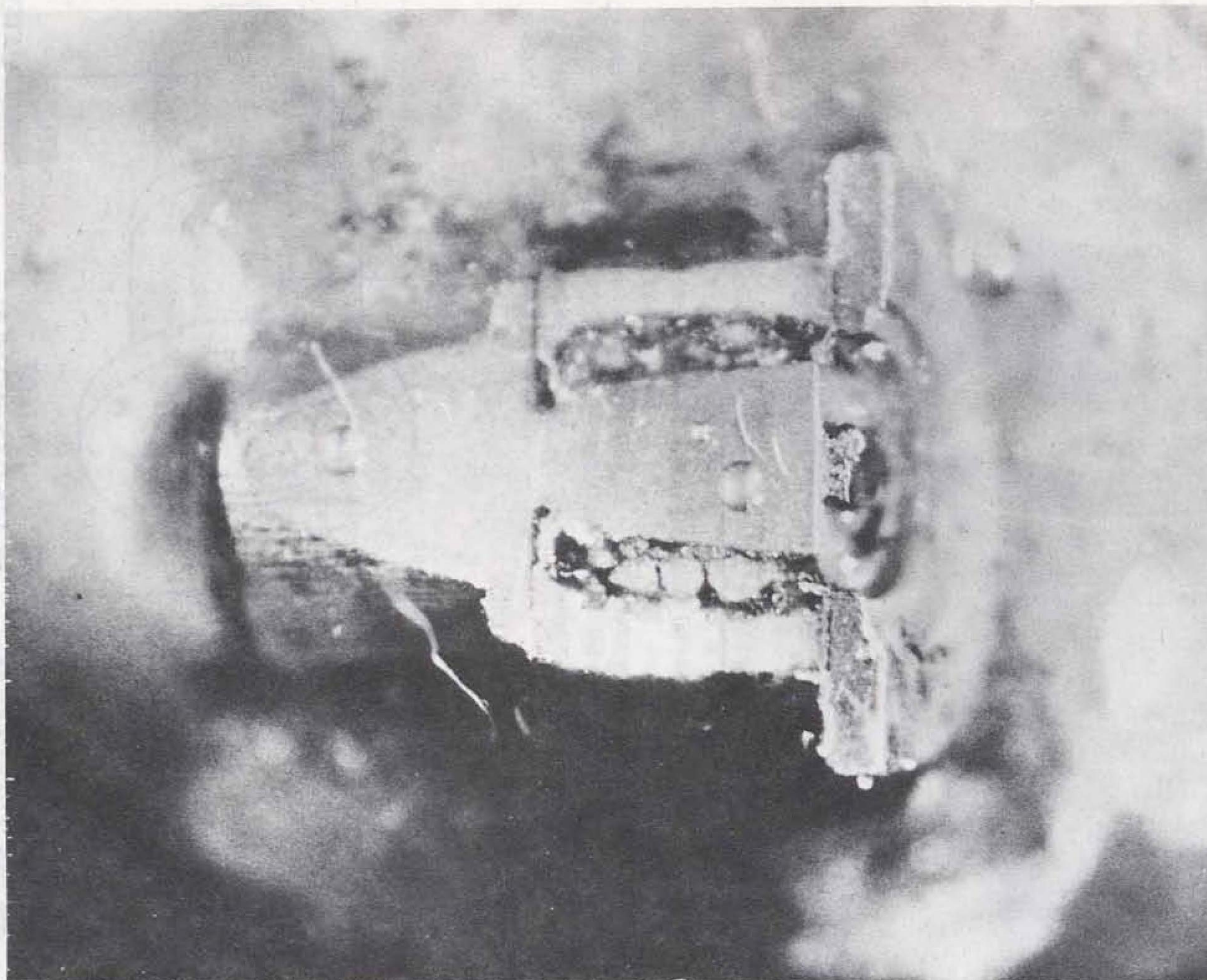

Figure 2. Section through a plastic-encapsulated diode

(a) Needle design

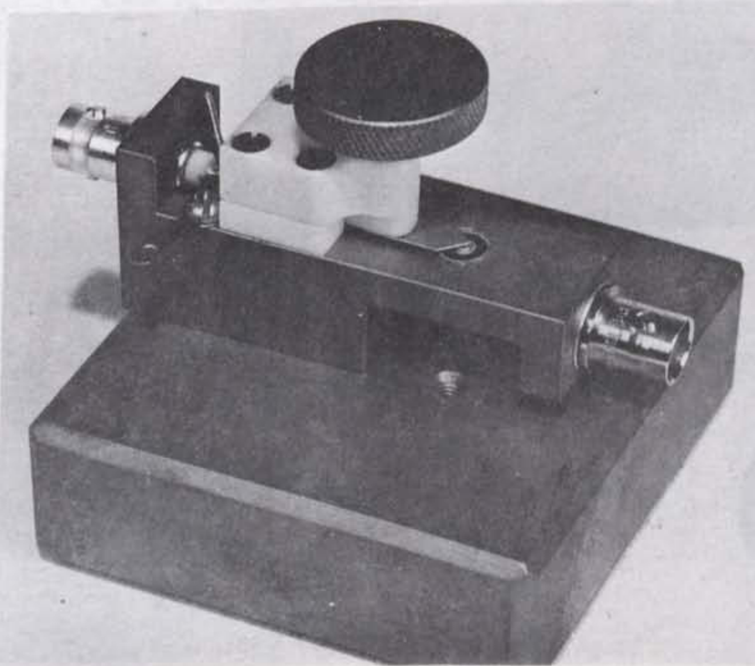

(b) Strip-line design

Figure 3. Stations for testing unencapsulated GaAs chips

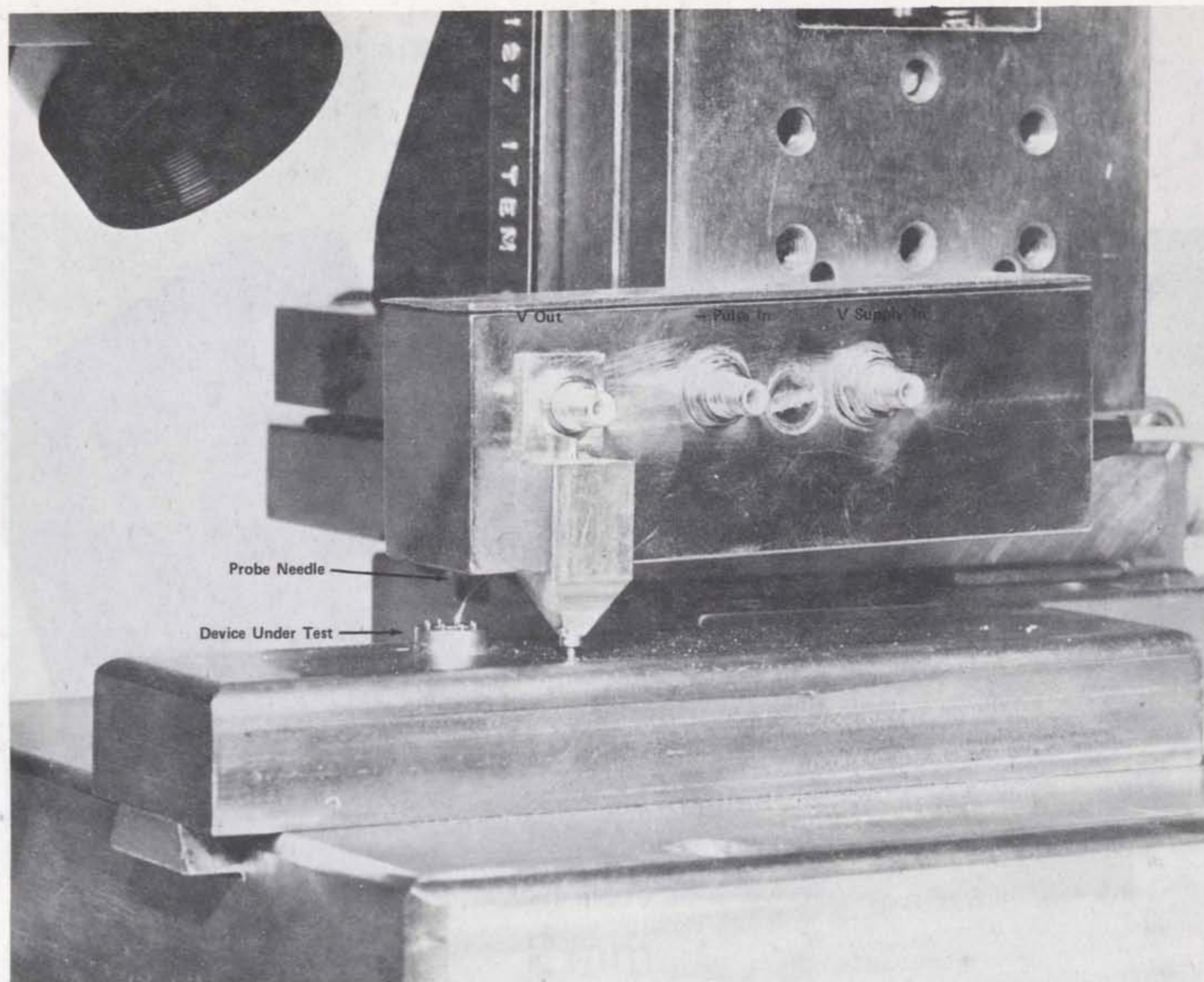

Figure 4. Detail of Figure 6 showing a tin-dot contact Gunn diode inserted for testing

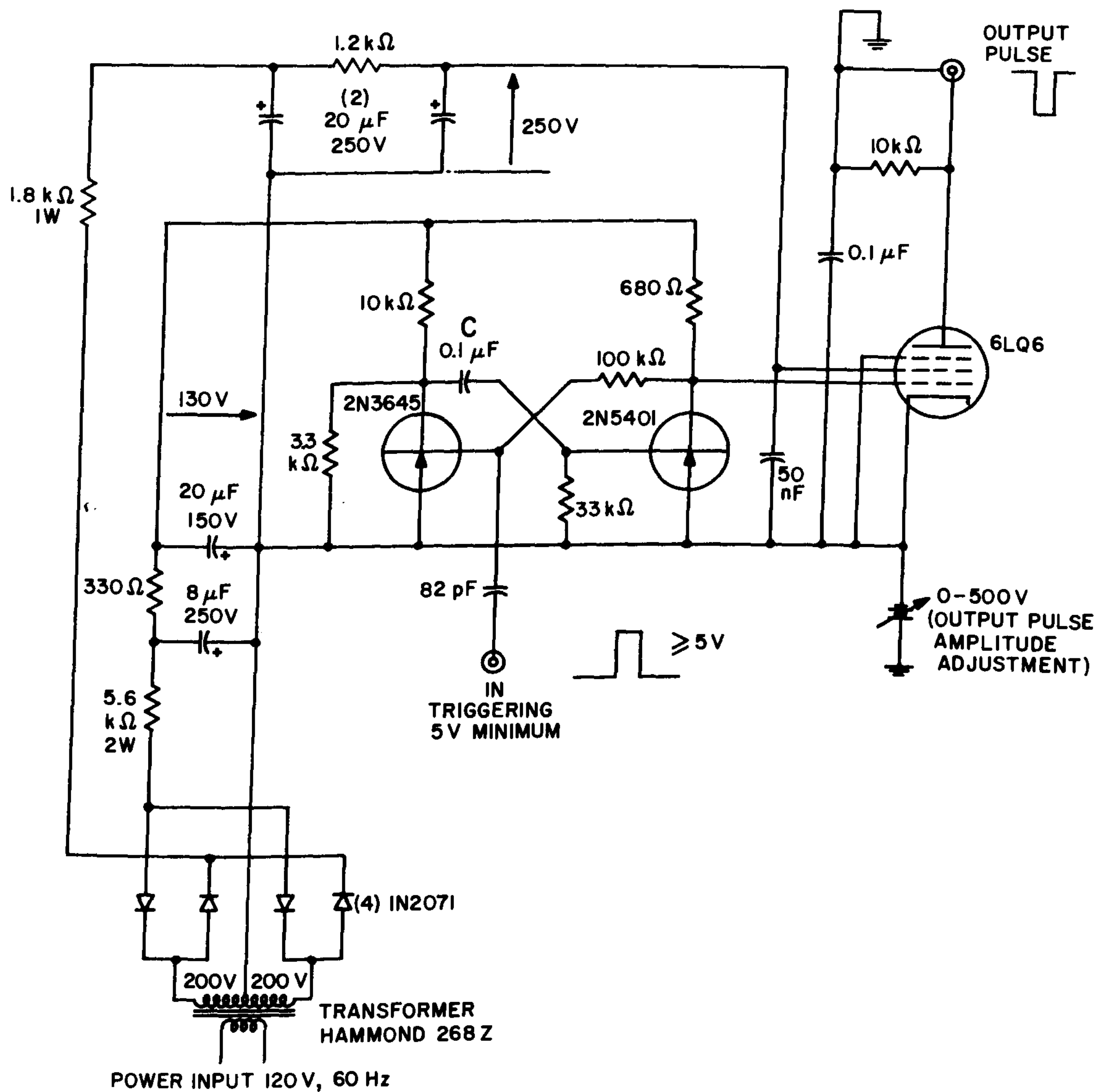

Figure 5. High-voltage pulse-generator circuit diagram. (Auxiliary circuits not shown.)

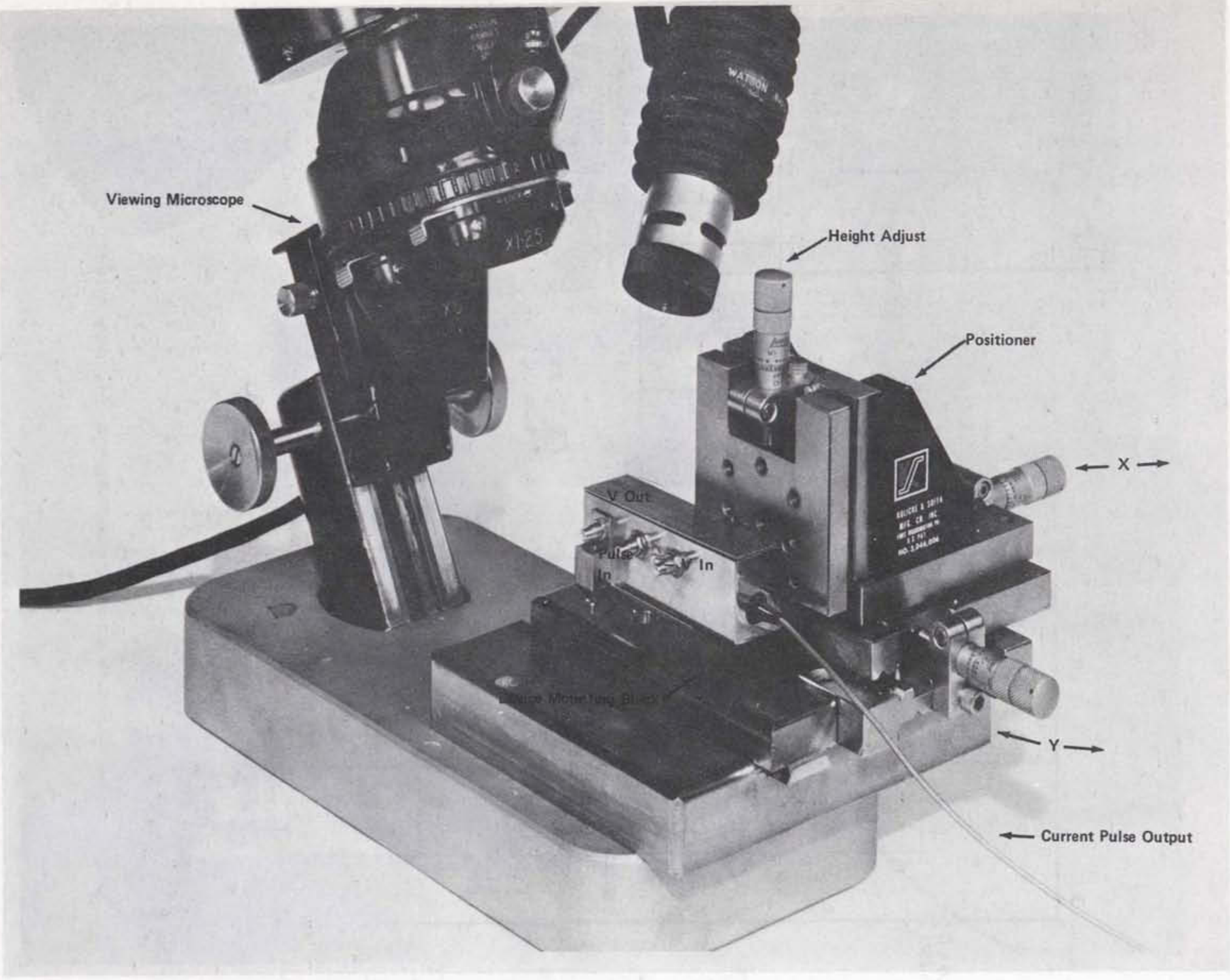

Figure 6. General view of the high-current pulser and its mechanical mounting

PULSER CONNECTIONS

OSCILLOSCOPE
SWEEP
SYNC OUT
1425A
A
B
140A
1411A
A vs B
TWO-CHANNEL SAMPLER
6dB
A INPUT
50Ω
CABLE
SYNC
B INPUT
50Ω
20dB
PULSE GENERATOR
PROBE HEAD
Vout
Vin
HP214A
VOLT ADJ.
TRIGGER LEVEL
VOLTAGE RANGE
TRIG IN
PULSE OUT
POWER SUPPLY
-40v

Figure 7. Diagram of the high-intensity current-voltage measuring facility

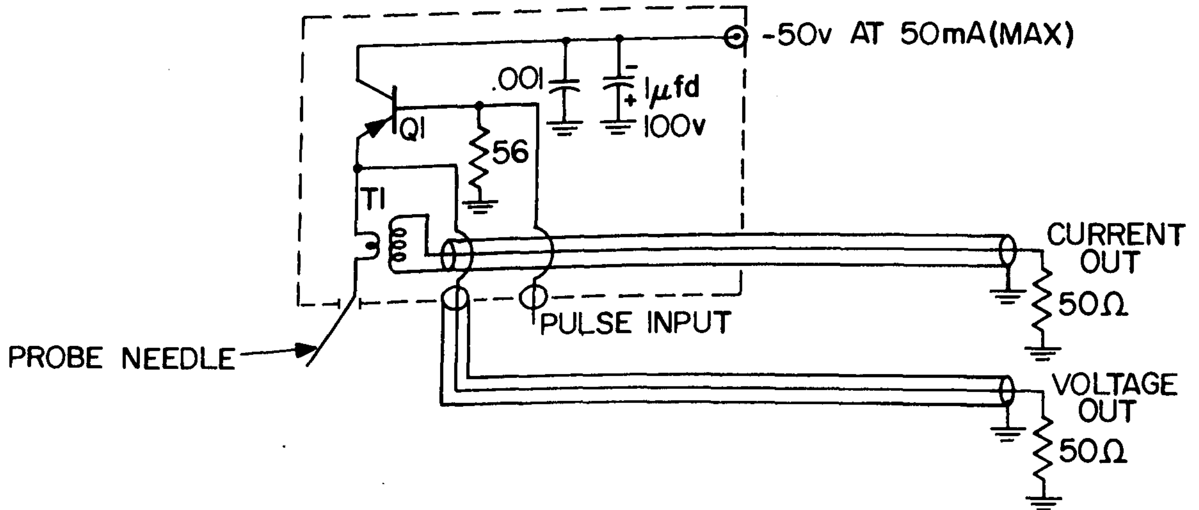

Figure 8. Circuit diagram of the high-current pulser

THIS PAGE INTENTIONALLY LEFT BLANK

GALLIUM ARSENIDE AND DEVICES AND THE GUNN EFFECT

by

W.D. Edwards, W.A. Hartman, A. Torrens and D.L. Butler

PART 7

THEORY OF STEADY HIGH-FIELD DOMAINS

by

A. Torrens

ABSTRACT

A high-field domain (HFD) is defined to be small if, between the uniform-region field E_U and the field maximum E_d, the velocity-field characteristic can be approximated by a parabola. An HFD is said to be quasi-neutral if, at all points, $|n-N| \ll N$. It is shown analytically that, for a carrier diffusivity D, the domain excess voltage U_d is proportional to $\sqrt{D(E_p-E_U)/N}$. Computations confirm this result, and show that (1) $U_d \propto N^{-1/2}$ holds for a quasi-neutral domain even if it is not small; (2) the domain length, minimum at $E_U = 0.27$ MV/m, tends to infinity as $E_U \rightarrow E_p$.

The new shape found for the U_d vs. E_U characteristic implies the existence of small-HFD oscillations near threshold, in agreement with particular small oscillations observed experimentally by some workers.

PART 7

THEORY OF STEADY HIGH-FIELD DOMAINS

1. INTRODUCTION

A common form of large-signal instability in a negative-differential-conductivity material is the high-field domain (Figure 1). For a domain propagating steadily in a given material, the outside field E_U and the domain excess voltage U_d, defined by $U_d \stackrel{d}{=} \int_{-\infty}^{+\infty} (E-E_U)dz$, are related. The relation is very useful, especially in the form of the plot of U_d vs. E_U [1,2], referred to as the *domain characteristic* C (Figure 2). If a steady domain propagates in a diode of length L subjected to a voltage U, the following relation holds [1,2]: $U_d = U-E_U L$. It shows that the "operation point" representing a steady domain in the diode is the intersection of the domain characteristic C and the "*device line*" D, plot of $(U-E_U\,L)$ vs. E_U. The operation point is important. For example, if it does not exist (C and D non-intersecting), it means that no HFD can exist in the diode. If the operation point exists, the corresponding field E_U yields the domain velocity ($c \simeq v(E_U)$) and, hence, the free-oscillation frequency c/L.

2. STUDY OF SMALL STEADY HFD'S

An HFD is said to be *small*, if, over the field range $[E_U, E_D]$, (Figure 1), the v vs. E characteristic of the material can be represented with sufficient accuracy by the second-order expansion at the peak point P (Figure 3):

$$v \simeq v_P + \tfrac{1}{2}\left(\frac{d^2v}{dE^2}\right)_P (E-E_P)^2 \tag{1}$$

If the diffusion coefficient D of the electrons over the same range $[E_U, E_D]$ is quasi-constant, the equal-areas rule [3] applies so that [4]

$$\frac{E_D-E_P}{E_U-E_P} = -2 \tag{2}$$

An HFD is said to be *quasi-neutral* if $|n-N| \ll N$ throughout the domain (cf. Figure 1). A small quasi-neutral domain is symmetric with respect to the plane $z = z_D$ where the field is maximum. The domain length L_d or, more generally, the distance over which E exceeds a given value chosen between E_U and E_D, is proportional to $N^{-\frac{1}{2}}$ [4]. Butcher obtained similar results [5], using a piece-wise linear approximation of v vs. E instead of eq. 1. The excess voltage U_d of the same small, quasi-neutral domain is given by the relation:

$$U_d = 12 \sqrt{\frac{\varepsilon D}{Ne} (E_U - E_P) / \left(\frac{d^2v}{dE^2}\right)_P} \qquad (3)$$

This relation shows that, for a *small* domain, U_d is proportional to $\sqrt{E_P - E_U}$: the domain characteristic C near P is approximately a parabola with a horizontal axis. This is in contradiction to the shape found by Copeland[1,2] (Figure 2).

3. COMPUTATIONS

Because the above conclusion contradicts Copeland's findings[1,2], direct computations (using no assumptions regarding the size or the quasi-neutrality of the domain) were carried out for verification purposes. The electron diffusivity was assumed to be constant, so that the velocity c of a domain with a given outside field E_U was known: $c = v_U$ [3]. The differential equations describing the steady HFD are [3,6]

$$\left.\begin{aligned} D\frac{dn}{dz} &= (v-c)\, n, \\ \frac{dE}{dz} &= \frac{e}{\varepsilon}\, (n-N), \\ \text{and} \quad \frac{dU_d}{dz} &= E-E_U. \end{aligned}\right\} \qquad (4)$$

The particular numerical values of e/ε, D and v(E) (Figure 3) are fairly representative of n-type GaAs, and are as chosen in ref. 6:

$$\varepsilon = 12.53\ \varepsilon_0,$$

$$D = 0.015\ \text{m}^2/\text{s},$$

$$v = \frac{\mu_a + G\,\mu_b}{1 + G}\, E,$$

with $\mu_a = 0.6\ T^{-1}$, $\mu_b = 0.025\ T^{-1}$, and $G = \begin{cases} 0 & \text{if } E \leq E_0 \\ \left(\dfrac{E-E_0}{E_1}\right)^2 & \text{if } E > E_0, \end{cases}$

with $E_0 = E_1 = 222.2$ kV/m. μ_a and μ_b are the electron mobilities in the lower and upper sub-bands of the conduction band, and G is the population ratio n_b/n_a.

Results

Solving numerically eq. 4 for a given value of E_U yields the corresponding value of U_d, hence one point of the domain characteristic. Figure 4 shows plots of U_d and L_d vs. E_U for various values of N. The shape shown in Figure 2b for the domain characteristic C is confirmed. Figure 4 also shows that, as E_U increases from its minimum $E_{Umin} \simeq 0.136$ MV/m, the domain length L_d first decreases, then increases again towards infinity as $E_U \to E_P$. This domain broadening occurs because NDC effects are very weak near P (Figure 3) and are overcome by diffusion

In Figure 5, $U_d\sqrt{N}$ (instead of U_d in Figure 4) is plotted as a function of E_U, together with the theoretical curve representing eq. 3. This figure shows that: (a) for $E_U \varepsilon [0.31$ MV/m, $E_P]$, the computations and eq. 3 agree, and $U_d\sqrt{N}$ is practically independent of N. (b) At lower values of E_U, computations and analysis disagree because the domains are no longer "small" (sec. 2). However, for $N > 10^{20} m^{-3}$, $U_d\sqrt{N}$ remains independent of N down to lower values (~0.23 MV/m) of E_U. This apparently corresponds to domains which are quasi-neutral but not small.

In Figure 6 $L_d\sqrt{N}$ (instead of L_d in Figure 4) is plotted as a function of E_U. $L_d\sqrt{N}$ is independent of N for $E_U \simeq E_P$. If the condition

$$N > N_{dif} \tag{5}$$

is satisfied with N_{dif} $10^{20} m^{-3}$, NL_d^2 is practically independent of N for $E_U \varepsilon [0.14$ MV/m, $E_P]$.

Over the somewhat more restricted range $E_U \ \varepsilon \ [0.15, 0.29]$ MV/m, if the condition 5 is satisfied, $L_d\sqrt{N}$ is fairly independent of E_U as well: $NL_d^2 \simeq 10^{10} m^{-1}$. This equation is related to the critical value of NL^2 below which diffusion-dominated diodes are stable [2, 7-10].

Figure 7 shows that, for N small, the ratio L_{de}/L_{ac} of the depletion and accumulation layer lengths increases rapidly from 1 as E_U decreases below E_P. However, for common values of N, namely for $N > 10^{20} m^{-3}$, this ratio remains less than 4.

4. DISCUSSION

The parabolic shape of the domain characteristic C near P (Figure 2b) implies that if a diode is biased near threshold, the device line can intersect the domain characteristic at three points, M_1, M_2, M_3 (Figure 2b), instead of two (M_1 and M_2) with Copeland's curve[1,2].

The domain corresponding to M_2 would usually be unstable [11] but either of the domains represented by M_1 and M_3 would be stable. The domain at M_3 would be small (U_d small) and fast ($c = v(E_{U3}) \simeq v_P$), and would disappear at higher diode voltages. Figure 4 and 2b show that the operation point M_3 can be obtained over a range of values of U/L which is relatively

small but increases as L decreases. This would explain why Foyt observed, only in short diodes, one mode of oscillation just above threshold, and another mode at higher voltages [12].

Hakki observed a particular mode of oscillation, just above threshold, over a voltage range which increased as the product NL decreased [13]. This mode also could be interpreted in terms of small HFD's. Similarly, Prew obtained small incoherent oscillations in InP diodes at threshold, and larger, spiky oscillations at higher voltages [14].

According to Butcher [5], and Copeland [1,2], NL_d^2 is finite as $E_U \to E_P$, and U_d is a linear function of $E_P - E_U$ near P. These results disagree with the curves shown in Figure 6 and 2b respectively. This apparent disagreement arises because Butcher assumed a v vs. E characteristic (Figure 3) for which dv/dE is discontinuous at P, so that $(d^2v/dE^2)_P$ is not defined (eq. 1). More specifically, the domain length L_d is related to the differential Debye length in the uniform region: $L_{D\delta U}\ \sqrt{\varepsilon D/Ne\mu_{\delta U}}$. As E_U approaches E_P, $L_{D\delta U}$ remains constant in Butcher's theory, but with the more realistic model used here, it becomes infinite because $\mu_{\delta U}$ tends to 0.

The disagreement between Copeland's conclusions and those obtained here could be explained as follows. Near the uniform region, the electron concentration n and the field E satisfy approximately the equation [6, pt. 2-7, sec. 3]:

$$D_U \frac{dn}{dx} = N\ (\mu + E\frac{d\mu}{dE})_U\ (E-E_U) - [c - v_U + \frac{Ne}{\varepsilon}\ \frac{dD}{dE}_U]\ (n-N)$$

Copeland's equation 8 is similar but does not contain the terms in $d\mu/dE$ and dD/dE. (see also ref. 15). These omissions are of little consequence at low values of E_U, where μ and D are fairly constant, but become significant near E_P. In particular, at E_P, μ is roughly equal to its equilibrium value, but the differential mobility $\mu + E\frac{d\mu}{dE}$ is zero. (If a piecewise linear v vs. E curve is assumed, then $d\mu/dE$ is zero, hence the accidental agreement between Copeland and Butcher.)

Finally, the shape of the I vs. U characteristic of a diode near threshold (Figure 8) is of interest. If A is the diode cross-section, $I = A\ Ne\nu_u$ and, using eq. 1, we obtain

$$I - I_P \propto (E_U-E_P)^2 \quad . \tag{6}$$

The equation

$$U - U_P = L(E_U - E_P) + U_d \tag{7}$$

and eq. 6 show that $I-I_P \propto (U-U_P)^2$ when there is no domain ($U_d = 0$). With a small domain present, eq. 3 and 7 show that, when $E_U \to E_P$, $U - U_P \propto (E_P-E_U)^{1/2}$, so that

$$I - I_P \propto (U-U_P)^4 \quad .$$

The shape of the I vs. U characteristic obtained is shown in Figure 8. With the piece-wise linear characteristic used by Butcher[5], one would obtain $I - I_P \propto U-U_P$ both below and above threshold, and the I vs. U characteristic would have, at P, a slope discontinuity which is absent from Figure 8. If, near P, the relation $U_d = L_0(E_P-E_U)$ predicted by Copeland[1,2] were exact, eq. 7 would become

$$U-U_P = (L-L_0)\ (E_U-E_P) \quad .$$

Therefore, the I vs. U curve would have a cusp at point P in the usual case when $L > L_0$. Intuitively, this would be less acceptable than the smooth curve shown in Figure 8.

5. CONCLUSION

If a high-field domain (HFD) is small (eq. 1) and satisfies the equal-areas rule, eq. 2 applies. If an HFD is small and quasi-neutral, eq. 3 applies, and the domain characteristic C has near P the shape shown in Figures 2b, 4 and 5. Consequences of this are discussed in sec. 4.1.

If an HFD is diffusion-dominated (but not necessarily small), the excess voltage U_d and length L_d corresponding to a given outside field E_U are proportional to $N^{-\frac{1}{2}}$ (Figures 5 and 6). Contrary to previously-reported conclusions, L_d increases indefinitely as E_U approaches E_P (sec. 4.2).

The above results can be compared with those relevant to the "Triangular" HFD, which occurs when diffusion is negligible[5,16,17]. Then, U_d and L_d corresponding to a given E_U are proportional to N^{-1}. In all cases, the average excess field U_d/L_d appears to be independent of N and to depend only on E_U, just as does the domain field E_D when the equal-areas rule is satisfied[3].

6. REFERENCES

1. Copeland, J.A., *Electrostatic Domains in Two-Valley Semiconductors*, IEEE Trans. ED13, 189-191 (January 1966).

2. Copeland, J.A., *Stable Space-Charge Layers in Two-Valley Semiconductors*, J. Appl. Phys. 37, 3602-9, (August 1966).

3. Butcher, P.N., W. Fawcett and C. Hilsum, *A Simple Analysis of Stable Domain Propagation in the Gunn Effect*, Brit. J. Appl. Phys. 17, 841-50 (July 1966).

4. Torrens, A.B., *Small and Quasi-Neutral Domains in Negative-Differential Conductivity Materials*, J. Appl. Phys. 45, 3041 (July 1974); 46, 980 (February 1975).

5. Butcher, P.N. and W. Fawcett, *Stable Domain Propagation in the Gunn Effect*, Brit. J. Appl. Phys. 17, 1425-32 (November 1966).

6. Torrens, A.B., *Negative Differential Conductivity Effects in Semiconductors*, Ph.D. Thesis, the University of British Columbia, Vancouver, (1969).

7. Ridley, B.K., *The Inhibition of Negative Resistance Dipole Waves and Domains in n-GaAs*, Trans. IEEE ED13, 41-3 (January 1966).

8. Sasaki, A., and T. Takagi, *Conditions for the Space-Charge Wave Growth and Differential Negative Resistance in 'Two-Valley' Semiconductors*, Proc. IEEE 55, 732-2 (May 1967).

9. Hakki, B.W., *Amplification in Two-Valley Semiconductors*, J. Appl. Phys. 38, 808-18 (February 1967).

10. Harrison, R., *Simple Transient and Non-Linear Analysis of High-Field Domains in GaAs*, J. Phys. D1, 973-82 (August 1968).

11. Torrens, A.B., *Equivalent Circuit and Domain Stability of a Generalized Gunn Diode; Application to Tunable Diodes*, J. Phys. D 4, 705-17 (May 1971).

12. Foyt, A.G., and A.L. McWhorter, *Gunn Effect in GaAs*, Bull. Amer. Phys. Soc. 10, 383-3 (1965).

13. Hakki, B.W., and S. Knight, *Microwave Phenomena in Bulk GaAs*, Trans. IEEE ED13, 94-105 (January 1968).

14. Prew, B.A., *High-Field Current Instabilities in InP*, Electron. Lett. 7, 584-5 (23 September 1971).

15. Aas, E.J., *Topological Study of Domain and Layer Propagation in a Gunn Diode*, J. Appl. Phys. 40, 4673-5 (October 1969).

16. Heinle, W., *Basic Equations of Gunn Domain Dynamics*, Phys. Lett. 24A, 533-5 (1967).

17. Heinle, W., *Principles of a Phenomenological Theory of Gunn-Effect Domain Dynamics*, Solid State Electron. 11, 583-98 (June 1968).

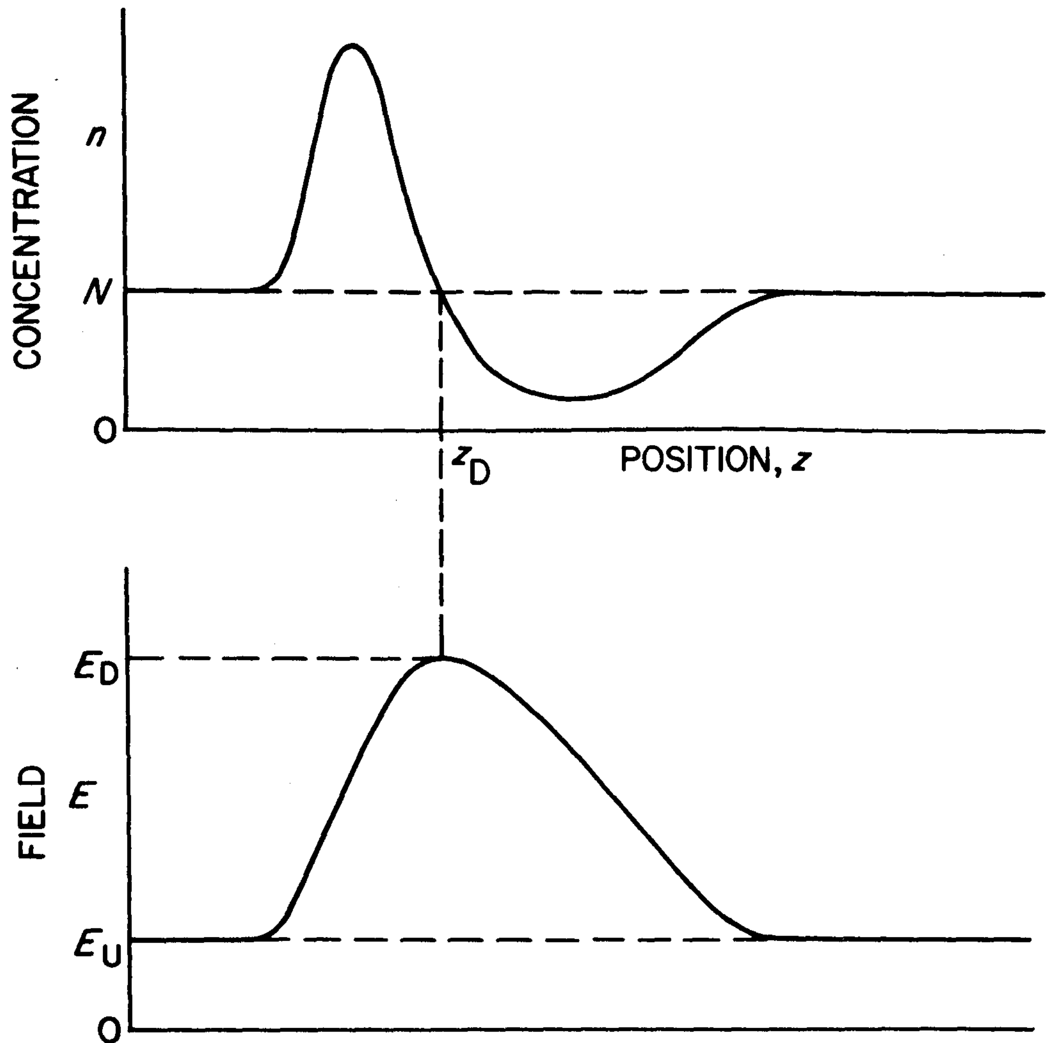

Figure 1. Steadily-propagating high-field domain (HFD) in an n-type negative-differential-conductivity (NDC) semiconductor: electron concentration n and electric field E as a function of distance z. Such a domain propagates with the electron stream at some 100 km/s. N is the doping concentration.

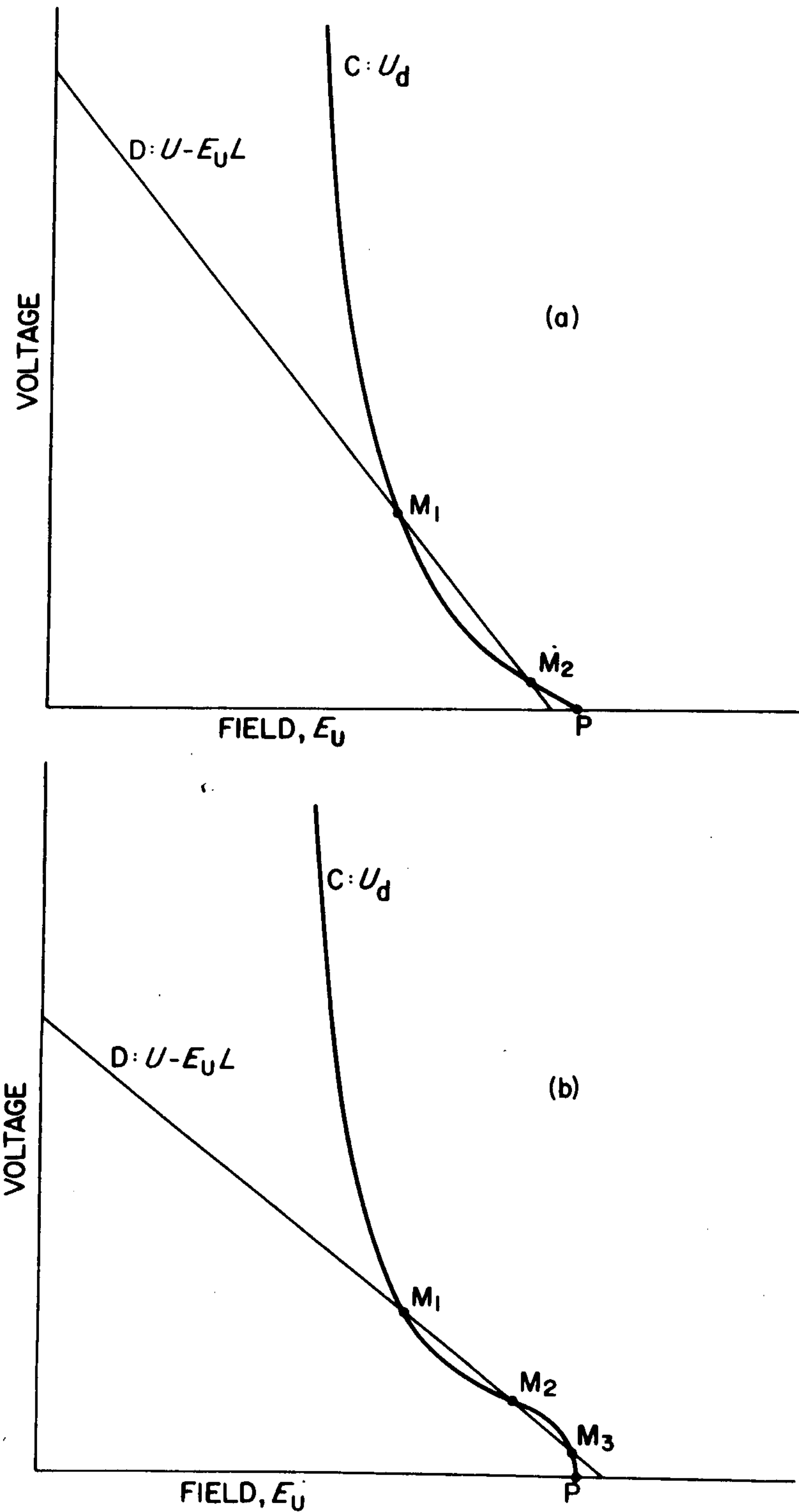

Figure 2. The domain characteristic C: domain excess voltage U_d vs. field E_U outside the domain, (a) according to Copeland [1,2], (b) according to the present analysis. D is the device line for a diode of length L subjected to a voltage U, and M is the operation point defining the steady domain in this diode.

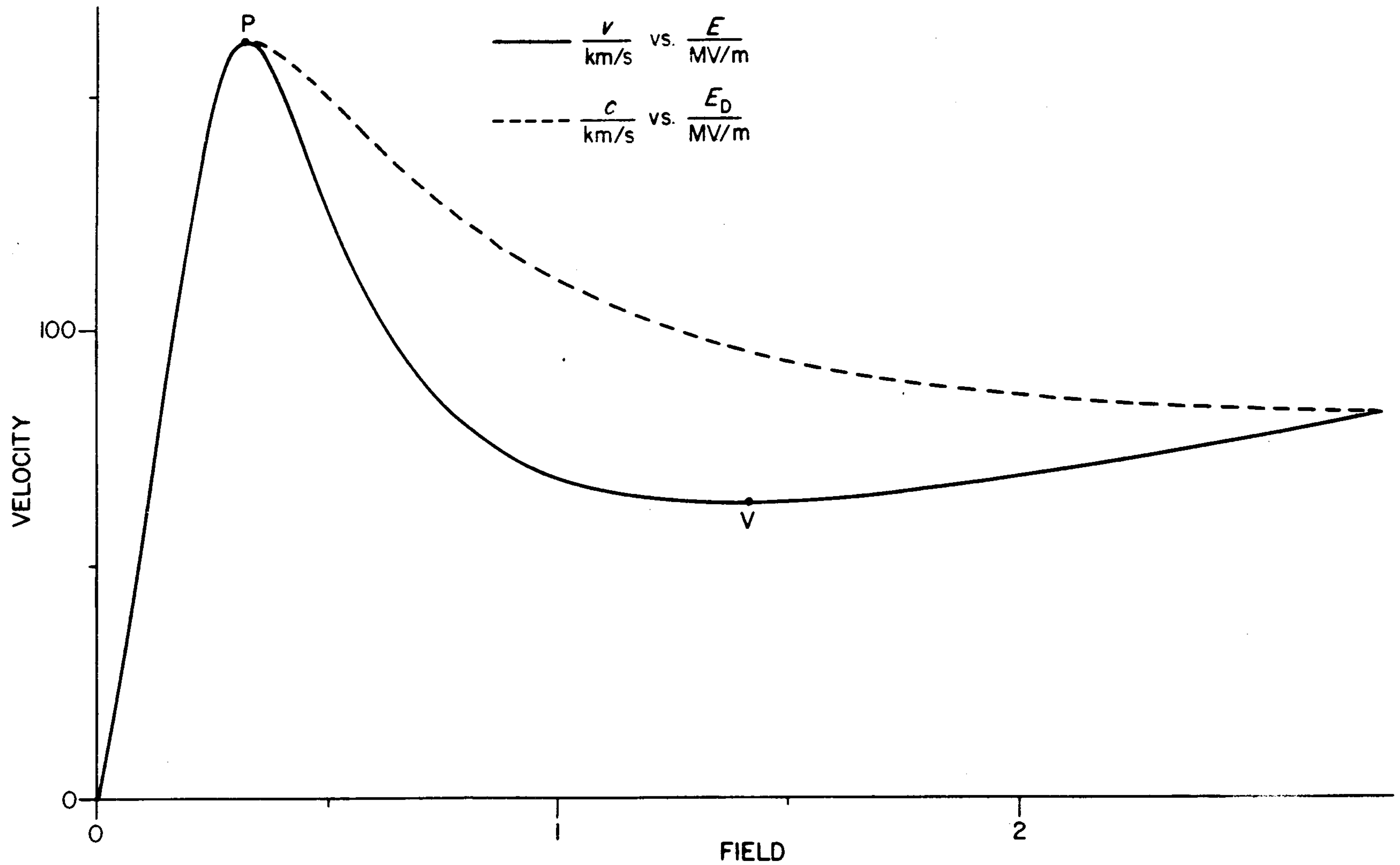

Figure 3. Electron velocity v vs. electric field E in n-type GaAs, at room temperature, as given by the analytical approximation used for the computations. Also shown is the relation between the velocity c and the maximum field E_D of a steadily-propagating domain, as obtained from the equal-areas rule [3].

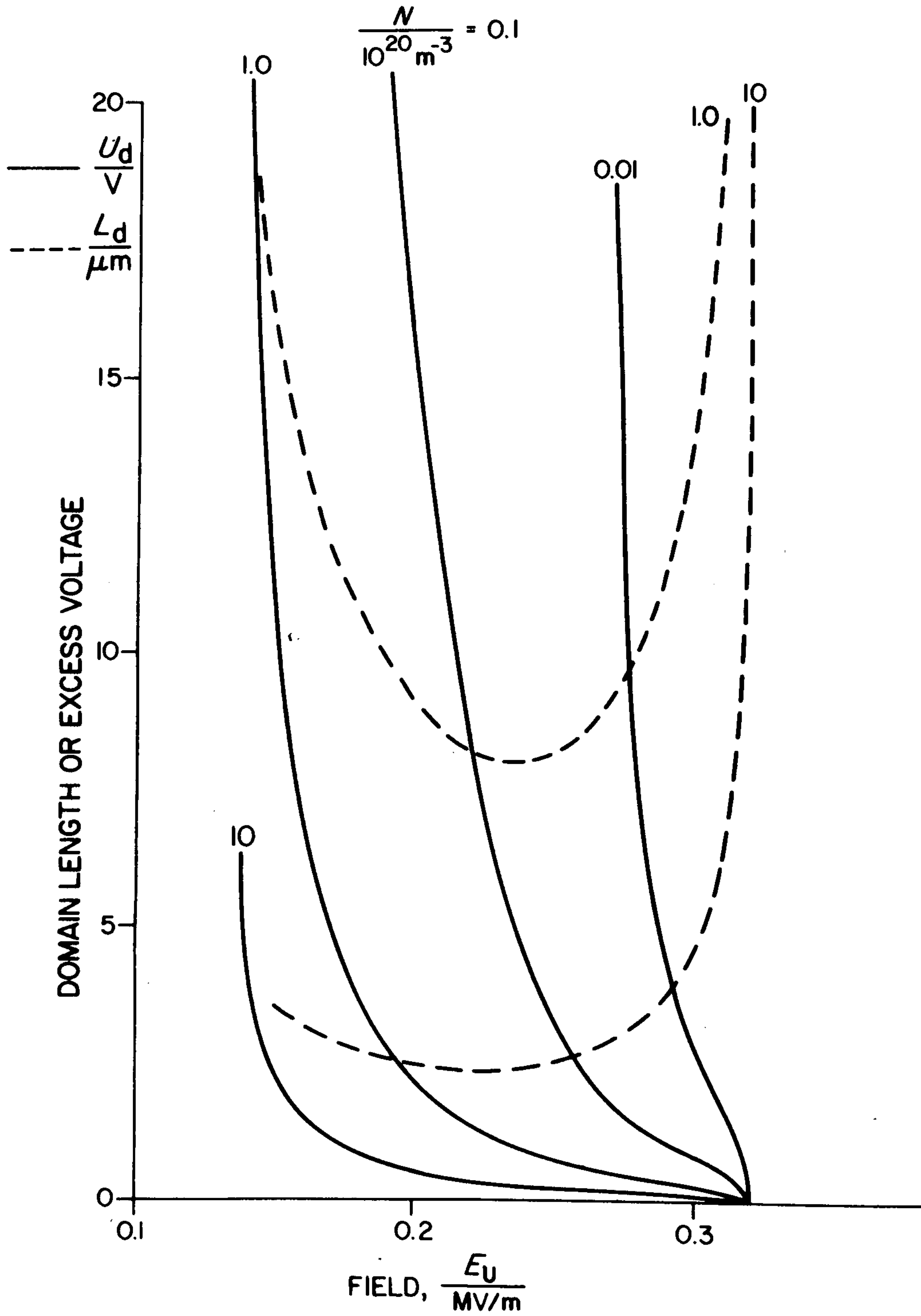

Figure 4. An HFD in GaAs. The excess voltage U_d and length L_d vs. the outside field E_U (cf. Figure 1), for various values of the doping N.

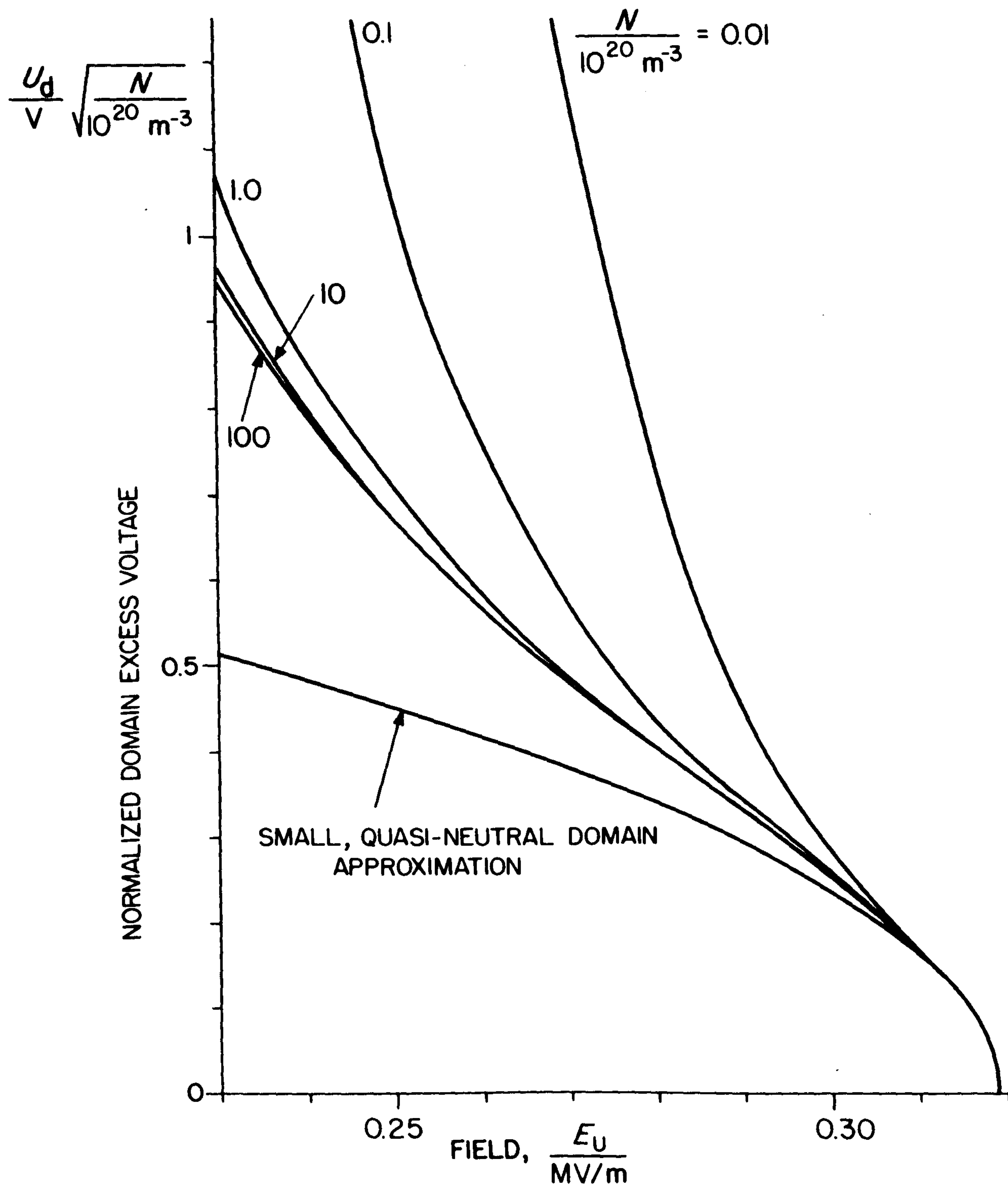

Figure 5. An HFD in GaAs: $U_d\sqrt{N}$ vs. E_U (see Figure 4).

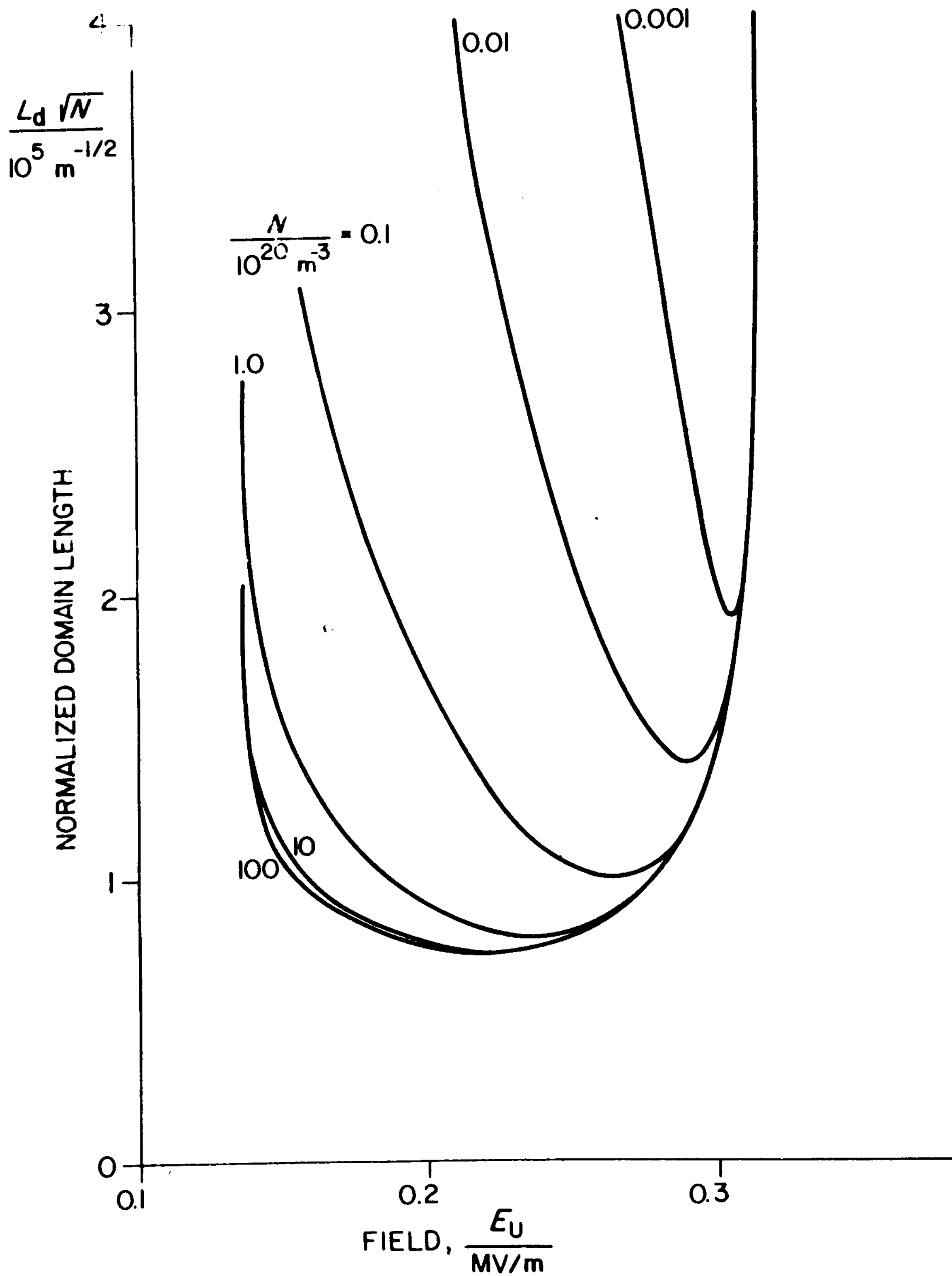

Figure 6. An HFD in GaAs: $L_d \sqrt{N}$ *vs.* E_U *(see Figure 4).*

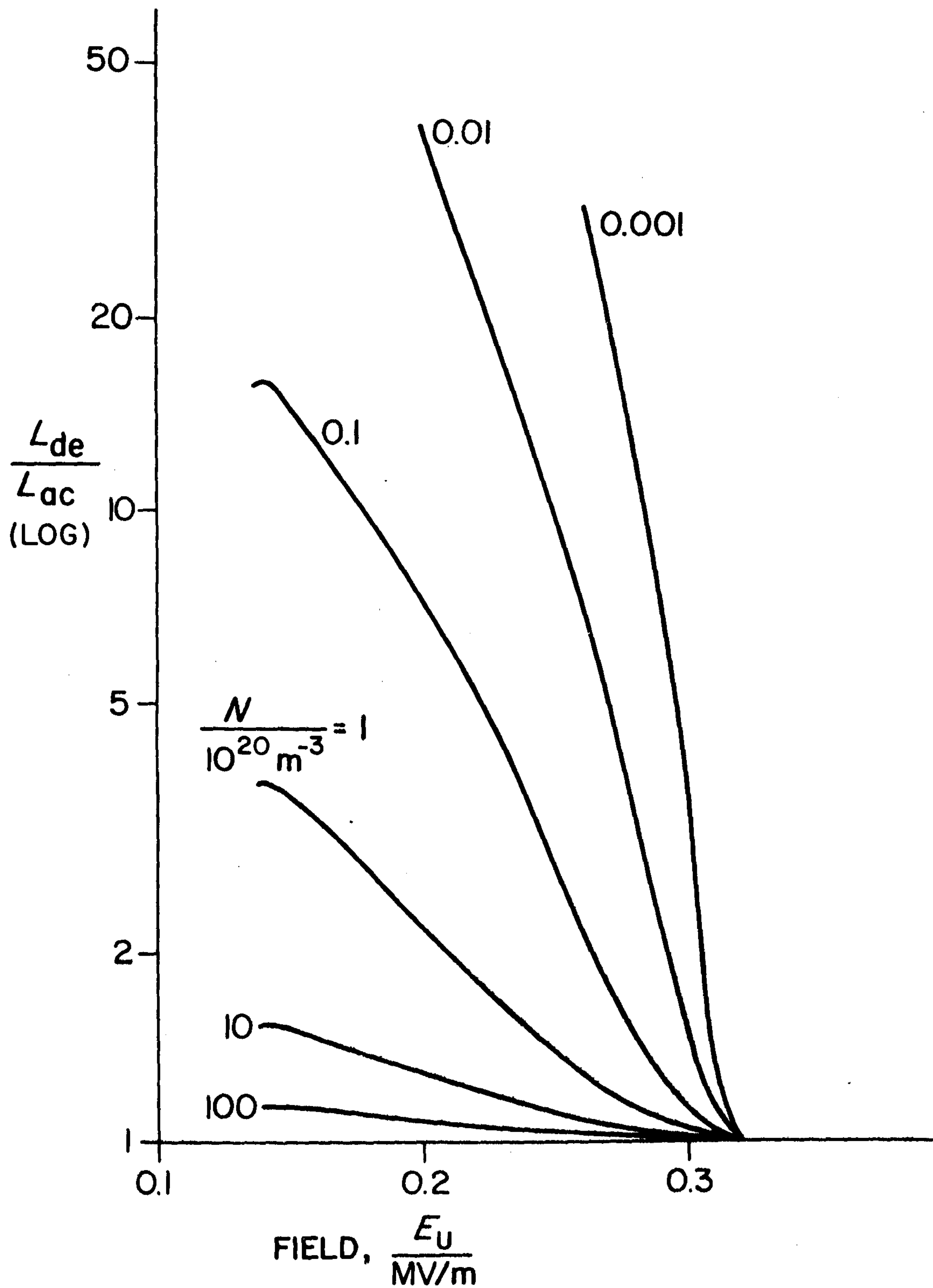

Figure 7. An HFD in GaAs: ratio L_{de}/L_{ac} of the depletion and accumulation layers lengths vs. the outside field E_U for various values of the doping N.

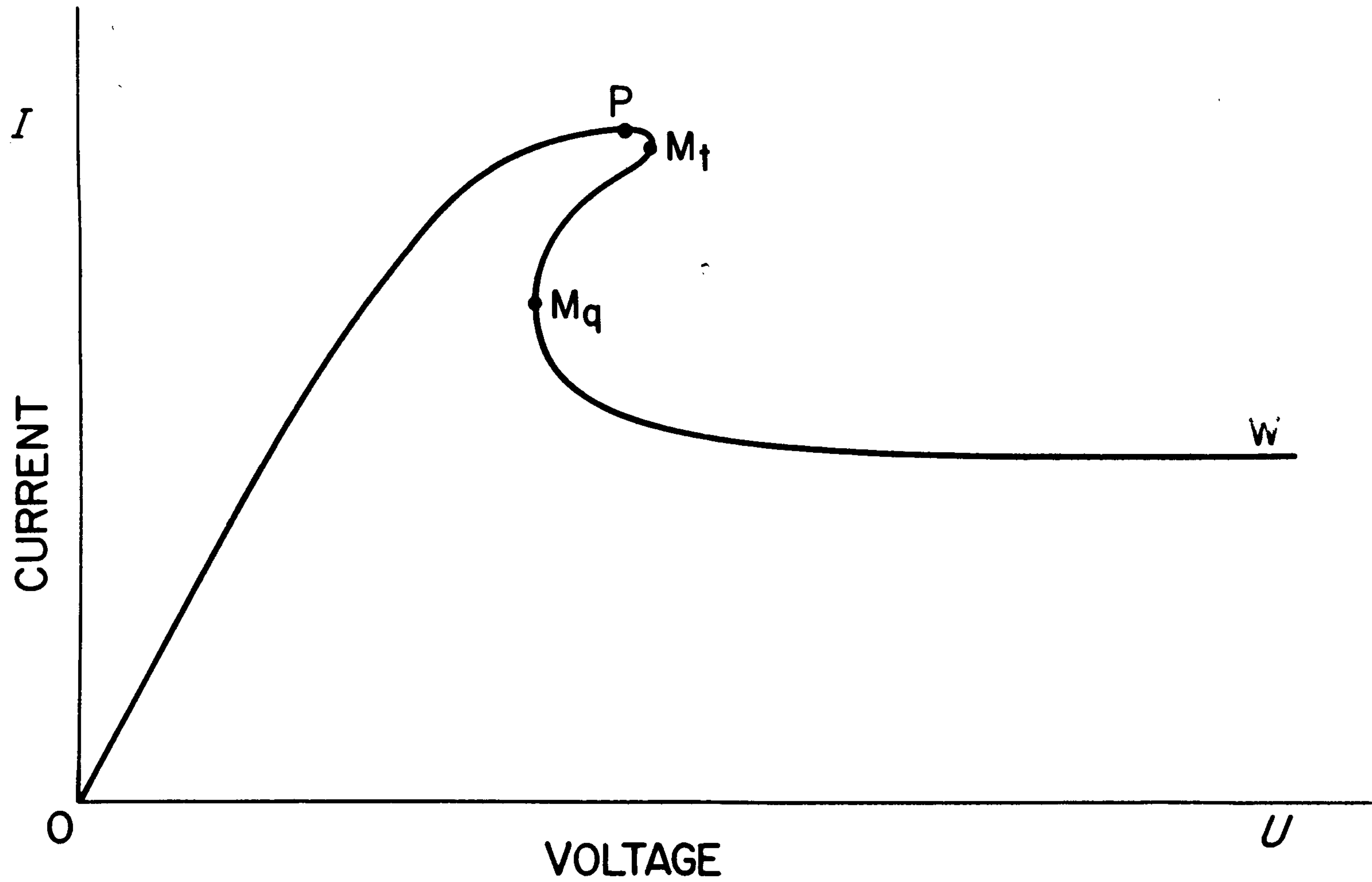

Figure 8. Current density J vs. voltage U of an NDC diode, without (arc OP) and with (arc PW) a steady HFD. The arc N_tM_q corresponds to an unstable HFD, in a diode biased through a zero external impedance [11].

THIS PAGE INTENTIONALLY LEFT BLANK

GALLIUM ARSENIDE AND DEVICES AND THE GUNN EFFECT

by

W.D. Edwards, W.A. Hartman, A. Torrens and D.L. Butler

PART 8

COMPUTER-SIMULATIONS OF NDC DIODES

by

A. Torrens

ABSTRACT

A computer model is used to simulate negative-differential-conductivity (NDC) effects in GaAs diodes. The simulations are focussed on parastability, a form of stability which occurs in diodes where the doping is sufficiently uniform and larger than about $1.1.10^{21} m^{-3}$. *In a parastable diode, above threshold, the field is uniform and below the peak field* E_p *except near the anode, where there is a stationary accumulation layer. If the bias is reduced below threshold, the current decreases but the parastable layer stays unless the doping increases towards the anode. If the doping increases towards the anode, the diode can be unstable over a range of bias, and parastable at high voltage, in agreement with experimental observations. If the bias voltage is modulated, a parastable diode exhibits negative AC conductance and can act as an amplifying device, as observed experimentally.*

PART 8

COMPUTER-SIMULATIONS OF NDC DIODES

1. COMPUTER PROGRAMS

The programs used were essentially the same as in ref. 1. They were altered to make optimal use of the more powerful FORTRAN language available on an XDS Sigma 7 computer. They were also expanded, for example to detect the extreme of the diode current and to record the values of the current for exterior plotting.

Also, the model described in sec. 3 of pt. 7 was modified to better approximate the v vs. E curve for GaAs[2,5]

$$v \overset{h}{=} \frac{\mu_e E + G v_V}{1 + G} , \quad (1)$$

with* $\mu_e \overset{h}{=} 0.6T^{-1}$, $v_V \overset{h}{=} 80$ km/s, $E_0 \overset{h}{=} 0.26729$ MV/m and $E_1 \overset{h}{=} 0.13$ MV/m. (The value of E_0 was chosen, for convenience, such that the peak field be exactly equal to 0.32 MV/m.)

A functional improvement was attempted, namely "zoning" of the diode being simulated. The basic idea of zoning is that, in a typical oscillating Gunn diode, most of the diode is uniform except in the neighbourhood of the HFD, whose length is typically only one tenth of the diode length. Thus, instead of dividing the diode from cathode to anode into a fairly large (typically 200 to 400) number of equal intervals (to solve the relevant partial differential equations), one could use a coarse grid of points except in the neighbourhood of the domain. This would reduce the number of points in the diode and, therefore, would increase the computation speed despite a small increase in programme complexity. It would be similar to adjusting the step-size of the independent variable in the numerical solution of an ordinary differential equation.

Each "zone" of the diode was divided into intervals of length h_m equal to $2^m h_0$, with $m = 0,1,2....,h_0$ being the length of the interval in the conventional method (diode uniformly divided). These values of h_m satisfy the condition for computation stability[1,6], $h_m^2 \geq Dk$, since h_0 itself is chosen so as to satisfy it. (k is the time increment used for the computations.) The interval size h_m was doubled where the gradient of n became too small in magnitude, and halved in the opposite case.

However, when zoning reduced the number of points in the diode to a value appreciably lower than in the conventional method, the computation became too inaccurate. The method was therefore abandoned.

---

* *the symbol $\overset{h}{=}$ means "equal by hypothesis".*

1.1 RELATION BETWEEN THE FIELD E AND THE VOLTAGE U

The change $\Delta\psi$ in internal potential across a diode of length L is given by:

$$\Delta\psi = \int_0^L E \, dz \quad .$$

Throughout most computations (as in ref. 1), the voltage U across the diode was equated to $\Delta\psi$. More rigorously, U should be written as the variation of the quasi-Fermi level ψ across the diode. Since [7, sec. 12.4]

$$d\psi = d\psi - \frac{D}{\mu}\frac{dn}{n} \quad ,$$

then

$$U = \Delta\psi - \int_{(\text{diode})} \frac{D}{\mu}\frac{dn}{n} \tag{2}$$

The second term on the right hand side of eq. 2 represents the difference between the anode and cathode contact potentials. (Cf. ref. 8, sec. 5.5.1). To illustrate the difference between U and $\Delta\psi$, let us consider a diode with a doping step in the middle. At equilibrium, such a diode contains a non-neutral region because of diffusion near the doping-step, so that $\Delta\psi$ is non-zero. Since $U = 0$ at equilibrium, U and $\Delta\psi$ cannot be equal. If D and μ are constant, eq. 2 yields the well-known result:

$$\Delta\psi = \frac{kT}{e} \ln \frac{n_A}{n_c}$$

(The subscripts A and C denote anode and cathode quantities, respectively.)

Eq. 2 was found by computations to be accurate for a non-uniformly doped diode at equilibrium (μ constant). It may not be rigorously applicable to an NDC material, but it does give meaningful results on parastable layers at equilibrium i.e., E_U and J are found to be zero for $U = 0$ (sec. 2.4). In any case, the second integral in eq. 2 is typically less than 30 mV in magnitude, which is small compared with U near or above threshold. Therefore, possible errors resulting from using eq. 2 with NDC materials should be negligible.

2. PARASTABILITY

2.1 GENERAL

The simulations were focussed on a new stability effect, fortuitously discovered in the course of computations and hereafter called "parastability", which was independently reported in elsewhere[9,13].

Parastability occurs in diodes where the doping N and the electron diffusivity D are large. A typical plot of diode stability in the N vs. L plane is shown in Figure 1. A boundary S emerges between two areas where diodes are respectively stable and unstable. At low N, this boundary coincides with the line D_c, of equation NL = $(NL)_c$, which separates subcritical and supercritical diodes[14,15], $(NL)_c$ is the critical NL-product). As N increases, the stability boundary S tends towards the line D_P, of equation $N = N_P$, above which diodes are parastable.

When a parastable diode, initially neutral, is biased in the NDC range, an accumulation layer (or high-field domain, depending on the nucleating inhomogeneity) is nucleated and propagates just as in an unstable diode. As the layer grows, the current decreases. When the layer reaches the anode, the field E_U behind the layer increases. At the anode, the layer does not disappear but settles into a stable, stationary layer, and E_U stays below E_P, so that no new layer nucleates. The diode current density J, equal to Nev_U, is less than the peak current density Nev_P. Figure 2 shows the electrical distribution in a parastable diode with stable anode layers at two different voltages. At the higher voltage, the accumulation is thicker and the electric field rises to a higher anode value. Other examples of parastable electrical distributions are shown in Figures 3, 4b, and 5.

2.2 OUTSIDE FIELD E_U

The outside field (i.e., the field in the uniform region) E_U is virtually independent of L and U as long as $U/L > E_P$. On the other hand, E_U is lower in a more densely doped diode, which is therefore more stable with respect to doping non-uniformities (see sec. 3). Thus, E_U is equal to a characteristic field $E_{par}(N)$ which, for a given D, is a function of N only. More generally, E_{par} appears to be a function of the product ND only, when L, N and D vary and U/L remains greater than E . For example, if $D = 0.02m^2/s$, E_{par}/MVm^{-1} is equal to 0.316, 0.298, and 0.280 respectively as $N/10^{21}m^{-3}$ equals 1.2, 1.5, and 2.0.

The electron velocity and current density corresponding to N and $E_{par}(N)$ will be called v_{par} and J_{par}:

$$v_{par}(N) = v[E_{par}(N)], \quad J_{par}(N) = Nev_{par}(N).$$

2.3 ANODE FIELD

In a thick layer, E becomes so high that the electron drift velocity reaches the saturation ("valley") value v_V (eq. 1), and current invariance implies that n reaches a saturation value n_{sat} such that:

$$n_{sat} v_V \approx n_U v_U \quad , \tag{3}$$

where U refers to the uniform, low-field region outside the layer.

Since $n_U \approx N$ and $v_U \approx v_P$, eq. 2 implies

$$\frac{n_{sat}}{N} \simeq \frac{v_P}{v_V} \simeq 2 \tag{4}$$

Poisson's equation implies that, in the thick accumulation layer:

$$\frac{dE}{dz} = \frac{e}{\varepsilon} (n_{sat} - N) \quad ,$$

hence an approximate value of E at the anode:

$$E_A \simeq E_U + \sqrt{\frac{2e}{\varepsilon} (n_{sat} - N) L \frac{U}{L} - E_U} \tag{5}$$

Since E_U is fairly independent of NL and U/L (sec. 2.2), and n_{sat} is proportional to N (eq. 4). Eq. 5 shows that the excess field E_A-E_U is at a given average field U/L proportional to NL. Since E_A may not exceed the avalanche field of the material, or some maximum beyond which holes are extracted from the anode, eq. 5 sets the maximum allowable value of the product NL $(U/L - E_U)$.

2.4 SUBTHRESHOLD PARASTABILITY

Once a stable threshold accumulation layer exists at the anode of a diode, it can (see sec. 3) *remain* there even if the voltage is reduced below threshold. (In fact, it is possible to obtain this layer by starting the simulation below threshold with, as initial condition, an accumulation layer vaguely approximating the final stable layer. This indicates that subthreshold layers can be quite stable.) As the voltage is reduced below threshold, the current begins to decrease below its saturation value and becomes a linear function of the voltage. This remains true down to zero bias. Then (Figure 3), the accumulation layer is very short and high, and the current in the diode is zero. The existence of a parastable layer at zero bias is very surprising. However, this finding is not a priori unacceptable since the field outside the layer, and the current through the diode, are then zero. The high-field region ($\Delta\psi > 0$) at the anode can exist at bias ($U = 0$) because the two terms on the right-hand side of eq. 2 cancel each other.

3. DEPENDENCE OF PARASTABILITY ON DOPING PROFILE AND VOLTAGE

In sec. 2, the doping profile was assumed to be uniform except for a slight overdoping (typically 10%) near the electrodes (cf. Figure 2). In fact, the results of sec. 2 hold in general if only the cathode is over-doped. The effects of non-uniform doping are discussed in this section, where N is assumed equal to a (nominal) reference value N_r everywhere except near the cathode and at specified local inhomogeneities.

3.1 EFFECT OF DOPING INHOMOGENEITIES IN THE BULK

The field E_{par} just behind a parastable layer is less than E_P (sec. 2.2). If there is a positive doping "hump" in this region, the field is locally decreased and the diode remains stable. If there is a negative doping "dip" behind the layer, the field is locally increased. If it is still less than E_p, the diode remains stable and, if the dip is far enough from the layer, the current density remains equal to $J_{par}(N_r)$; the extra voltage drop across the dip is compensated by a decrease of the layer, as if U had been reduced. However, if the dip is large enough that the field there rises above E_p, then a high-field domain is nucleated and the diode is no longer stable. For example, a 5-μm long diode with $D = 0.01\ m^2/s$ and $N_r = 3.10^{21} m^{-3}$ is stable at U/L = 0.4 MV/m with a 1μm-long, 2% doping dip, but unstable with a 4% doping dip.

The larger the difference $E_p - E_{par}(N_r)$, i.e., the larger N_r (sec. 2.2), the larger the doping dip must be to destroy parastability. In other words, highly-doped diodes ($N >> N_p$) are more stable than lightly doped diodes (N only slightly larger than N_p, see Figure 1). This conclusion was also obtained by Mircea[9].

3.2 EFFECT OF AN ANODE DOPING-INHOMOGENEITY

If the doping N increases with position near the anode, the diode can be unstable at low voltage and parastable at higher voltage. For example, a diode with $N = N_r = 1.2 \cdot 10^{21} m^{-3}$ except for a small overdoping near the cathode and a smooth increase up to 2.1 N_r at the anode is unstable if U/L = 0.32 MV/m, and stable above 0.35 MV/m (Figure 4).

Figure 5 illustrates a diode with an anode doping so large that the parastable layer is detached from the anode itself. The field drops, at the anode, to a value (0.107 MV/m) in the ohmic range, which shows that the parastable layer does not depend on particular boundary conditions.

Simulations with time-dependent doping have indicated that the diode current is controlled by the doping N_E at the back (cathode-side) edge of the parastable layer. If N increases with time over a region containing the layer and is kept constant elsewhere, the diode current density, equal to $eN_E v_{par}(N_E)$, increases as N_E increases (sec. 2.2). Consequently, the field increases where N is kept constant, until it reaches the peak value E_p, at which point the diode becomes unstable. However, if the voltage is then increased, the edge of the would-be stable layer moves towards the less doped region, where N_E is less, and the diode becomes stable again (Figure 4a).

One example is illustrated in Figure 6. The total doping is the sum of a constant and a variable profile:

$$N(z) = N_0(z) + g(t)N_1(z)$$

Figure 6b shows that the diode is initially parastable with U/L = 0.32 MV/m and g = 0. It becomes (1) unstable when g is increased up to 0.4905, then

(2) stable when U/L is increased up to 0.34 MV/m, then (3) unstable when g is increased up to 0.9505, and, finally (4) stable when U/L is increased up to 0.35 MV/m. At this last value of U/L, the diode remains stable up to the highest value of g of 7.5: when U is sufficiently high that the layer edge is in the region where the modulated doping N_1 is zero, the diode is parastable regardless of g.

If the diode average field U/L is appreciably lower than E_P, it is still possible to have a parastable layer (sec. 2.4). However, the field behind the layer is then less than $E_{par}(NE)$. Only very large doping inhomogeneities can then make the diode unstable by raising the field behind the layer above E_P. In this sense, parastable layers are less sensitive to doping inhomogeneities when the diode is biased below threshold than above. On the other hand, parastable layers "detached" from the anode by a large overdoping could be simulated above threshold only (Figures 4, 5).

4. RESPONSE OF A PARASTABLE DIODE TO VOLTAGE MODULATION

4.1 VOLTAGE VARIATIONS

The steady-state current is independent of the voltage U above threshold, in which case $E_U = E_{par}(N)$. The current is proportional to U below threshold. Thus, for slow voltage variations, a diode with an anode layer stable below and above threshold behaves as a current-limiting device. This statement must be qualified as follows:

1. If the device has no initial parastable layer, the current goes through a minimum lasting a time of the order of the transmit time L/v_p, as the voltage crosses threshold (Figure 7).

2. As the voltage is increased, the extra charge in the anode layer (Figure 2) is provided by one or several growing layers nucleated at the cathode, because the increase of voltage "pushes" E_U into the NDC range. As they propagate through the diode, these growing layers modulate the current transiently (Figure 8).

3. There is no such current oscillation during a voltage decrease, because the value of E_U is not "pushed" up. The charge removed from the layer simply disappears at the anode.

4.2 SINUSOIDAL MODULATION

For microwave applications sinusoidal modulation of the diode voltage is of particular interest. The problem includes many independent parameters: diode length L, electron diffusivity D, nominal doping N_r, doping profile (e.g., zero, small or large anode overdoping), average voltage U_0, modulation amplitude $\hat{U}_1$, modulation frequency f. A systematic study of the various possible cases would therefore be very lengthy and tedious and only a few simulations were performed. Depending on the values of f and U_0, a few simple classes of behaviour can be distinguished.

(a) $U_0 \simeq LE_P$, $f \simeq 0.5\ v_P/L$.

U equals LE_P about every half-period. When U crosses this value while increasing (t = 0.3 ns in Figure 9) an accumulation layer is launched at the cathode (cf. sec. 4.1) and causes a current decrease (Figure 9). Later (t/ns = 0.35 to 0.4), the current is fairly constant because the diode is in the saturated current range ($J \simeq J_{par}(N)$, sec. 2.2). When U is less than LE_P, the parastable layer stays at the anode but the diode becomes ohmic (sec. 2.4), hence a decrease of J accompanying that of U (t/ns = 0.4 to 0.5 Figure 9).

(b) $U_0 > LE$, $f < v_P/L$, anode overdoping.

The diode behaves as in (a), except that the single current dip may be replaced as a short oscillation, and the anode layer disappears every cycle if the minimum, $\check{U}$, of U is sufficiently low, e.g., $\check{U} \simeq LE_P$ (see sec. 3.2).

(c) $U_0 > LE_P$, $f < 2v_P/L$, anode overdoping.

A in (a), an accumulation layer is nucleated at the cathode as U increases. However, the frequency is so high that the layer amplitude goes through a maximum, then decreases down to a low value before the layer reaches the anode. As a result, no stable layer ever settles at the anode, and the diode actually operates in the LSA mode. A typical oscillation is illustrated in Figure 10a, b. The efficiency is about 2.5% in this case, and becomes 3.4% if U_0/L is increased to 0.45 MV/m (Figure 10c). Higher efficiencies should be possible since the diodes operate in the LSA mode[16,18]. In the example of Figure 10, N/f is equal to $2.4 \cdot 10^{10} sm^{-3}$ and therefore lies within the range where LSA should be possible[17].

Amplification by stable, over-critical diodes has been reported and could be explained by parastability[10,19,20]. In particular, diode stabilization was obtained (1) only above a voltage appreciably higher than the threshold voltage[19,20], and (2) more easily if N decreased towards the anode[19]. This is in agreement with sec. 3.2.

5. CONCLUSION AND SUMMARY

Flexible, efficient computer programs were developed and used to simulate negative-differential-conductivity (NDC) diodes with constant diffusivity D and arbitrary doping profiles. These programs were used mainly to study parastable diodes.

Parastability is a new mode of stability for NDC diodes. It occurs if the product of the doping N by D exceeds a limiting value. For GaAs, this corresponds to a limiting value of N is about $10^{21} m^{-3}$, which is well within the doping range of commonly-used devices. Published experimental results indicate that parastability has already been observed, even though it was not always recognized as such.

A parastable diode contains an accumulation layer at the anode, which initially forms and settles there when the voltage reaches threshold.

In a parastable diode above threshold, the normalized steady-state current I/N is saturated to a value which decreases slowly as N increases. However, the current response to high-frequency voltage modulation shows that the diode exhibits broadband negative conductance, which makes parastable diodes applicable as microwave amplifiers.

A parastable layer can remain as the voltage is reduced below threshold, if the doping is sufficiently uniform. Otherwise, if the doping increases near the anode, parastability may occur only above a voltage limit which is higher than threshold.

6. REFERENCES

1. Torrens, A.B., *Negative Differential Conductivity Effects in Semiconductors*, Ph.D. Thesis, the University of British Columbia, Vancouver (February 1969).

2. Butcher, P.N., and W. Fawcett, *Calculation of the Velocity-Field Characteristic for GaAs*, Phys. Lett. 21, 489-90 (June 1966).

3. Ruch, J.G., and G.S. Kino, *Transport Properties Of GaAs*, Phys. Rev. 174, 921-31 (15 October 1968).

4. Fawcett, W., *Recent Developments in the Calculation of Hot Electron Distribution Functions*, 10th Int. Conf. Phys. Semicond: Proc, 51-9, (August 1970).

5. Fawcett, W., A.D. Boardman and S. Swain, *Monte Carlo Determination of Electron Transport Properties in Gallium Arsenide*, J. Phys. Chem. Sol. 31, 1963-90 (September 1970).

6. Richtmyer, R.D., *Difference Methods for Initial Value Problems*, Interscience (1957).

7. Schockley, W., *Electrons and Holes in Semiconductors*, Van Norstrand (1950).

8. Gibbons, J.F., *Semiconductor Electrons*, McGraw-Hill (1966).

9. Mircea, A., *The Influence of Electron Diffusion on the Oscillation Characteristics of Short Gunn Diodes*, Device Res. Conf., Rochester (June 1969).

10. Magarshack, J., and A. Mircea, *Stabilization and Wide-Band Amplification Using Over-Critically Doped Transferred-Electron Diodes*, 8th Internat. Conf. on Microwaves and Optical Generation and Amplification, Amsterdam; Proc.: MOGA 70, 16.19-23 (September 1970).

11. Thim, H., *Experimental Verification of Bistable Switching with Gunn Diodes*, Electron, Let. 7, 246-7 (20 May 1971).

12. Thim, H., *Stability and Switching in Over Critically Doped Gunn Diodes*, Proc. IEEE 59, 1285-6 (August 1971).

13. Gueret, P., and M. Reiser, *Switching Behavior of Over-Critically Doped Gunn Diodes*, Appl. Phys. Lett. 20, 60-2 (15 January 1972).

14. Kroemer, H., *Theory of the Gunn Effect*, Proc. IEEE 52, 1736-6 (December 1964).

15. McCumber, D.E., and A.G. Chynoweth, *Theory of Negative Conductance Amplification and of Gunn Instabilities in 'Two-Valley' Semiconductors*, Trans. IEEE ED13, 4-21 (January 1966).

16. Copeland, J.A., *A New Mode of Operation for Bulk Negative Resistance Oscillators*, Proc. IEEE 54, 1479-80 (October 1966).

17. Copeland, J.A., *LSA Diode-Oscillator Theory*, J. Appl. Phys. 38, 3096-101 (July 1967).

18. Copeland, J.A., *LSA Oscillator Waveforms for High Efficiency*, Proc. IEEE 57, 1666-7 (September 1969).

19. Perlman, B.S., C.L. Upadhyayula and R.E. Marx, *Wide-Band Reflection-Type Transferred-Electron Amplifiers*, IEEE Trans. MTT18, 911-21 (November 1970).

20. Perlman, B.S., C.L. Upadhyayula and W.W. Siekanowicz, *Microwave Properties and Applications of Negative Conductance Transferred Electron Devices*, Proc. IEEE 59, 1229-37 (August 1971).

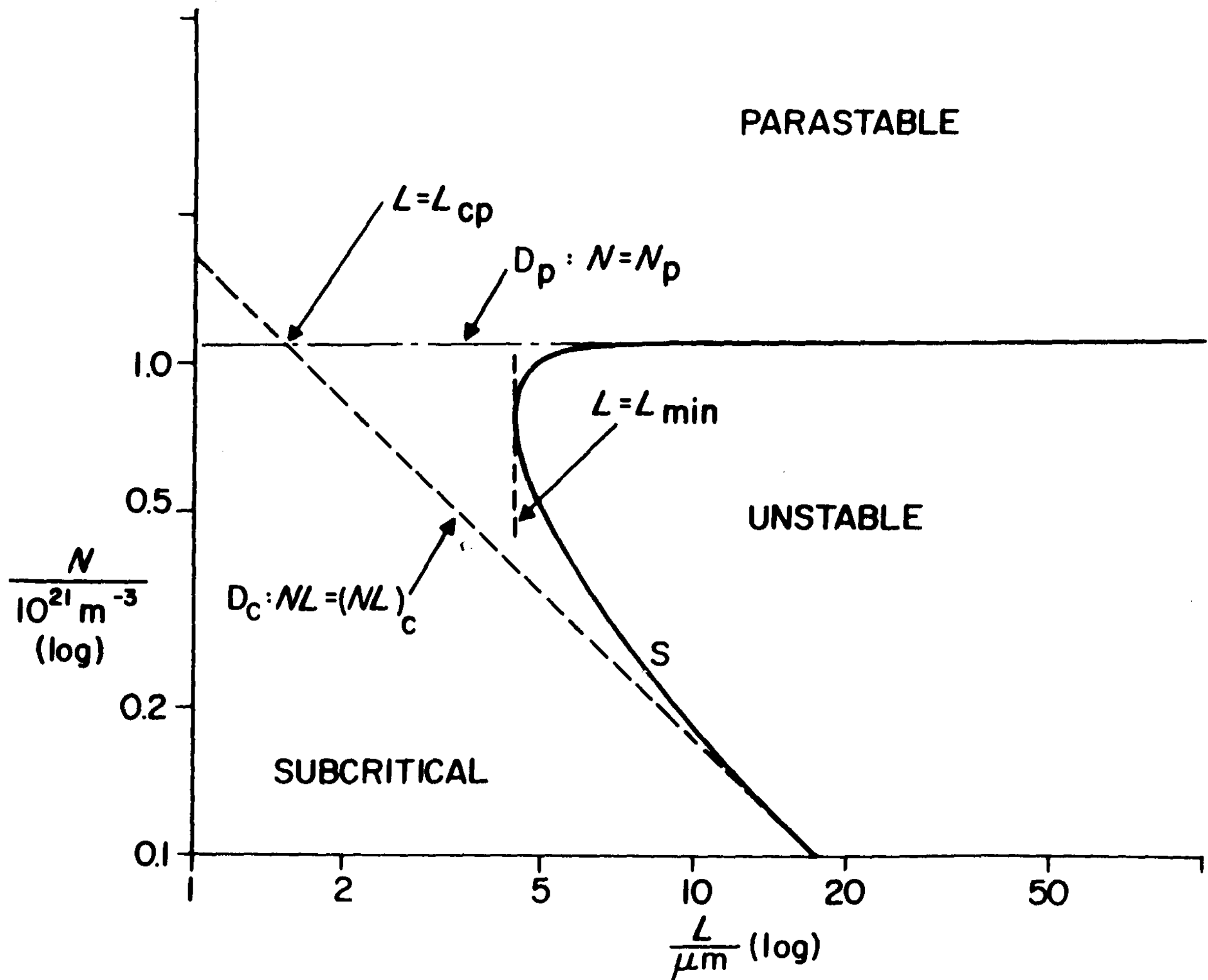

Figure 1. Stability of an NDC (n-GaAs) diode as a function of its doping N and its length L. Electron diffusivity: $D = 0.02\ m^2/s$.

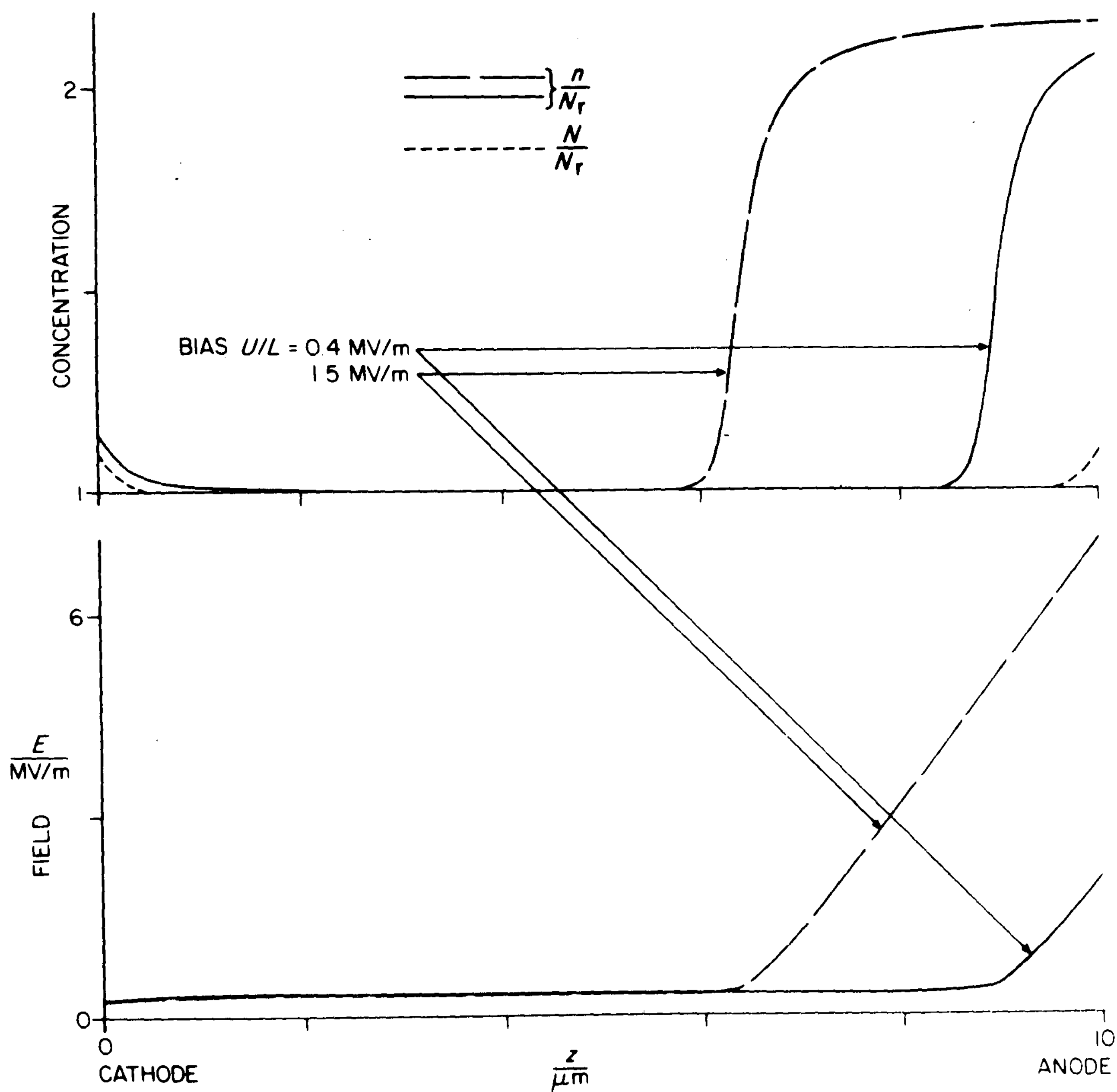

Figure 2. Electric field E, electron concentration n and doping N as a function of position z in a diode with a nominal doping N_r of $1.2 \cdot 10^{21} m^{-3}$, for two values of the average field U/L.

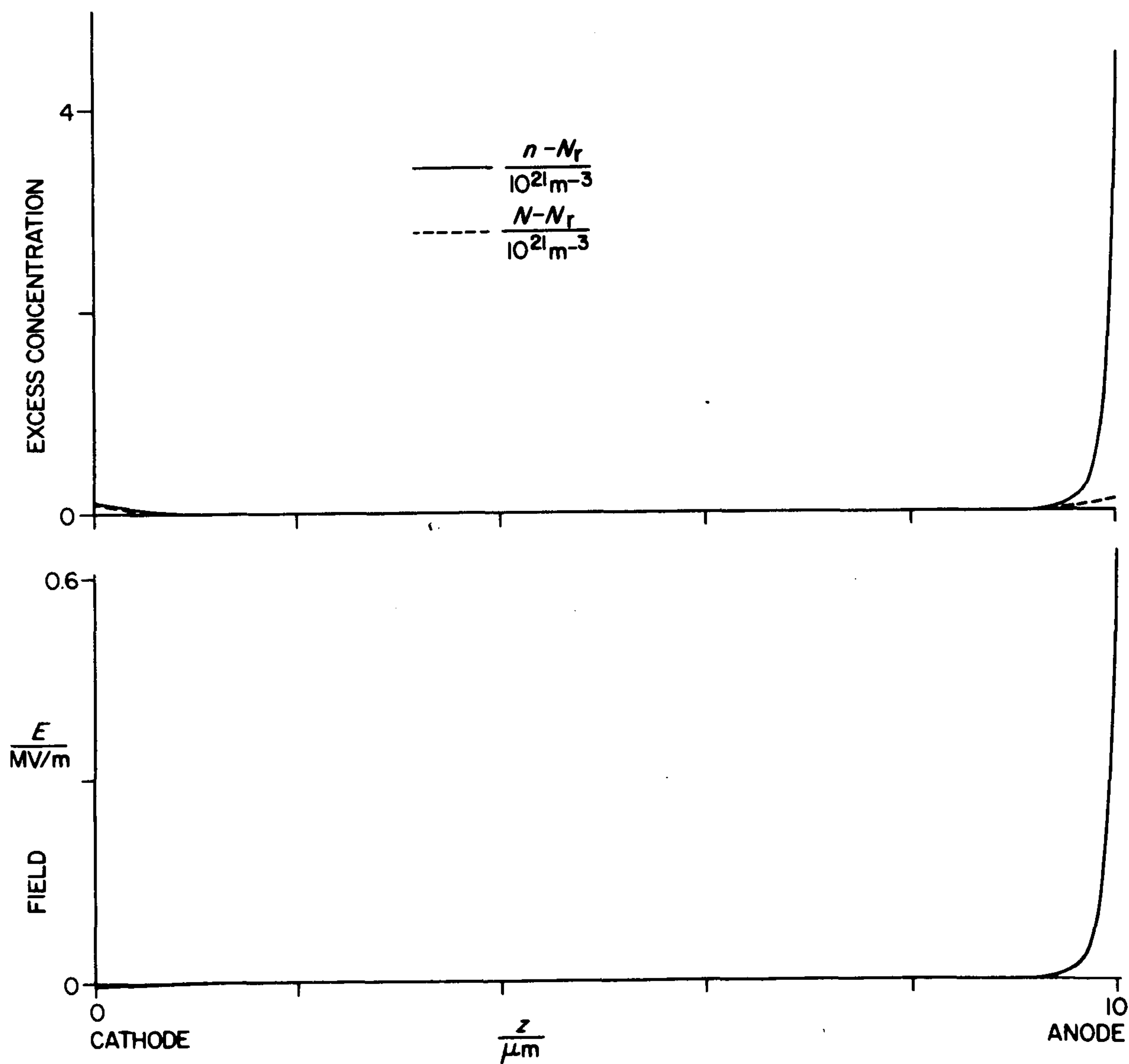

Figure 3. Parastable electrical distribution in a diode whose voltage has been reduced to zero. $N_r = 1.2 \cdot 10^{21} m^{-3}$. E is the electric field, n the electron concentration, N the doping.

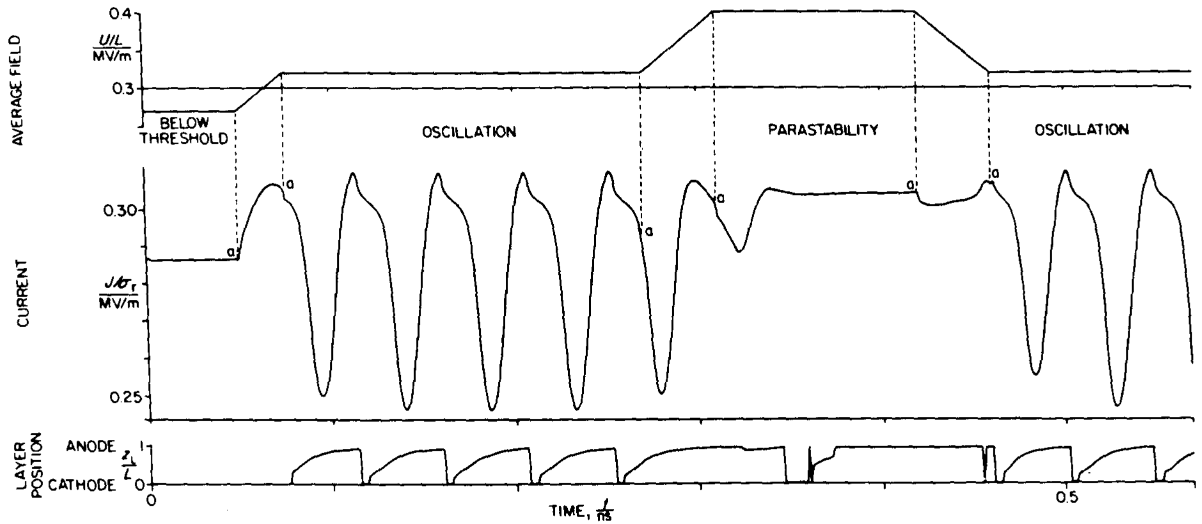

(a) Current density J vs. time t in response to a varying average field U/L. Also shown is the position z_L of the accumulation layer normalized to the diode length L. The current jumps marked "a" are due to discontinuities of the displacement current which occur when dU/dt is discontinuous.

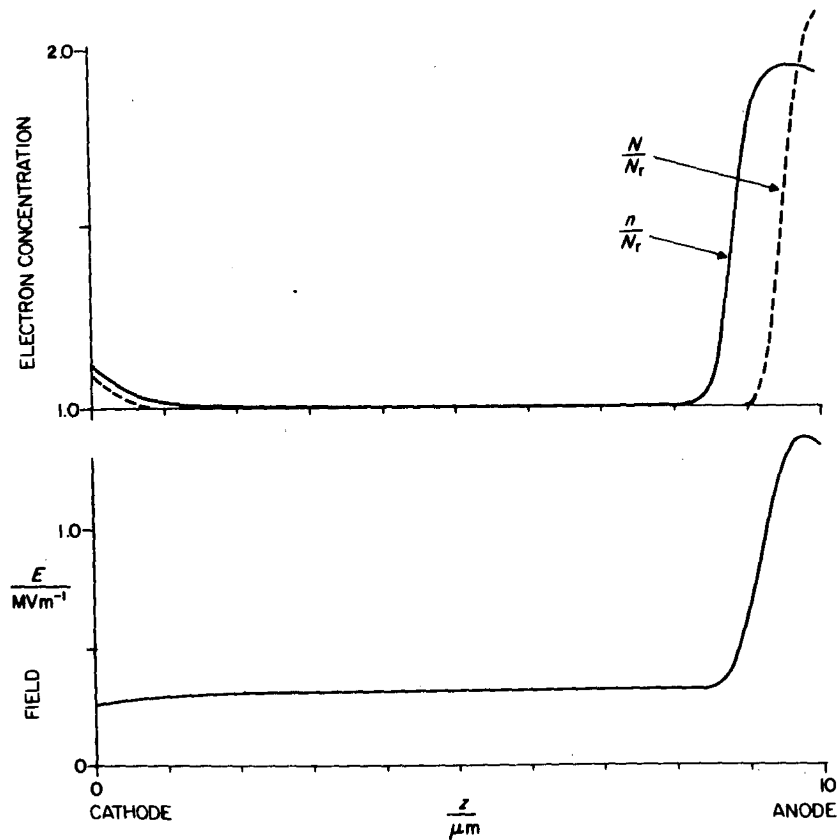

(b) Electrical distribution in the parastable diode (U/L = 0.36 MV/m, t = 0.42 ns in (a)).

Figure 4. Voltage-dependence of the stability of a diode with anode overdoping. $N_r = 1.2 \cdot 10^{21} m^{-3}$.

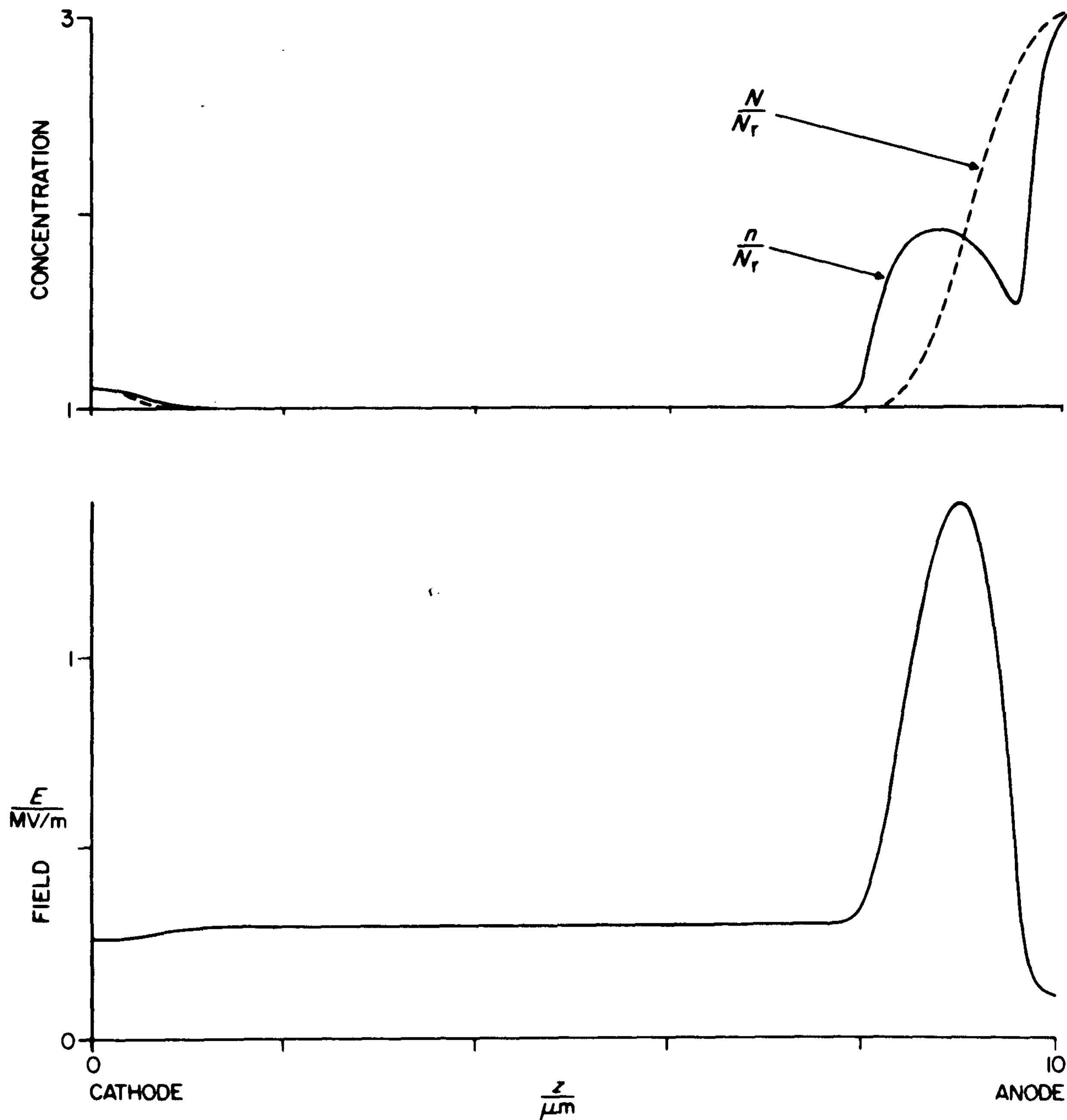

Figure 5. Electric field E and electron concentration n in a parastable diode with U/L = 0.4 MV/m, $N_r = 1.5 \cdot 10^{21} m^{-3}$ and a large overdoping near the anode (dashed curve). N is the doping.

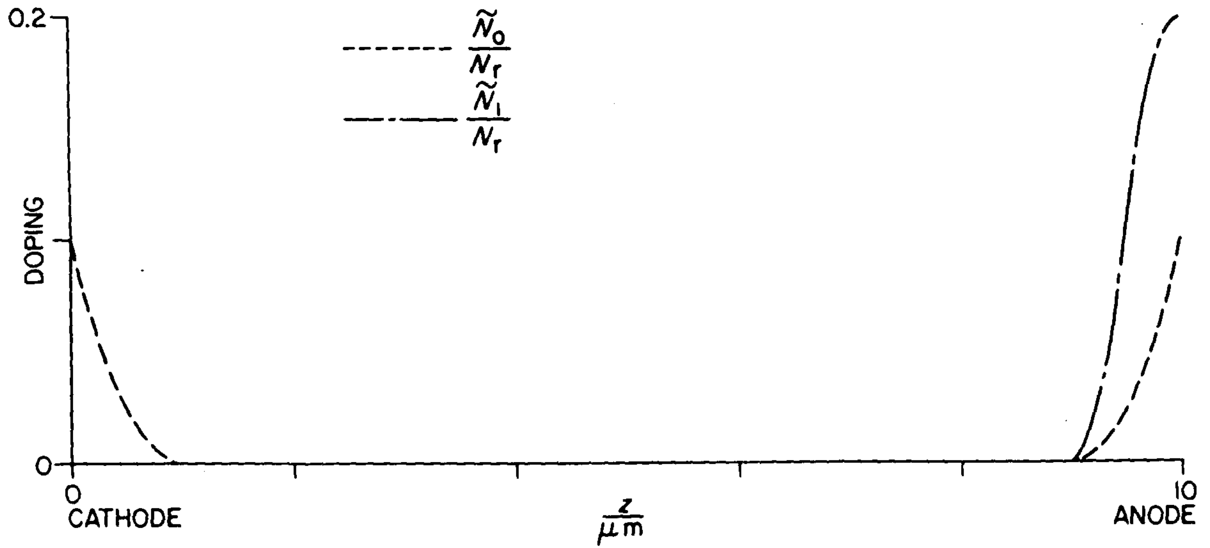

(a) Constant and modulated doping profiles N_0 and N_1 vs. z. The total doping at time t is $N_0 + g(t)\,N_1$.

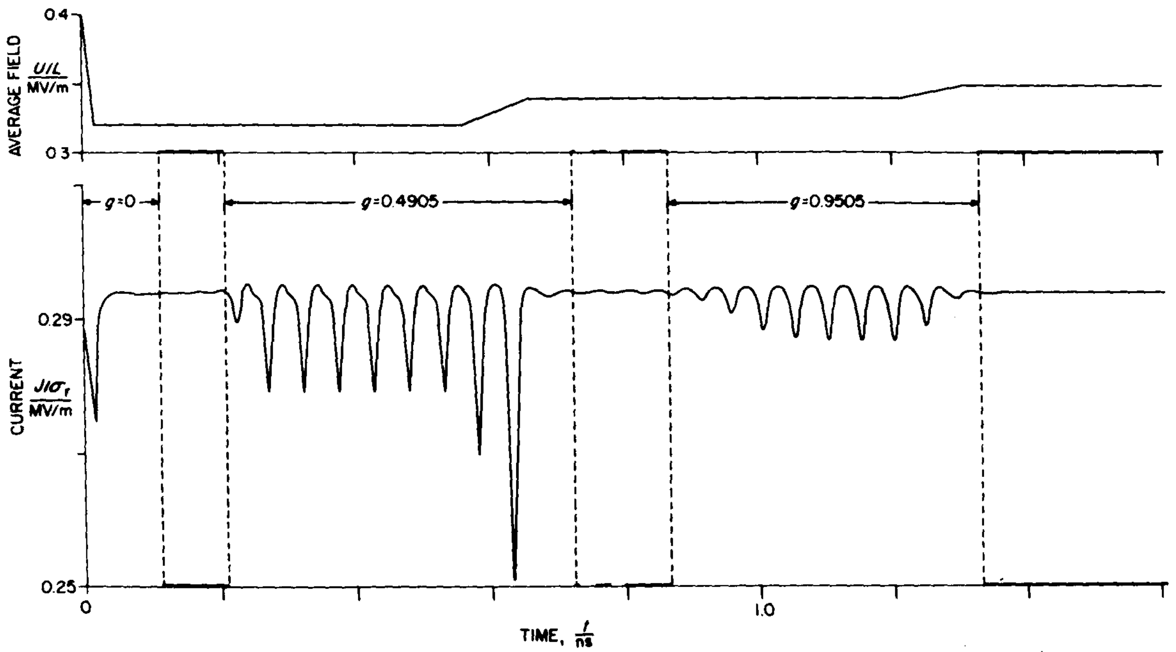

(b) Diode current J in response to changes of the voltage U and the doping factor g. L is the diode length and σ_r the reference conductivity of the material. The thicker sections of the time axis indicate when g increases linearly with time.

Figure 6. Diode with $N_r = 1.2 \cdot 10^{21} m^{-3}$.

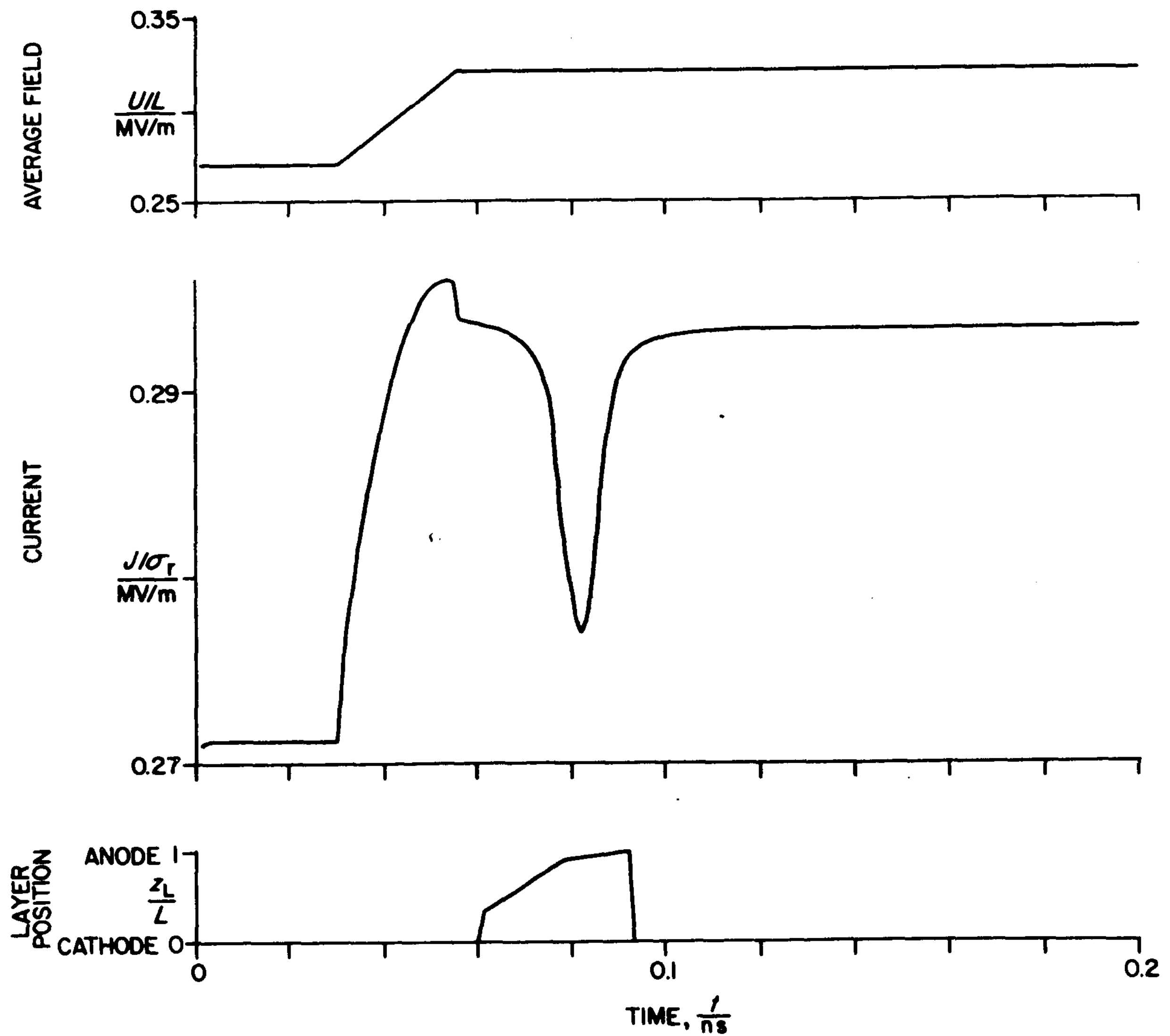

Figure 7. Current transient accompanying the formation of a parastable layer. The diode is the same as in Figure 3 except that the anode has no overdoping. U/L is the average electric field, J the current density, σ_r the equilibrium conductivity, z_L the accumulation-layer position and L the diode length.

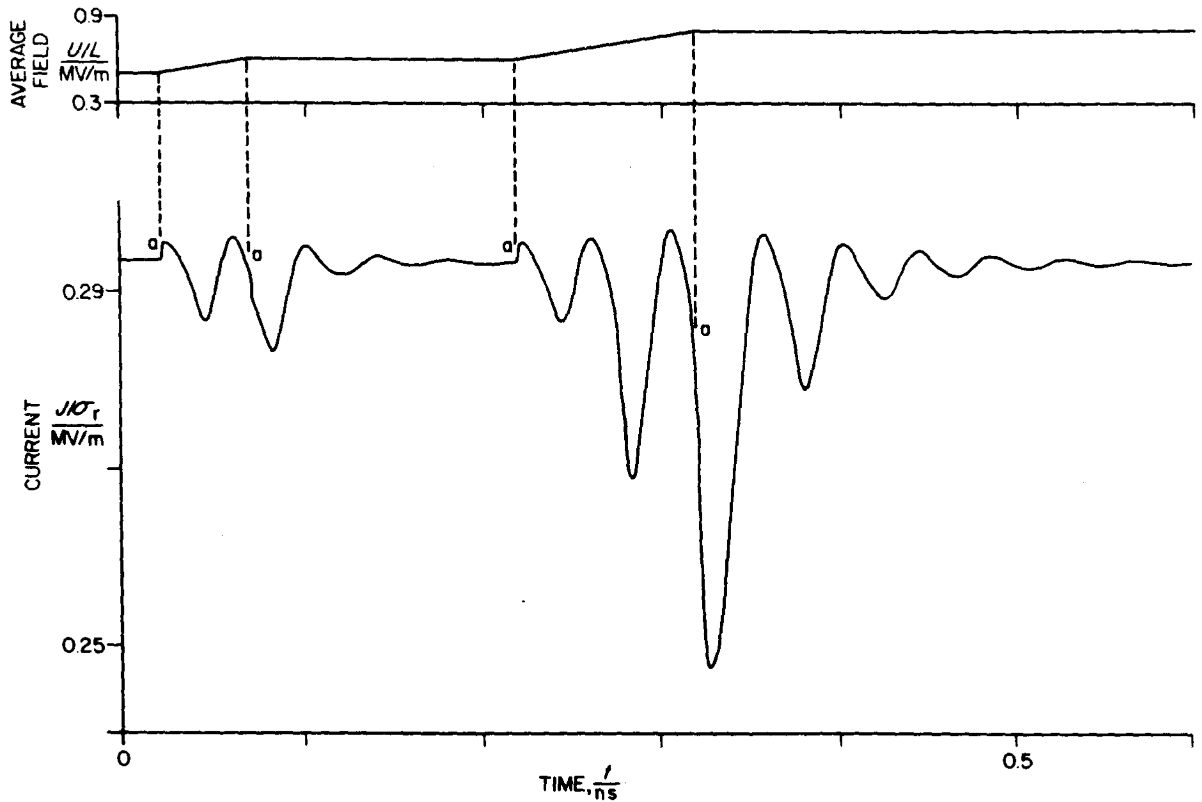

Figure 8. Same diode as in Figure 2: response to an increasing average field U/L. J is the current density and σ_r the reference conductivity. The current jumps marked "a" are due to discontinuities of the displacement current which occur when dU/dt is discontinuous.

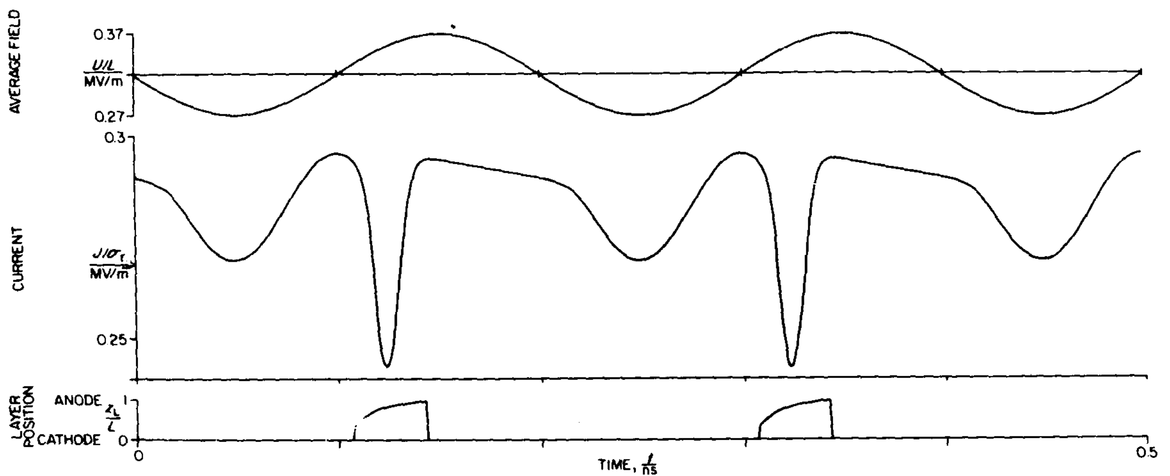

Figure 9. Same diode as in Figure 3: current density J and accumulation-layer position z_L vs. time t when the voltage U is modulated:

$$U = U_0 + \hat{U}_1 \sin(2\pi ft - \psi), \text{ with } U_0/L = 0.32 \text{ MV/m}, \hat{U}_1/L = 0.05 \text{ MV/m}, f = 5 \text{ GHz}.$$

σ_r is the reference conductivity and L the diode length ($\sigma_r = N_r e \mu_e$).

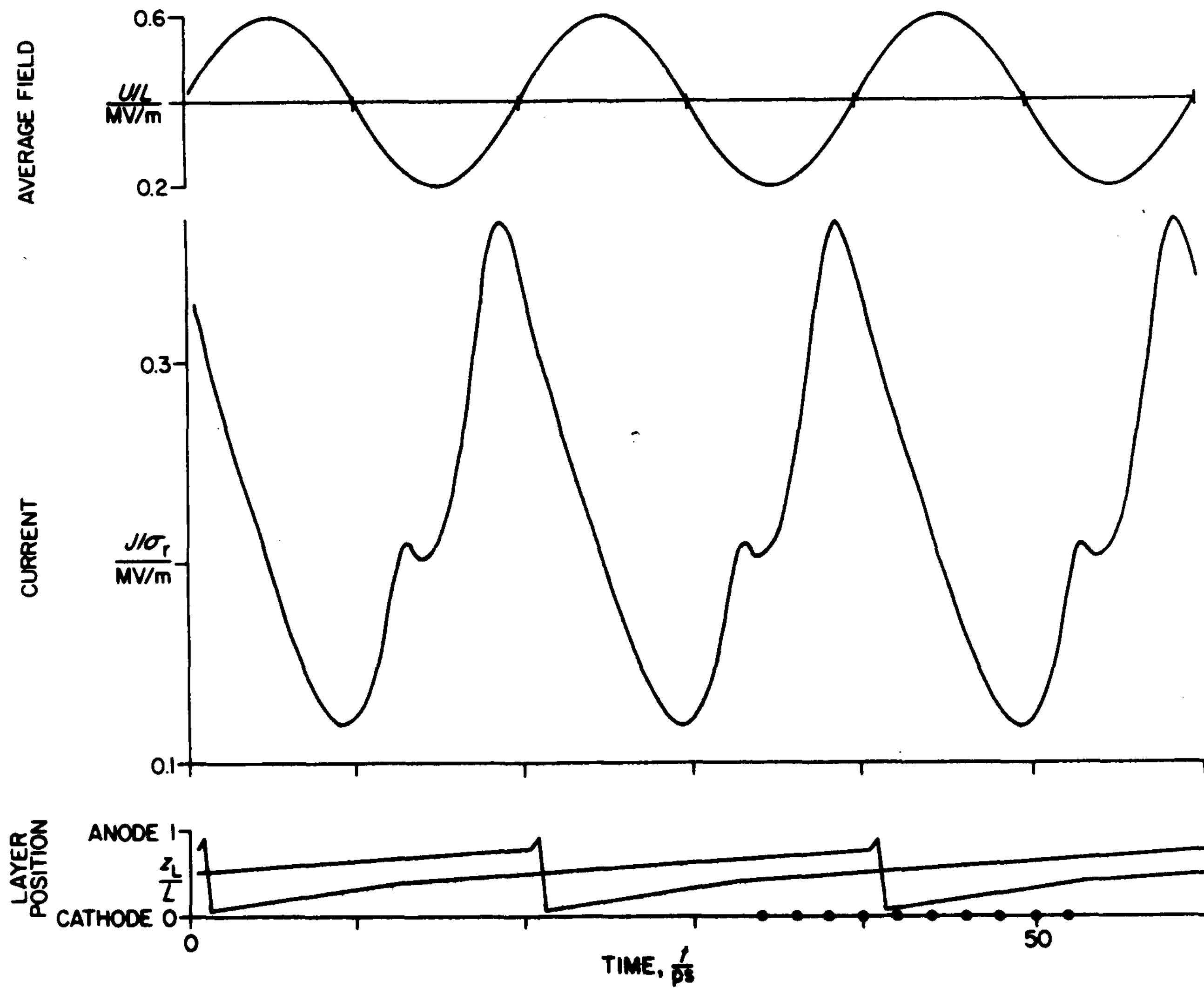

(a) Current density and layer position for U_0/L = 0.4 MV/m, U_1/L = 0.2 MV/m and f = 50 GHz

Figure 10. Same diode as in Figure 9. (Sheet 1 of 3)

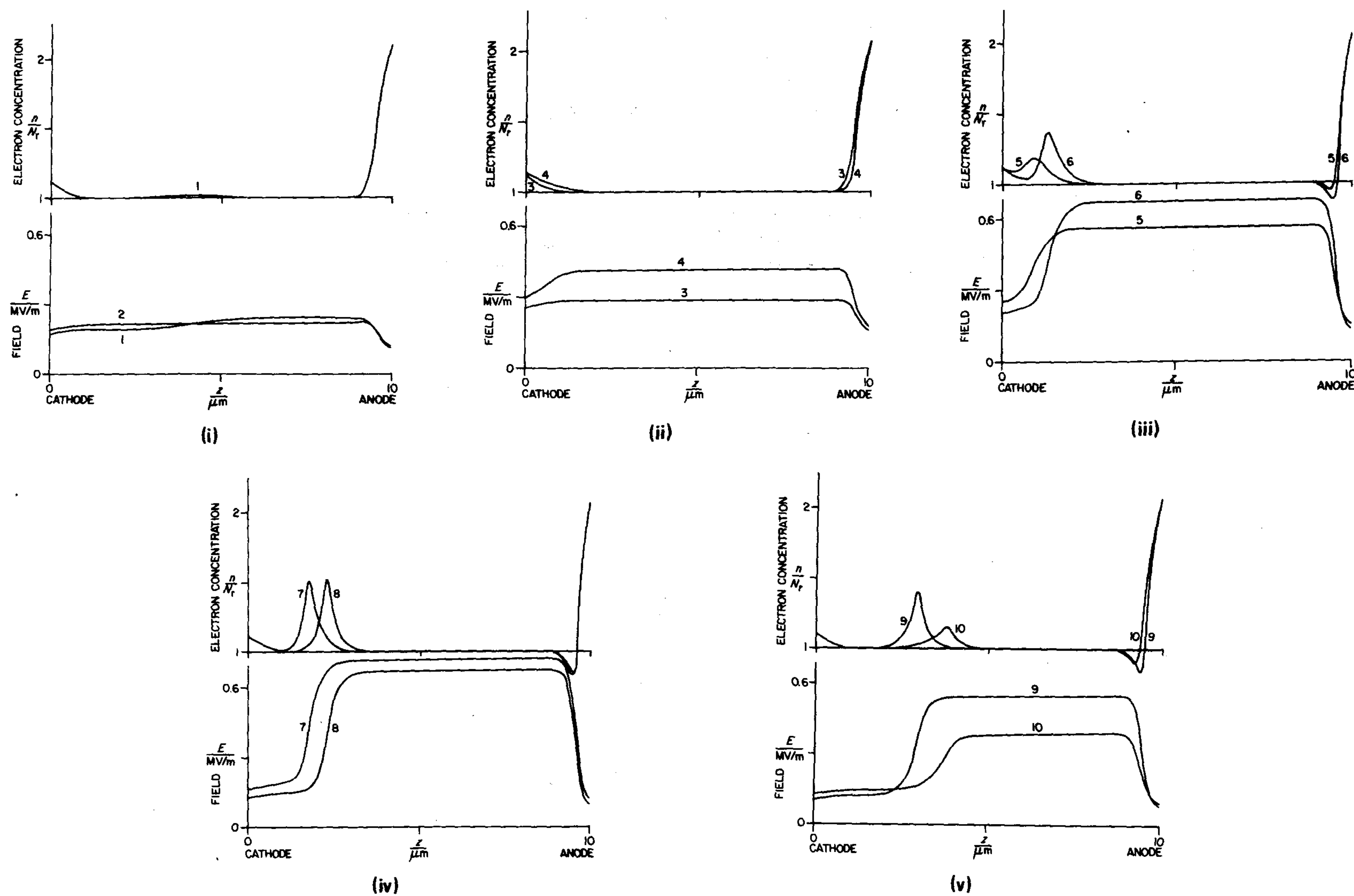

(b) Electrical distribution in the diode at the times marked by dots in (a). E is the electric field and n the electron concentration. The numbers 1, 2, 3,.... indicate the time sequence in 2-ps intervals.

Figure 10. Same diode as in Figure 9. (Sheet 2 of 3)

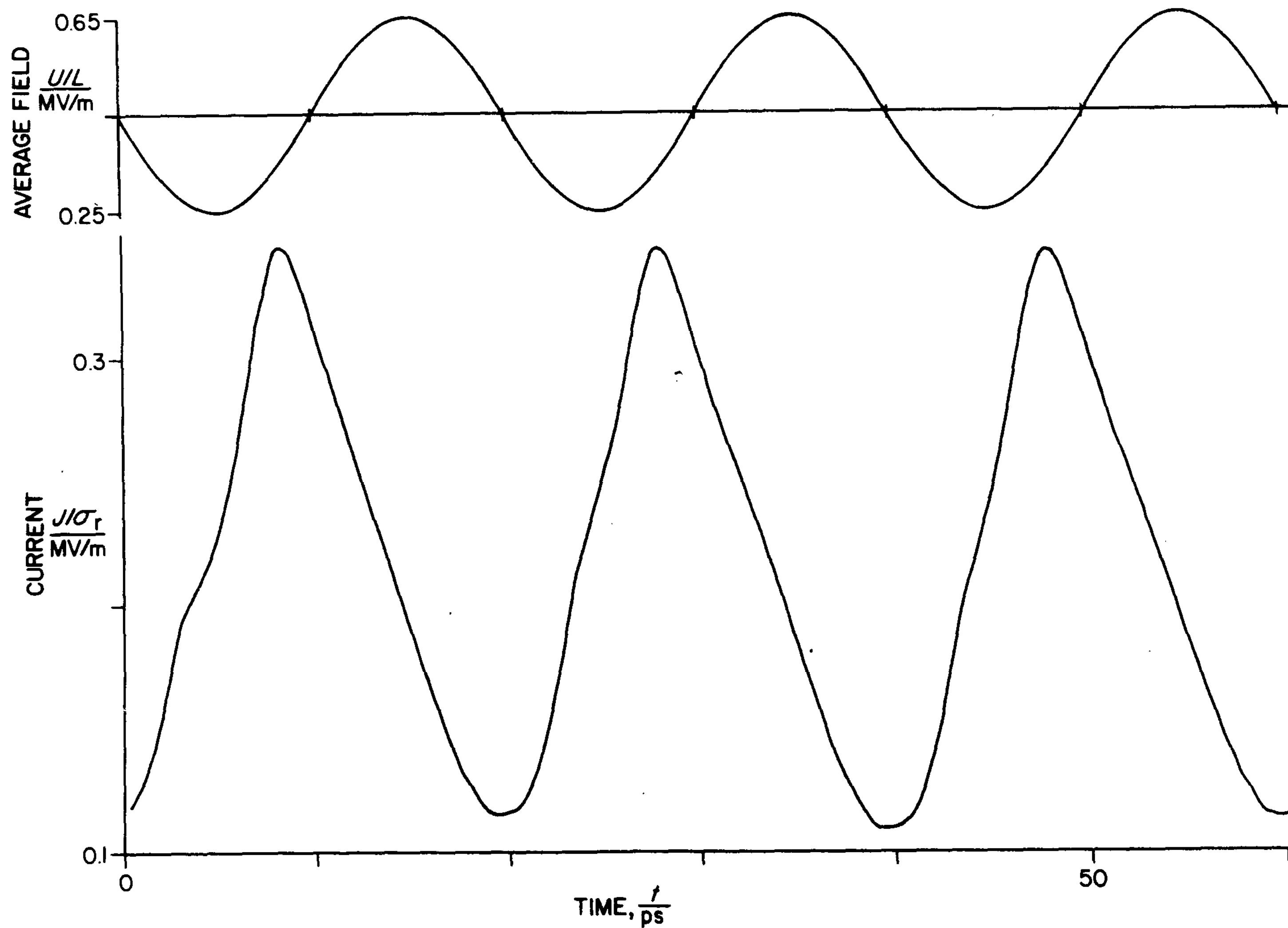

(c) Current density and layer position for U_0/L = 0.45 MV/m, U_1/L = 0.2 MV/m and f = 50 GHz

Figure 10. Same diode as in Figure 9. (Sheet 3 of 3)

THIS PAGE INTENTIONALLY LEFT BLANK

GALLIUM ARSENIDE MATERIALS AND DEVICES AND THE GUNN EFFECT

by

W.D. Edwards, W.A. Hartman, A. Torrens and D.L. Butler

PART 9

THE GUNN EFFECT – FUTURE APPLICATIONS

by

W.D. Edwards, W.A. Hartman, A. Torrens and D.L. Butler

ABSTRACT

NDC devices can be used in a variety of applications which exploit the one effect particular to these devices, namely domain propagation. These applications include the generation of special periodic waveforms with or without external control electrodes, high speed electronic or optical scanning, FM pulse generation, and optical modulation using the electro-optic effect in gallium arsenide.

PART 9

THE GUNN EFFECT: FUTURE APPLICATIONS

1. INTRODUCTION

Propagating high-field domains in a gallium arsenide diode (pt. 1) lead to the possibility of a basic change in circuit design concepts and to thoughts of several very interesting devices.

Silicon integrated circuits are based on a well-established technology, but are also based upon traditional ideas of single resistors, capacitors, and active elements. (The advertisements often quote the number of elements per unit area.) The Gunn domain in a GaAs sample is a new phenomenon and it may be used to perform interesting electrical operations.

In an oscillating Gunn device the current through the sample at any instant depends upon the material conductivity and cross-section at the position of the domain. Thus the variation of the current through the sample as the domain moves from cathode to anode gives a scan record proportional to the conductivity and cross section along the sample. Typically the domain (or scan) moves through a 100-micron sample in 10^{-9} seconds.

Among the many applications of Gunn devices, those which employ specifically the fast scanning by moving domains include:

(a) *Circuit Function Generator (Sandbank 1967; ref. 1)*

By modification of the sample conductivity (by diffusion, alloying) it should be possible to get a range of desired function shapes and pulse trains at the repetitive rate given by the basic Gunn frequency (Figure 1). It should be possible to achieve similar pulses by modifying the sample cross-section at the time of manufacture. With either of these methods, there is the possibility of producing complex functions at high speeds from a single two-terminal device.

(b) *Function Generator with External Control*

In the approaches given in (a), the function generated is essentially defined at the time of manufacture. However, we may apply side contacts to the Gunn device and use control voltages to modify the pulse train or function by injection or capacitive effects. Side-contact voltages can also be used to modify the basic Gunn frequency.

(c) *High-speed Scanner*

Circuits may be attached to side contacts and hence "scanned" by the high-speed, high-field Gunn domain at the basic Gunn diode frequency.

(d) *Optical Scanner*

Since GaAs is photoconductive, it is possible to consider modifying the function shape or wave train (see (a)) by optical injection. Alternatively,

we could consider using uniform GaAs that is modulated in conductivity by the optical signal and this modulation is then scanned by the Gunn domain. In this latter case the output current is proportional to the optical signal and we have a solid-state optical scanner of very high speed with low applied voltage. A variation which is at least as feasible is to use the GaAs as a scanner only and to use photodetectors such as cadmium-sulphide cells attached to the side contacts of the Gunn device to perform the actual optical detection [2]. With present technology, a scan of 50 "points" in a nanosecond can be visualized.

(e) *Coding Devices*

A capacitive contact produces output pulses whose duration is the time it takes a domain to pass under a contact. This is much less than the total transit time of the device. One could presumably put several contacts on the side and get a train of pulses over a range of frequencies compared with the basic Gunn oscillation.

(f) *Pulse-frequency Modulation*

With certain electrode shapes, e.g. an annular one, there can be wide frequency variations with low operating-voltage swings. A frequency change by almost a factor of 3 has been reported by Clarke (1969 [3]). Since the voltages are low this brings to mind a useful analogue to digital converter.

(g) *Optical Modulator*

The field in the domain is sufficiently high to give a band-edge shift that may be useful in modulating an optical signal at this band-edge wavelength at very high frequency [4]. The electro-optic effect in GaAs itself can also be used to modulate polarized light [5]. The advantage of the Gunn diode over conventional ADP or KDP modulators is that it auto-oscillates, and uses a small bias voltage. For wider band use there is also the possibility of using Gunn devices in series to provide sufficient voltage to modulate the ADP and KDP crystals themselves.

All of the above possibilities are best achieved in the co-planar configuration.

(h) *Memory Devices*

The impact ionisation of deep traps in GaAs and their stability in more than one ionisation state opens up the possibility of non-volatile memory and two-state devices.

2. REFERENCES

1. Sandbank, C.P., *Synthesis of Complex Electronic Functions by Solid State Bulk Effects*, Solid State Electron, 10, 369, (1967).

2. Engelbrecht, R.S., *Bulk Effect Devices for Future Transmission System*, Bell Lab. Rec. 45, 192 (1967).

3. Clarke, G., A.L. Edridge and J.C. Bass, *Planar Gunn-Effect Oscillators with Concentric Electrodes,* Electron Lett. 5, 471 (1969).

4. Guetin, P. and D. Boccon-Gibod, *Trans-Keldysn Effect with Gunn Domains in Bulk GaAs,* Appl. Phys. Lett. 13, 161 (1968).

5. Cohen, M.A., S. Knight and J.P. Edward, *Optical Modulation in Bulk GaAs using the Gunn Effect,* Appl. Phys. Lett. 8, 269 (1966).

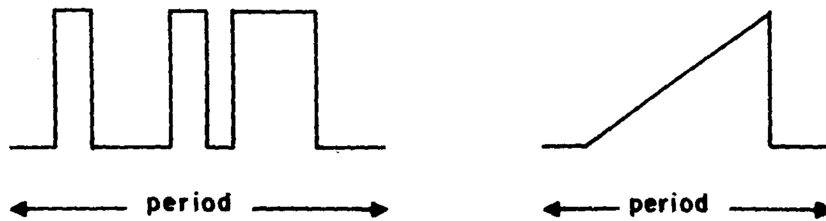

Figure 1. Waveforms which could be generated by specially-profiled NDC diodes oscillating in the free-domain mode.

CRC DOCUMENT CONTROL DATA

1. ORIGINATOR: Department of Communications/Communications Research Centre

2. DOCUMENT NO: CRC Report No. 1303

3. DOCUMENT DATE: December 1976

4. DOCUMENT TITLE: Gallium Arsenide Materials and Devices and the Gunn Effect

5. AUTHOR(s): W.D. Edwards, W.A. Hartman, A.B. Torrens and D.L. Butler

6. KEYWORDS: (1) Gallium-Arsenide
(2) Gunn
(3)

7. SUBJECT CATEGORY (FIELD & GROUP: COSATI)

20 Physics
20 12 Solid State Physics

8. ABSTRACT: For abstract see Page vii of this report.

9. CITATION:

EXECUTIVE SUMMARY

DOCUMENT NO: CRC Report No. 1303

TITLE: Gallium Arsenide Materials and Devices, and the Gunn Effect

AUTHOR(S): W.D. Edwards, W.A. Hartman, A.B. Torrens and D.L. Butler

DATE: December 1976

Gallium arsenide is a semiconductor material which is becoming increasingly important in the fabrication of electronic semiconductor devices, particularly microwave devices for communications applications above 3 GHz.

The work described in this report was begun in 1968 as a research project at the Communications Research Centre, and the results obtained from this record preceded much of the current technical knowledge pertaining to gallium arsenide. In this regard, much of the material described herein is largely historical. Nevertheless, it is a valuable reference document, particularly the section dealing with the formation of metallic contacts to gallium arsenide, and one of the authors (W.D. Edwards) is regarded as a leading authority on this topic.

The report describes techniques for preparing gallium arsenide substrate wafers, growing epitaxial layers of gallium arsenide by vapour deposition, assessing the products, forming metallic contacts, and fabricating and testing diodes. The Gunn effect, currently being utilized to build stable oscillators, is also described from the theoretical and practical standpoints.

SOMMAIRE À L'INTENTION DE LA DIRECTION

N° DU DOCUMENT: Rapport du C.R.C. n° 1303

TITRE: Les matériaux et dispositifs à arséniure de gallium et l'effet Gunn

AUTEUR(S): MM. W.D. Edwards, W.A. Hartman, A.B. Torrens et D.L. Butler

DATE: décembre 1976

L'arséniure de gallium est un matériau semiconducteur qui a une importance de plus en plus grande dans la fabrication de dispositifs semiconducteurs électroniques, particulièrement pour la fabrication de dispositifs micro-ondes devant servir aux communications sur des fréquences supérieures à 3 GHz.

Les travaux décrits dans ce rapport ont débuté en 1968, sous forme d'un projet de recherche effectué au Centre de recherches sur les communications, et les résultats obtenus étaient à l'avant-garde des connaissances techniques du moment en ce qui concerne l'arséniure de gallium. De ce fait, le rapport contient des renseignements qui sont pour la plupart de caractère historique, quoique très intéressants, particulièrement en ce qui concerne la formation de surfaces métalliques de contact avec l'arséniure de gallium, et l'un des auteurs, M. W.D. Edwards, est considéré comme un expert en la matière.

Le rapport décrit les techniques de préparation de substrats d'arséniure de gallium en tranches, de croissance de couches épitaxiales d'arséniure de gallium par évaporation, d'évaluation des produits, de formation de surfaces métalliques de contact et de fabrication et d'essai des diodes. L'effet Gunn, employé à l'heure actuelle pour fabriquer des oscillateurs stables, y est également décrit des points de vue théorique et pratique.

GALLIUM ARSENIDE MATERIALS AND
DEVICES AND THE GUNN EFFECT

TK
5102.5
C673e
#1303

DATE DUE
DATE DE RETOUR

OCT - 2 1997

LOWE-MARTIN No. 1137

CRC LIBRARY/BIBLIOTHEQUE CRC
TK5102.5 C673e #1303 c. b

INDUSTRY CANADA / INDUSTRIE CANADA

209171

Government of Canada

Gouvernement du Canada